Pressure Drop through a Packed Bed

A dissertation submitted in partial fulfilment of the requirements for the degree Master in Nuclear Engineering at the Post-graduate School of Nuclear Science and Engineering

AJK van der Walt

Study Supervisor:
Prof CG du Toit

1 December 2006

Acknowledgements

This study would not have been successfully completed without the help of a number of people. I would firstly like to thank my study leader, Professor Du Toit and co-study leader Professor Rousseau for the guidance throughout the study. Also for my colleagues Jean and Tiaan who contributed to the successful completion of the pressure drop tests and data reduction. Special thanks to my wife Michelle for the support and patience through the past two years. This study would not have been possible without the grace of our Heavenly Father, to whom all praise is given.

ABSTRACT

The importance of the development of PBMR technology for the generation of electricity in South Africa is undeniable. Part of the development includes simulation models to predict operating and transient thermal-fluid behaviour of the reactor core. With regard to thermal-fluid simulations pressure drop correlations are very important, and must be validated experimentally. The High Pressure Test Unit (HPTU) was designed, built and successfully commissioned to provide a facility capable of producing the range of experimental results required. Two types of pressure drop tests are performed on the HPTU, namely integrated and separate effects tests.

In this study a data processing methodology is established that is used to convert raw experimental data into meaningful results. The data processing methodology includes criteria for the prediction of steady state conditions and an uncertainty analysis to investigate the total uncertainty in the Euler number and the friction factor for packed beds. The data processing methodology was implemented and used to estimate the uncertainty in the desired variables. The methodology proved to be successful, and the estimated uncertainties were within the desired range and confidence interval. The repeatability of the results proved to be excellent, which further supports that the tests were successfully conducted.

The final results were compared with relevant correlations identified from a literature survey. The results from the separate effects tests could not be predicted by any correlations obtained from the literature and the Euler numbers were found to be significantly lower. The reason for the large deviation from existing correlations seems to be the result of an inherent characteristic of the packing arrangement of the beds. The results from the integrated effects tests were predicted reasonably well by correlations from the literature. Methods of including the influence of the walls in the prediction of the pressure drop showed that the walls could play an important role in the pressure drop through annular packed beds.

This study showed that the integrity and quality of the data obtained from the HPTU is high and that the results can be used with confidence in further research of pressure drop through packed beds.

UITTREKSEL

Die ontwikkeling van korrel bed modulêre reaktor (PBMR) tegnologie is ongetwyfeld uiters belangrik vir die voorsiening van elektrisiteit in Suid Afrika. Termo-vloei simulasies speel 'n groot rol in die voorspelling van die vloei en hitte oordrag eienskappe van korrel bed reaktors. Drukval korrelasies vorm deel van termo-vloei simulasies, en word voorspel deur korrelasies wat eksperimenteel ondersoek moet word. 'n Eksperimentele opstelling genaamd die High Pressure Test Unit (HPTU) is vir hierdie doel ontwikkel en suksesvol in gebruik geneem. Twee tipe drukval toetse word op die fasiliteit gedoen; naamlik die aparte effek toetse en die geïntegreerde effek toetse.

In hierdie studie is 'n data-verwerkings metodologie ontwikkel om rou data van die HPTU in bruikbare verwerkte data om te skakel. Hierdie metodologie sluit gestadigde toestand kriteria in om te voorspel wanneer die termo-vloei toestande in die fasiliteit geskik is om lesings te neem. 'n Onsekerheidsanalise word uitgevoer op die data om die onsekerheid in die Euler getal en wrywingsfaktor te bereken. Die dataverwerkingsmetodologie is suksesvol geïmplementeer en gebruik om die onsekerhede te bereken. Daar is aangetoon dat die integriteit van die data van so aard is dat die onsekerheid binne die gewenste beryk is. Die herhaalbaarheid van die toetse is ondersoek en gevind om uitstekend te wees.

Die finale resultate is vergelyk met korrelasies wat geïdentifiseer is uit 'n literatuur oorsig. Die korrelasies kan die resultate van die aparte effek toetse nie voorspel nie, waaruit dit blyk dat die resultate aansienlik laer is as voorspel deur bestaande korrelasies. Dit wil voorkom of die rede vir die verskil tussen bestaande korrelasies en die resultate toegeskryf kan word aan inherente eienskappe van die pakkings-struktuur. Bestaande korrelasies voorspel die resultate van die geïntegreerde effek toetse redelik goed. Metodes wat geïdentifiseer is om die invloed van die wande op die drukval in ag te neem toon aan dat die wande se invloed moontlik belangrik kan wees in die voorspelling van die drukval in annulêre gepakte beddens.

Die studie het aangetoon dat die resultate verkry van die HPTU drukval toetse van hoë kwaliteit is en dat die resultate sinvol gebruik kan word in die verdere ondersoek van die drukval deur gepakte beddens.

TABLE OF CONTENTS

LIST OF FIGURES

LIST OF TABLES

NOMENCLATURE

Variables

a - Constant representing physical characteristics of bed

b - Constant representing physical characteristics of bed

d , d_{or} - Orifice throat diameter

d_p - Particle diameter

e Outer

f_k - Friction factor'

i - Inner

j - Number of spacers

k - The k_{th} measured value in the steady-state criteria

k - Coverage factor in the uncertainty analysis

k_1 , k_2 - Constants in B_w

m - Value in steady-state criteria

$\dot{m}$ - Mass flow rate

n - Empirical constant related to the dependency of the friction factor on the Reynolds number

n - Value in the steady-state criteria

n - Number of measurements in the calculation of the standard deviation in the mean

n - Number of particles in the bed

p - The fluid pressure

Δp - Pressure drop

Δp_{or} - Pressure drop over the orifice plate

$|\Delta r|$ - Distance from nearest wall

s - Length of the spacers

u_s - Standard uncertainty

u_g - General uncertainty with an associated confidence interval

z - Dimensionless distance in the radial porosity approximation

Axial direction

A - Empirical constants in the friction factor for laminar flow

- Area

B - Empirical constants in the friction factor for turbulent flow

B_w - Parameter in friction factor dependent on the bed-to-particle diameter ratio

C - Correction factor for the constants in the friction factor

C - Discharge coefficient in mass flow rate calculation

C_1 - Constant in the radial porosity approximation

$C_1(k)$ - First steady-state criteria

C_2 - Constant in the radial porosity approximation

$C_2(k)$ - Second steady-state criteria

D - Bed diameter, Pipe diameter

D_H - Hydraulic diameter

Eu - The Euler number

L - Length

M - Modification factor for the hydraulic radius

P - Any parameter evaluated for steady-state conditions

Re - Reynolds number

Re_D - Pipe Reynolds number

R_h - Hydraulic radius

T - The fluid temperature

U - Velocity

V_{balls} - Volume of the balls in the bed

V_{bed} - Volume of the bed without the particles

Greek Symbols

α - Variable used in explanation of uncertainty

β - Diameter ratio d/D

- Variable used in explanation of uncertainty

$\bar{\varepsilon}$ - Average porosity

ε - Porosity

ε - Expansion factor

μ - Fluid viscosity

ϕ - Any variable in the uncertainty analysis

ρ - Fluid density

σ - Standard deviation

σ_m - Standard error

ψ - Friction factor

Subscripts

1 - Indicates before the orifice plate

2 - Indicates after the orifice plate

$1\min avg$ - Average of the evaluated parameter over one minute

$5\min avg$ - Average of the evaluated parameter over five minutes

avg - Average

bed - Of the bed

d_p - Based on the particle diameter

dyn - Dynamic

eff - Effective

i - Interstitial

m - Modified

m - In the mean value

min - Minimum

o - Superficial

p - Particle

z - Axial direction

∞ - Bulk

1 INTRODUCTION

1.1 Background

1.1.1 Background to the PBMR

It is predicted that moderate growth in South Africa will result in peak electricity demands which will exceed the current generating capacity (PBMR (Pty) Ltd, 2006a). In an effort to provide electricity and better public services to everybody, the Pebble Bed Modular Reactor (PBMR) Demonstration Project has been recognized by the South African electric utility Eskom as a strategic National Project with major macro economic, social and strategic benefits (PBMR (Pty) Ltd, 2006b). In 2004 the South African Government has committed themselves towards significant funding of the safe Pebble Bed Modular Reactor technology (PBMR (Pty) Ltd, 2006c).

PBMR technology has significant advantages over coal-fired power stations (which are the major source of electricity in South Africa), and conventional Light Water Nuclear Reactors (LWR). Coal-fired power stations have to be located close to coal mines to reduce the very expensive transportation costs of coal. These location restrictions on coal-fired power plants result in an imbalance between electricity supply and demand centers in South Africa (Eskom, 2006). Since the placement of nuclear power plants has a different set of criteria and is not restricted by fuel transportation costs they can more easily be placed close to demand centers. By doing so transmission costs are significantly reduced (Eskom, 2006).

Pebble Bed Modular Reactors are designed to provide inherently safe and clean nuclear power. The concept of a pebble bed reactor was well proven by the 45 MW thermal German AVR plant. The AVR plant ran for 21 years as an experimental demonstration of a pebble bed core. Various fuel and safety experiments were performed on this reactor through which the pebble bed concept was established as proven High Temperature Reactor (HTR) technology. The use of pebble bed reactors for the production of electricity was further proven by the German Thorium High Temperature Reactor (THTR).

Pebble bed fuel consists of coated fuel kernels embedded in a spherical carbon matrix. The so-called TRISO (TRistructural ISOtropic) particles are made up of Uranium Dioxide fuel kernels coated with a buffer Carbon layer followed alternately by two dense pyrolytic carbon layers and a Silicon-carbide layer. Figure 1.1 shows the composition of such a TRISO particle and pebble fuel sphere.

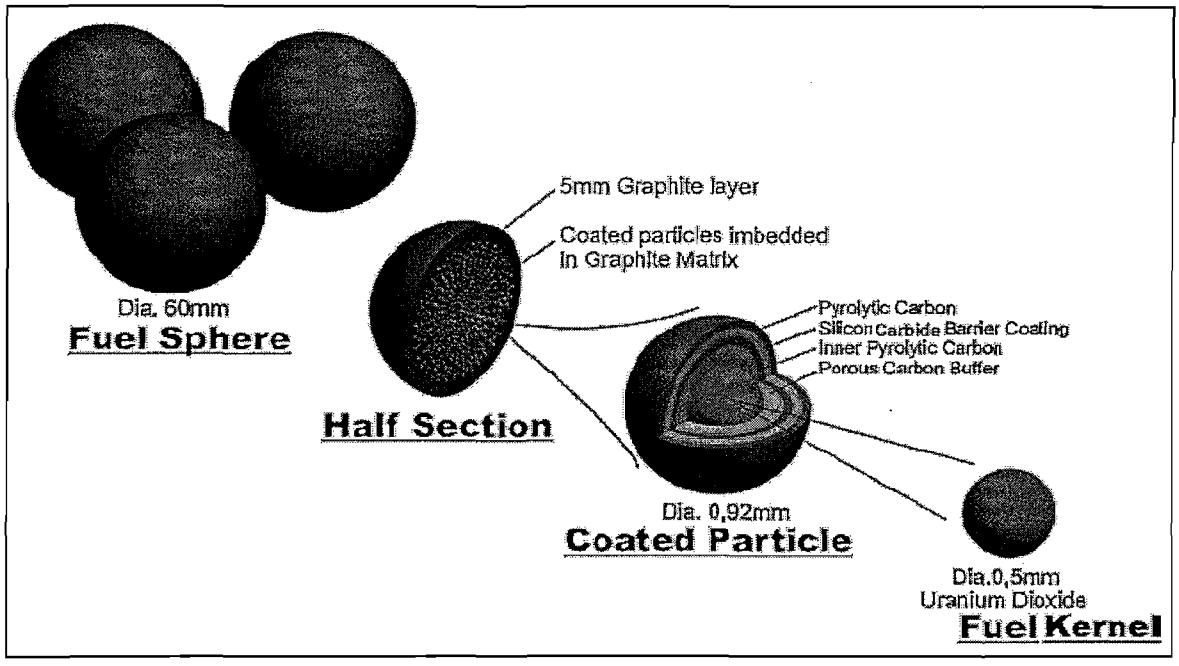

Figure 1.1 *Schematic example of a TRISO particle and a fuel pebble (Matzie, 2004)*

The fuel along with the heat transfer characteristics of the core plays a critical role in the safety of a pebble bed reactor. The integrity of the TRISO coated particles is virtually guaranteed for fuel temperatures below 1600 °C, with the release of fission products below a factor of 10^{-5} of the inventory. To maintain inherent safety and control capabilities certain limits is placed on the core diameter. The 200 MW Siemens HTR-Modul on which the PBMR design was originally based was limited to a 3m diameter core. For larger cores sufficient heat removal without intervention cannot be guaranteed and the neutron control capabilities of the control rods in the reflector are reduced.

With safety being a primary consideration in nuclear technology, PBMR plants are designed for the abovementioned reasons to have a much lower thermal and electrical power output than coal-fired power stations or other forms of nuclear power plants. The simplicity of PBMR plants and the fact that no backup safety equipment is needed in the case of a total loss of active coolant accident makes it economically competitive with other forms of power generation. PBMR designers have however realized that an increase in thermal power will be necessary.

The first step towards increasing the thermal power, while maintaining control capabilities, was to shift the design to an annular configuration with a dynamic centre reflector (Koster *et al.*, 2003:232). The centre reflector in this case consisted of graphite balls circulating with the fuel pebbles through the core. The dynamic reflector would inevitably result in a mixing zone

of graphite balls and fuel pebbles. The mixing zone and dynamic core have certain neutronic and thermal-hydraulic implications which limit the power of the core for the event of an accident (Koster *et al.*, 2003:236). With a dynamic centre reflector an increase in thermal power from 200 to 300 MW was possible (Koster *et al.*, 2003:232).

In order to stay within commercial goals a further increase in power was necessary. By replacing the dynamic centre reflector with a replaceable solid reflector a safe thermal power increase from 300 to 400 MW was possible (Koster *et al.*, 2003:232). Figure 1.2 shows the annular core with the reflectors.

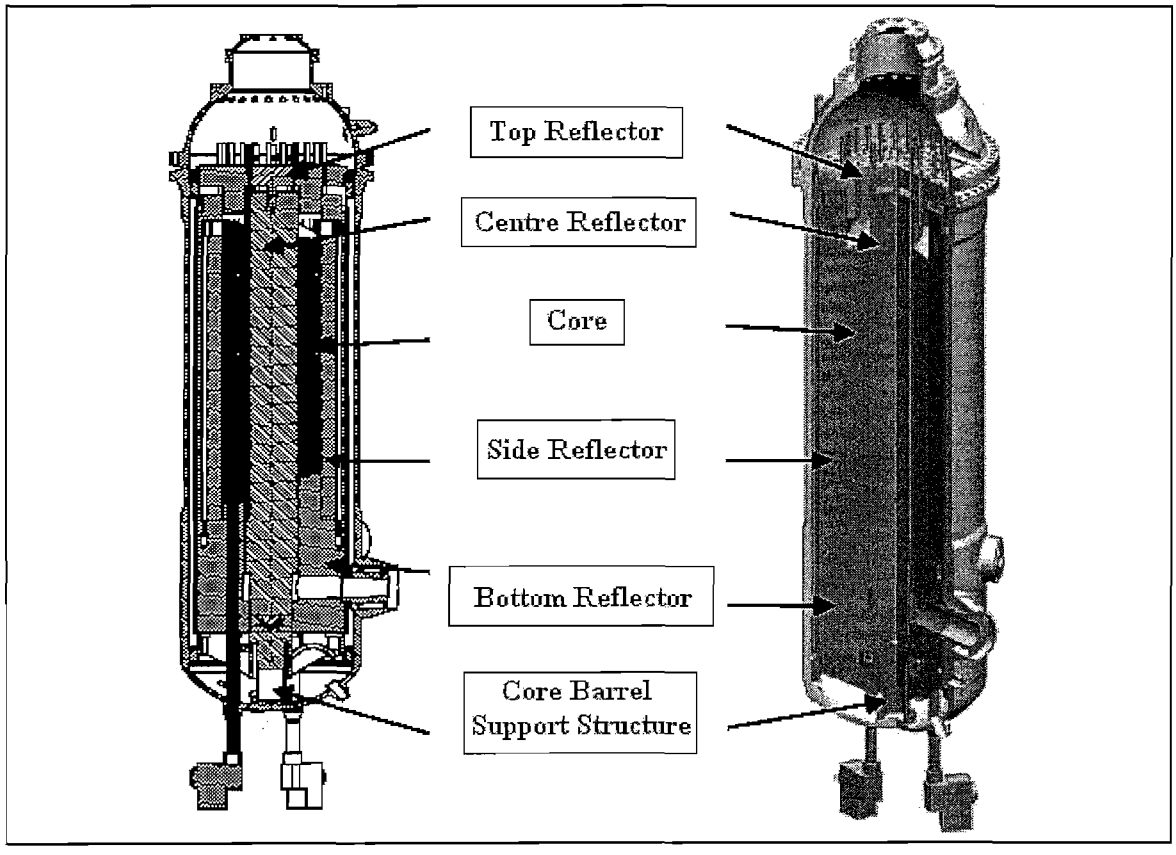

Figure 1.2 *A schematic layout of the proposed PBMR core showing the annular core and reflectors. (Matzie, 2004)*

Fuel handling for the PBMR plant is based on the so-called MEDUL (MEhrfavh-DUrchLauf)-concept, which means that the fuel pebbles are added regularly at the top of the core and circulated through until fully burnt. The fuel pebble circulation rate is expected to be 2900 balls per day (Matzie, 2004), or 0.64 % of the total number of pebbles in the core. The PBMR can therefore be approximated as a fixed bed reactor. Fluid flow through packed bed

reactors forms part of the larger research area of porous media. This study will focus on fluid flow and pressure drop through packed beds consisting of spherical particles with the specific intention of increasing the knowledge about the pressure drop through annular packed beds. The study will also be of benefit to the broader research area of flow through porous media.

1.1.2 Importance of pressure drop for the development of PBMR

For any power generation plant it is very important that the predicted power output and plant efficiency is met within certain limits when operation commences. With regard to the prediction of the power output the accurate prediction of the pressure drop is very important. Pressure drop influences the efficiency of the plant, and is directly linked to the temperature rise and power density in the core.

Pressure drop through the core constitutes a major part of the total pressure drop through the cycle. The design of the helium circulators and compressors therefore rely in part on the accurate prediction of the pressure drop through the core (Kugeler *et al.*, 2003).

1.1.3 Modelling approaches

The use of thermal-fluid simulations has become indispensable for the prediction of the reactor power output and accident behaviour in the development of the PBMR, and along with experimental verification it forms a strong basis for the safety case of the PBMR. System performance prediction is important in both steady-state and transient conditions. Transient analyses are required for control studies and for studying operating procedures such as start-up, load rejection, load following and accident events (Du Toit *et al.*, 2006). Detailed modelling of the PBMR components are very time consuming. Modelling approaches that are less time consuming while providing sufficiently accurate answers are therefore desirable, especially for the integrated simulations of the PBMR plant and transient analysis.

In order to obtain a sufficiently accurate engineering answer, the computational time desired must be weighed against the detail required. Since transient simulations are for example computationally very expensive, some detail will be compromised for faster answers. For this purpose the reactor core is coarsely discretized into a number of one-dimensional elements

(Du Toit *et al.*, 2006) in thermal-hydraulics codes such as Flownex (2006). The amount of detail compromised can however be reduced if the thermal-hydraulic correlations used are thoroughly verified and validated experimentally for the use in the simulation code. This verification and validation process of all the thermal-hydraulic processes present must take place for the flow and packing characteristics of all the typical unit cells in the bed. The primary flow and packing characteristics include the variation in porosity, the influence of the walls and the range of Reynolds numbers (laminar and turbulent flow).

1.1.4 Experimental verification and validation

The need for experimental verification and validation of heat transfer and pressure drop correlations has led to the development of the Heat Transfer Test Facility (HTTF) by M-Tech Industrial Pty (Ltd). This facility is of utmost importance for the safety case of the PBMR as it will investigate the important thermal hydraulic phenomena present in the PBMR core. A part of the HTTF is dedicated to the investigation of the thermal-hydraulic phenomena important for the prediction of the PBMR core performance as well as correlations that are of specific importance in the safety calculation. These tests will be carried out over the whole range of relevant Reynolds numbers. To obtain the high Reynolds numbers the tests will be performed over a range of pressures. This part of the HTTF is known as the High Pressure Test Unit (HPTU). Some correlations need to be verified at high temperature. For this reason the second part of the HTTF will be developed known as the High Temperature Test Unit (HTTF). Pressure drop experiments will be performed on the HPTU.

The types of tests performed on the HPTU can be divided into two groups namely the separate effects tests (SET) and the integrated effects tests (IET). Separate effects tests are performed to investigate the different thermal-hydraulic phenomena separately from each other and at different uniform porosities. These tests form the building blocks of thermal-hydraulic codes such as Flownex (2006). For each typical unit cell or control volume, verified correlations can be used to describe the different thermal-hydraulic phenomena present. In each control volume the structure or porosity is assumed to be homogenous. Through this bottom-up approach the reactor can be modelled by the integration of typical control volumes each with individually verified thermal-hydraulic correlations. For the purpose of the pressure

drop investigation different homogenous porosity test sections will be used which represent the typical control volumes encountered in the PBMR core.

The purpose of the IETs is to obtain experimental data for the integrated phenomena. The pressure drop through a randomly packed annular bed which is dimensionally similar to the actual PBMR core must for example be measured and compared with the prediction of a code based on the integration of control volumes. Results from the IETs will therefore be used for the verification of the thermal-hydraulic codes and establishing a database for comparison between models and experimental data. For the purpose of the pressure drop investigation both a cylindrical packed bed and an annular packed bed will be investigated experimentally.

1.2 Problem definition

As a result of the High Temperature Reactor (HTR) technology development in Germany a significant amount of research has been done on flow through cylindrical cores consisting of randomly packed beds of spheres. This could be used by the developers of PBMR technology in South Africa, especially during the early design stages. The changes in the core design from a cylindrical core to an annular core do have certain implications. All the heat transfer and pressure drop correlations were developed for cylindrical packed beds where the ratio of the cylinder diameter to particle (or pebble) diameter is very large. This ratio is 50 for the AVR and 85 for the THTR. In such large beds the variation in the average radial porosity encountered is relatively small in comparison with the rest of the bed, and can therefore be assumed to be negligible. The assumption of a homogeneous packing arrangement in thermal-fluid simulations of the PBMR core is however not necessarily correct, and must be investigated for the regions close to the walls.

The pressure drop correlations developed in Germany were not based on experiments performed under the required quality control systems. This reduces the confidence in the existing pressure drop correlations, especially for the purpose of proving PBMR's safety case.

The problem pertaining to the prediction of the pressure drop through the PBMR core can be summarized as the following:

- The pressure drop correlation currently used in the unit cell approach for the modelling of the PBMR core has not been verified for the physical characteristics of

the packed bed in the near wall region, and has not been derived within the required quality assurance environment.

- Limited research has been done on the pressure drop through annular packed beds and therefore:
    - Very little experimental data on pressure drop through annular packed beds are available for the verification of the different pressure drop correlations found in the literature;
    - The approach to model the PBMR core by the integration of homogenous porosity control volumes cannot be properly evaluated without data from integrated pressure drop experiments.

1.3 Aim of the study

The aim of this study is not to address and solve the entire problem as stated above. The construction and commissioning of the HPTU provided a test facility capable of investigating the pressure drop through packed beds over the whole range of Reynolds numbers required within a controlled quality assurance environment. It is now left to obtain raw experimental data and process them into useable results. With regard to the tests to be performed and the processing of the raw data this study will mainly contribute to solving the problem stated above by developing a data processing and evaluation methodology which will indicate whether the data obtained are of high quality.

In summary this study aims is to contribute in the following ways:

- An extensive literature survey will be performed with the following goal:
    - ➢ To establish a database of pressure drop correlations to compare and evaluate the SET and IET pressure drop experiment data.
    - ➢ To obtain pressure drop correlations pertaining to annular packed beds.
    - ➢ To identify possible methods of evaluating the experimental data from the HPTU.
- Develop and establish a data reduction and processing methodology which can be used to extract and convert raw experimental data into meaningful information which can be evaluated and compared with correlations. This will include:
    - ➢ The calibration of the measuring instruments to reduce systematic errors.

- Defining steady-state criteria which can be used in real time to evaluate whether flow conditions have reached steady-state and when data could be extracted.
- A thorough uncertainty analysis to investigate the influence of random and systematic errors from the measurements and the measuring instruments on desired variables such as the Euler number.
- Adding a certain confidence in the processed data from the uncertainty analysis.
- Investigating the precision of the calculations made by the control system implemented on the HPTU.
- Investigating the repeatability of the measurements.

- Compare the processed data with the important correlations identified in a meaningful way.
- Evaluate the data at the hand of the methods identified in the literature survey.

Note that the last two outcomes do not imply that a final verdict will be given regarding the correlations investigated. The study rather aims to give a preliminary verdict regarding the success of the test sections used, i.e. whether the purposes of the SETs and IETs were actually realized. The emphasis throughout the study is therefore to obtain and develop tools for the evaluation of the quality and integrity of the data and the success of the pressure drop tests. Through this process of evaluation the study also aims to point out where further research could be done to improve the understanding of pressure drop through packed beds.

1.4 Research Methodology

The aim of the study outlined above can clearly be divided into two distinctive parts. The first part is to identify important correlations and methods to investigate the importance of different flow phenomena in the prediction of the pressure drop. This is very important since the correlations identified will serve as points of reference against which the data can be compared, while the methods to investigate secondary influences will further add to evaluating the data. This will be done through an extensive literature.

The second part of this study will focus on the experimental aspects of investigating the pressure drop, with the focus on the processing of the raw data. To achieve this goal the

existing HPTU plant must first be understood and the important aspects of the design will be examined. Tests will be performed and raw data will be obtained. A first set of data will then be used to establish a data processing methodology which can be implemented to identify usable data and to prove the quality and integrity of the data.
The two main goals will be combined in the comparison of the data and correlations, with the literature survey serving as a means to further evaluate the integrity of the data.

1.5 Contribution of the study

The literature survey performed will contribute to the database of pressure drop literature and will be available for future use. The literature will not only contribute to evaluating the data in a meaningful way, but the possible methods of evaluating the phenomena influencing the pressure drop through packed beds will also indicate whether secondary influences are truly important.
The data processing methodology will form the basis for the data processing of the results from other tests performed on the HPTU, and possibly the HTTU. It will therefore form the basis of a general data processing philosophy. The preliminary evaluation of the pressure data will indicate further areas of research pertaining to pressure drop through the PBMR core.
This research will further benefit the larger scientific community to further the understanding of the complex nature of the fluid dynamics found in porous media which will probably be a topic of research for still some time in the future.

1.6 Overview of the dissertation

An account of the background and the role of this research in the development of the PBMR have been given in Chapter 1. As a starting point to this study, previous research performed will be investigated through a thorough literature survey. As part of the literature survey some theoretical aspects of the different phenomena influencing the pressure drop will be discussed to form a basis for the evaluation and interpretation of the experimental results. The test facility used to obtain the experimental results is described in chapter 3. In chapter 4 the data processing and data reduction methodology will be discussed at length. A number of results will also be presented to show the success of the data processing methodology. Chapter 5 is

dedicated to the comparison and evaluation of the experimental results at the hand of the literature survey and the theoretical aspects of the difference important phenomena. The main focus of the conclusions in Chapter 6 will be to summarize the results and to indicate the areas where further research will be beneficial for the understanding of pressure drop through packed beds. A survey of the literature will now be used to identify the most relevant correlations against which the experimental results could be compared, as well as methods to describe influences that are of secondary importance in the evaluation of the experimental results.

2 LITERATURE SURVEY

2.1 Introduction

In the previous chapter the problem definition was outlined and placed within the context of High Temperature Reactor technology with specific reference to the modelling approach employed in Flownex (2006) for the simulation of the thermal-hydraulic phenomena of the PBMR core and the test facility developed to address the questions regarding the correlations found in the literature.

This comprehensive literature survey can be divided into two main sections. The relevant and important correlations are firstly identified, with the correlation generally used for predictions of the pressure drop through the PBMR core underlined. The correlations discussed are mostly concerned with the pressure drop due to the particles.

The second part aims to explain the secondary pressure losses in more detail. Through this part of the literature survey methods will also be pointed out that can be used to evaluate experimental data and show whether the secondary pressure losses are important and whether they should be investigated further.

A general background will now follow, explaining different pressure drop prediction methodologies.

2.2 General Background

Before continuing with the literature survey, some basic phenomena encountered in packed beds must be mentioned. A brief discussion of the different ways of predicting the pressure drop in different simulation methodologies is also given to outline the boundaries within which the important literature and evaluation methods fall.

2.2.1 Some important phenomena

In packed beds the largest part of the pressure loss is due the flow resistance of the particles. This is generally a good approximation if the bed diameter to particle diameter ratio is large.

In the near wall region the particles are forced by the walls to arrange in such a way that the void fraction, or porosity, is larger. The result of this porosity variation is a bypass effect resulting in higher flow velocities near the walls.

Friction due to the walls also plays a very important role. The wall friction enforces a no-slip condition on the flow and therefore influences the flow distribution in the near wall region. The porosity variation and wall friction is therefore very important and will be referred to throughout the discussion.

2.2.2 Pressure drop in macroscopic flow modelling

Different thermal-fluid simulation methodologies exist. The difference between thermal-fluid simulation methodologies generally lies in the level of detail for which a solution is sought. The level of detail varies between lumped one dimensional models, network codes, detailed macroscopic Computational Fluid Dynamics (CFD) codes and even CFD simulations of microscopic flow phenomena.

In the case of the PBMR reactor core the level of detail can be expressed as the extent to which the complex geometry is represented. In microscopic flow modelling the pressure drop is explicitly calculated by solving the Navier-Stokes equations for the flow around each particle. For engineering purposes microscopic flow phenomena are not modelled, as this is computationally extremely expensive for the complex geometry found in the PBMR core. Microscopic flow modelling should however not be ruled out as a possible way of investigating the complex flow phenomena in packed beds, especially with present day computing capabilities.

The use of dimensionless parameters such as the Euler number and is however preferred for design purposes. In the investigation of the pressure drop the Euler number is correlated to a friction factor (similar to pressure drop through pipes) and the bed geometry (average porosity and the bed length-to-particle diameter ratio). By doing so the complexity of the problem is reduced to the determination of empirical constants which depend on the geometric characteristics of the bed. The advantage of this method is that a bed can be discretized into a large number of control volumes for "detailed" flow modelling while making use of a macroscopic representation of the geometry and in which the pressure drop is then calculated implicitly. It is however clear that the empirical constants must be valid for each control

volume encountered in the discretized bed and for both the radial and axial directions (if an axial-symmetric discretization is assumed).

Two very important observations can now be made: firstly constants obtained from experiments where the wall influence is not negligible should not be used in a control volume far from the wall. Secondly, constants obtained from average porosities of a bed with a large bed-to-particle diameter ratio cannot be used for control volumes close to the wall where the average porosity is significantly larger.

From the first observation mentioned above it follows that it is important to distinguish between correlations where the influence of the wall friction could possibly have been significant in the calculations of the empirical constants and those where the influence was possibly negligible. This influence of the wall friction must also be quantifiable to aid in determining certain characteristics of a packed bed in the design of an experiment. From the second statement given it is clear that the pressure drop correlation used for control volumes close to the wall where a high average porosity is encountered should also investigated.

The geometry of packed beds (or average and local porosity) is therefore also of importance for this study, even though it will not be investigated in particular.

2.3 Pressure drop correlations for packed beds

The first purpose of the literature will now be pursued in which the important correlations predicting the influence of the particle resistance on the pressure drop is summarized. The correlations will then be used in the second part of the literature survey in more detailed methods of evaluating the secondary influences to predict the particle resistance to the flow.

2.3.1 Background to the fundamental equation

A number of methods exist to describe the pressure drop through packed beds. The most common and by far the most established method makes use of the hydraulic diameter concept developed by Blake (1922). Blake suggested that the dimensionless groups,

$$f_k = \frac{\Delta p}{\rho \cdot U_i^{\,2}} \cdot \frac{D_H}{L} = \frac{\Delta p}{\rho \cdot U_o^{\,2}} \cdot \frac{d_p}{L} \cdot \frac{\bar{\varepsilon}^3}{1-\bar{\varepsilon}} \qquad (1)$$

and

$$\mathrm{Re}_m = \frac{\rho \cdot U_i \cdot D_H}{\mu} = \frac{d_p \cdot \rho \cdot U_o}{\mu \cdot (1-\bar{\varepsilon})} \tag{2}$$

should be used to characterize the pressure loss due to the particulate system for different mass-flow rates (Ergun, 1952:90). The variables are declared as ρ the fluid density, Δp the pressure drop, U_i the interstitial fluid velocity, D_H the hydraulic diameter, L the bed length, $\bar{\varepsilon}$ the average porosity and d_p the particle diameter. The first term, f_k is recognized as the Darcy-Weisbach friction factor for pipe flow, modified by using the hydraulic diameter of a packed bed of spheres in terms of the average porosity $\bar{\varepsilon}$:

$$D_H = \frac{2 \cdot \bar{\varepsilon} \cdot d_p}{3 \cdot (1-\bar{\varepsilon})} \tag{3}$$

The interstitial velocity U_i is rewritten in terms of the superficial average velocity, U_o and the average porosity. The second term is the Reynolds number, where the same modifications have been made. These two groups are known as the modified friction factor and modified Reynolds number, Re_m respectively. In general the hydraulic diameter concept used for packed beds is derived for perfectly spherical particles, as should be clear from the definition of D_H, and excludes the hydraulic diameter associated with the walls. Note that the value of $2/3$ is not included in equation(1), but is generally implicitly included in the constants in the correlations derived for the friction factor.

Early attempts failed to predict the pressure drop for both laminar and turbulent flow with a single correlation. The additive nature of the viscous and kinetic or inertial energy losses was not recognized and correlations were restricted to either low or high Reynolds numbers. The transition from laminar to turbulent flow in porous media is very smooth, unlike that found for fluid flow in pipes.

The resistance offered by friction to the motion of fluid was first formulated by Reynolds (1900) as the sum of the viscous and kinetic energy losses:

$$\frac{\Delta p}{L} = a\mu U + b\rho U^n, \tag{4}$$

with $n = 2$. The first term on the right-hand-side presents the viscous energy losses and the second term the kinetic energy losses. The parameters a and b represent the physical characteristics of the bed and therefore depend amongst others on the porosity. It has been shown by various authors that a is proportional to $(1-\bar{\varepsilon})^2/\bar{\varepsilon}^3$ and b to $(1-\bar{\varepsilon})/\bar{\varepsilon}^3$. According

to Carmen (1937:158) Forchheimer (1930) suggested that the value of n is also dependent on the characteristics of the bed and that n can take on a value between 1.6 and 2. If equation (4) is written in terms of the friction factor for the general case, the following equation is obtained:

$$\psi = \frac{\Delta p}{\rho U_o^{\,2}} \cdot \frac{d_p}{L} \cdot \frac{(\bar{\varepsilon})^3}{(1-\bar{\varepsilon})} = \frac{A}{\dfrac{\mathrm{Re}_{dp}}{(1-\bar{\varepsilon})}} + \frac{B}{\left[\dfrac{\mathrm{Re}_{dp}}{(1-\bar{\varepsilon})}\right]^{2-n}}, \qquad (5)$$

where Re_{dp} is the particle Reynolds number defined as $(\rho \cdot U_o \cdot d_p)/\mu$.

This is the most general form of the friction factor for fluid flow through packed beds based on the hydraulic diameter concept. The values of A and B are empirically determined constants. It is important to note that the average porosity is used throughout, and that a uniform velocity profile, or plug flow is assumed.

2.3.2 Carmen- and Ergun-type correlations

There are two variations on the general form of the friction factor. Firstly the constant n can be taken as 2, as originally proposed by Reynolds as quoted by Ergun (1952). This is generally known as the Ergun-type equation and is most frequently encountered in the literature and is the most common variation. The second variation is where $1.9 \leq n \leq 1.95$, as proposed by Carmen (1937), and is therefore generally known as the Carmen-type equation.

The Ergun equation (Ergun, 1952), with A = 150 and B = 1.75 was developed by fitting equation (5) to 640 experimental data points. These data included pressure drop measurements for flow through beds packed with various particle shapes and sizes, including various sized spheres, sand and crushed materials (pulverized coke) (Ergun, 1952:91). The Ergun equation is applicable to the particle Reynolds number range $1 < \mathrm{Re}_{d_p} < 2500$, and average bed porosities of the range $0.36 < \bar{\varepsilon} < 0.4$. In chemical packed bed reactors various particle shapes are used. Bed-to-particle diameter ratios are generally low, and the influence of wall friction on the pressure drop is in most cases substantial. Since the Ergun equation does not explicitly account for the walls (whereby the wall effects are assumed to be negligible), and is not correlated for specific particle shapes, its use for certain applications

has been questioned. Therefore many researchers correlated equation (5) to their own experimental data, defining the values of A and B differently, while assuming n equal to 2. By varying the bed-to-particle diameter ratios of packed beds in experimental investigations, many researchers tried to establish a way of including the influence of the walls in the empirically determined constants. As a result of these attempts a large number of correlations exist. Only a few of these correlations are however meaningful for further investigation, with the gross number applicable to such small ranges of Reynolds numbers, average porosities and bed-to-particle diameter ratios, that they bear no further significance in this study.

The Carmen-type equation is less known and has not received as much attention or credit as the Ergun-type equation in certain applications. The constants A and B were originally proposed by Carmen as 180 and 2.871 respectively (Carmen, 1937:160). A number of variations on the constants A and B are known to exist. Brauer (1960) empirically correlated the values of A, B and n as 160, 3.1 and 1.9 respectively. This was done for pressure drop data from packed beds with spherical particles over the modified Reynolds number range $0.04 < Re_m < 8000$. Jeshar (1964) evaluated this correlation further for spherical particles over the modified Reynolds numbers range $2 < Re_m < 30000$. Barthels (1972) correlated the values of A, B and n to experimental data and proposed the values as 150, 2.855 and 0.095. Included in Barthels' (1972) data were pressure drop data from a structured packed bed with a porosity of 0.476, and the correlation is valid over the Reynolds number range $2 < Re < 8000$. The correlation by Barthels (1972) is therefore to some extent valid at high average porosities up to 0.476, as well as Reynolds numbers well into the turbulent flow regime.

2.3.3 The KTA equation

As part of the development of thermal-fluid correlations for pebble bed HTR cores a German research group made a considerable effort of establishing a pressure drop correlation for cylindrical packed beds of spherical particles over a very large range of Reynolds numbers. The development of the correlation and the participants of the research groups are given in the KTA (Kerntechnische Ausshluß) 3102.3 (Anon, 1981) report. The derivation of the correlation is based on the investigation of various well-tested correlations. A new correlation was obtained from a regression analysis on the semi-empirical data obtained from each

correlation. All the correlations used were investigated beforehand and had to adhere to certain criteria. The criteria included the following:

- The influence of the walls on the pressure drop must be negligible. From various experimental investigations of various authors the research team chose data points at bed-to-particle diameter ratios and Reynolds numbers where the influence of the walls was negligible. By plotting the bed-to-particle diameter ratio to the Reynolds number they were able to draw a curve which indicates the range in which the influence of the walls is negligible. The theoretical basis for this curve is however not clear from the KTA report.
- The average porosity of the bed must be known from the original documents.
- The bed length must be larger than 4 particle diameters.
- Only correlations developed for unstructured (randomly packed) bedswere used.
- Only experiments with particles larger than 1mm diameter were considered.

From the different correlations a new correlation was proposed with the values of A, B and n as 160, 3 and 1.9 respectively. It is clear that a Carmen-type equation was proposed with constants very similar to the correlation by Brauer (1960) and Barthels (1972). The correlations of Brauer (1960) and Barthels (1972) were also used in the regression analysis. The application of the correlation by Barthels (1972) for this purpose was restricted to the Reynolds number range where data for randomly packed beds were used in the original correlation. Any data for structured beds were excluded. Each correlation used in the investigation is restricted to a certain Reynolds number range, average porosity and bed-to-particle diameter ratio. The application of the correlation is therefore not restricted to two single values of the average porosity over the whole Reynolds number range. If the minimum and maximum average porosities of all the different correlations are assumed to be valid over the whole Reynolds number range it can be assumed that the KTA equation is valid for $0.366 < \epsilon < 0.43$. The correlation is likewise valid for bed-to-particle diameter ratios larger than 5. An uncertainty analysis was performed to calculate the uncertainty with a 95% confidence level. The claimed uncertainty is ±15%. This is based on the deviation of the correlations used from the average calculated. Experimental results from Achenbach (1995) confirmed the validity of the KTA equation up to $\frac{\mathrm{Re}}{1-\bar{\varepsilon}} < 10^5$. For higher Reynolds numbers the friction factor seems to become independent of the Reynolds number (Achenbach, 1995).

The equation developed by the research group is of particular importance to the PBMR, as it is the equation adopted for the German development of Pebble Bed HTRs. In the context of the PBMR development this correlation is generally referred to as the KTA equation.

2.3.4 Comparisons and modifications of different correlations

A very valuable overview of pressure drop correlations is given by Eisfeld and Schnitzlein (2001). The primary objective of their study was to establish which correlations are valid when the wall effects are not negligible, i.e. for low bed-to-particle diameter ratios. This was done from more than 2300 experimental data points from various authors. Pressure drop data from experiments with characteristics in the range $1.624 < D/d_p < 250$, $0.330 < \bar{\varepsilon} < 0.882$ and $0.01 < \mathrm{Re}_{dp} < 17635$ were used. Both the Ergun-type and Carmen-type equations were investigated, as well as alternative approaches. The relative root mean square deviations were calculated for each correlation. This was done independently for pressure drop data from spherical, cylindrical and combinations of particles.

Eisfeld and Schnitzlein (2001) concluded from their study that if an Ergun-type equation is assumed to be valid, the correlation proposed by Reichelt (1972) gives the best results for spheres and cylinders. It was thereby shown that an Ergun-type equation is indeed capable of predicting the pressure drop for low bed-to-particle diameter ratios, where the average porosities are very large.

The correlation proposed by Reichelt (1972) with the modifications by Eisfeld and Schnitzlein (2001) is the most important Ergun-type correlation considered in this study.

The correlation is based on the method proposed by Metha and Hawley (1969) of including the walls into the hydraulic diameter. The method and the subsequent correlation will be discussed in more detail in further in the Literature Survey and will also be used to quantify the influence of the wall friction which will explain why the wall friction must be negligible in the experimental investigation in this study. It is however important at this point to mention that the correlation of Reichelt (1972) predicts a significant influence of the walls on the pressure drop for bed-to-particle diameter ratios lower than 10, contrary to the assumption made in the KTA correlation.

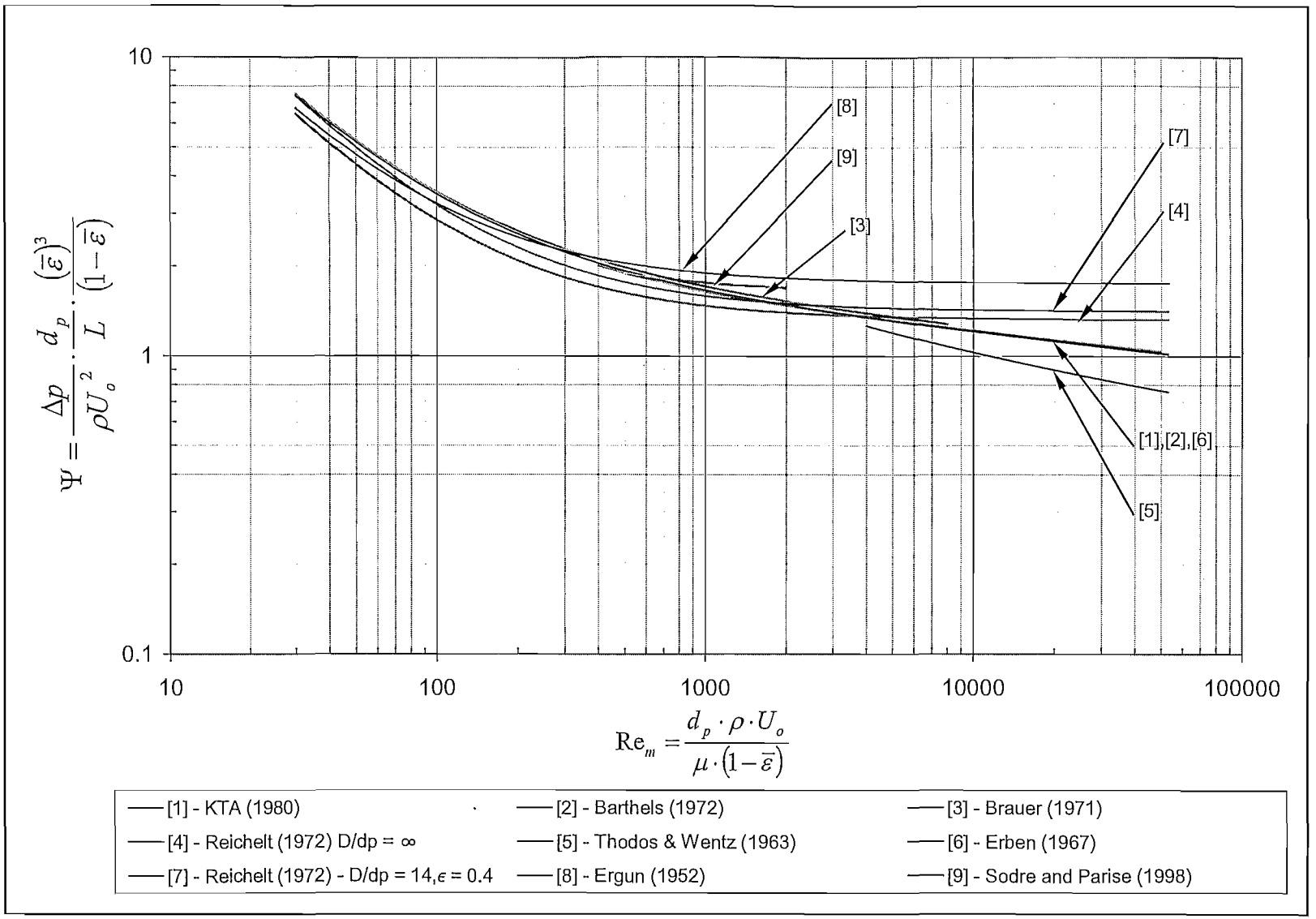

Figure 2.1 *Qualitative comparison between the most important pressure drop correlations*

As far as the Carmen-type correlation is concerned, the study by Eisfeld and Schnitzlein (2001) showed that the correlation by Barthels (1972) predicts the pressure drop overall slightly better than the correlation by Brauer (1960), and is in general better than the Ergun-type correlations. The correlations by Brauer (1960), Barthels (1972) and the KTA equation are very similar as indicated in Figure 2.1. Since the correlation by Barthels (1972) is valid for the ranges given in Figure 2.1, it seems reasonable from a qualitative comparison that the KTA equation should also hold over this range of average porosities and Reynolds numbers. Above the Reynolds number range tested by Barthels (1972) the validity of the KTA equation at high average porosities remains in question, and must be clarified.

2.3.5 Pressure drop through structured and distended beds

For the use of homogeneous porosity control volumes in modelling the reactor core, pressure drop correlations applying to homogenous porosities must be investigated. When the bed-to-particle diameter ratio of a randomly packed bed is very large, the porosity can be assumed to be homogeneous. For such cases the porosity is however far below the average porosity of the typical control volume found close to the walls. Such high porosities can only be realized in structured packed beds.

Unfortunately limited research has been done on the pressure drop through structured packed beds and no conclusive answer can as yet be given as to whether the same general pressure drop correlations are valid. Of the experimental research performed the most thorough work is that of Wentz and Thodos (1963) for cylindrical test sections and Erben (1967) for rectangular test sections. Pressure drop measurements were taken for flow through cubic, body-centred cubic and face-centred cubic packing arrangements. To obtain high porosities the particles were distended by means of thin wires, and various porosities were tested ranging from 0.615 to 0.882. Structured packed beds (i.e. without wires) were also investigated, one being a body-centred cubic arrangement with a porosity of 0.354 and the other a cubic arrangement with a porosity of 0.48. All the packing arrangements had a length of 5 particle diameters. At the sphere-wall interface the particles were shaped to follow the wall curvature thereby eliminating the wall channelling phenomena. From the experimental data Wentz and Thodos (1963) empirically correlated the friction factor of the modified Reynolds number (equation (2)) in the following form for the total pressure drop across the bed:

$$\psi = \frac{0.396}{\left(\mathrm{Re}_m\right)^{0.05} - 1.2}. \tag{6}$$

Pressure drop measurements were also made for a single layer of particles in the middle of each packing arrangement with purpose to eliminate any entrance and exit effects. From these measurements the following correlation was obtained:

$$\psi = \frac{0.351}{\left(\mathrm{Re}_m\right)^{0.05} - 1.2}. \tag{7}$$

The experimental data from Wentz and Thodos (1963) follows a general trend for all the types of packing arrangements and porosities which suggests that there is not a significant difference in the friction factor for different average porosities in homogenous packing arrangements.

As previously mentioned the data used by Barthels (1972) also included measured pressure drops from structured packed beds. Pressure drop experiments were performed for a cubic packing arrangement in a square column with an average porosity of 0.476 over the particle Reynolds number range of $4 \cdot 10^3 \leq \mathrm{Re}_{dp} \leq 10^5$. The data of the structured packing arrangement showed no deviations from the randomly packed beds of lower porosities, which suggests that there is little difference in the basic phenomena governing the pressure drop through structured and random packing arrangements. A comparison between the correlations of Barthels (1972) and a correlation by Erben (1967) further supports this notion. Erben (1967) performed pressure drop experiments on structured packing arrangements with porosities of 0.26 and 0.476 in square columns over the Reynolds number range $10^4 \leq \mathrm{Re}_{dp} \leq 10^5$. The following correlation was suggested:

$$\psi = \frac{3.3615}{\left(\mathrm{Re}_m\right)^{0.11}}. \tag{8}$$

It should be clear that this correlation only applies to flow far into the turbulent regime. In both the experiments of Barthels (1972) and Erben (1967) no effort was made to exclude the bypass flow phenomena.

2.3.6 Pressure drop through annular packed beds

To further support the problem definition it is relevant to show the results of the only pressure drop correlation found in the literature that specifically pertain to annular packed beds. The correlation derived from the experimental investigation of pressure drop through annular packed beds by Sodré and Parise (1998) is given as:

$$\psi = \frac{\Delta p}{\rho U_o^{\,2}} \cdot \frac{d_p}{L} \cdot \frac{\left(\bar{\varepsilon}\right)^3}{\left(1-\bar{\varepsilon}\right)} = \frac{A \cdot C}{\mathrm{Re}_m} + B \cdot C^2 . \tag{9}$$

The values of A and B are the constants originally proposed by Ergun (1952), and C is a correction factor accounting for the variation in the porosity (and axial velocity) close to the wall and the wall friction. The way in which the wall friction is accounted for is based on including the wall surface area in the hydraulic diameter as proposed by Metha and Hawley (1969). The variation in the velocity close to the walls is based on an exponential approximation of the radial porosity variation through the bed. The influence of the wall friction on the flow is assumed to be restricted to one particle diameter from the wall.

An experimental investigation was carried out to test the model. This was done for a randomly annular packed bed with an annular width-to-particle diameter ratio, $\frac{D_o - D_i}{2 \cdot d_p}$ of 4.127 over the modified Reynolds number range $500 < Re_m < 2000$. The predicted friction factor had a maximum deviation of 8% from the experimentally calculated friction factor.

2.3.7 Summary of the important correlations

The relevant correlations found in the literature survey are summarized in Table 2.1 for comparison between the coefficients, ranges, type of packing arrangements and the way the influence of the walls are taken into account, and graphically compared in Figure 2.1. The predicted friction factors as a function of the modified Reynolds number are shown in Table 2.1 to give a qualitative comparison of the different correlations. As reference the Ergun equation (1952) is also included.

A number of observations can now be made. If a bed-to-particle diameter ratio of 14 is assumed (which is approximately the value for the annular width-to-particle diameter ratio of the proposed PBMR core) with an average porosity of 0.4, the correlation of Reichelt (1972)

as adjusted by Eisfeld and Schnitzlein (2001) shows a significant deviation from the Carmen-type correlations over most of the modified Reynolds number range, especially above a 1000. It is further apparent that the main difference between the Ergun- and Carmen-type correlations lies in the prediction of the pressure drop in the turbulent flow regime. The Ergun-type equation predicts the pressure drop to be independent of the Reynolds number in the turbulent flow regime, while the Carmen-type correlations show a clear dependency. Since the PBMR core will mainly operate in the turbulent flow regime the prediction of the pressure drop in this region is very important.

Concerning the prediction of the friction factor for structured beds Figure 2.1 once again shows some contradicting behaviour. The friction factor predicted by Barthels (1972) and Erben (1967) shows no difference from the predicted friction factors for randomly packed bed. This is clearly not the case for the friction factor correlated by Wentz and Thodos (1963). The last observation from Figure 2.1 is that the friction factor predicted for annular packed beds by Sodré and Parise (1998) is very similar to the Ergun equation and differs significantly from the KTA equation for high Reynolds numbers.

Table 2.1: Summary of the coefficients, ranges, type of packing arrangements and accounting for wall influence for the important correlations

Author	Type	ψ	Re_m	ϵ	Packing Structure	Wall Influence
Barthels (1972)	Carmen	$\psi = \frac{150}{Re_m} + \frac{2.885}{Re_m^{0.95}}$	$4 \cdot 10^3 - 10^5$ $400 - 5 \cdot 10^4$	0.476 0.369 – 0.404	Structured – Cubic packed Random	By-pass flow and wall friction in constants
Brauer (1960) Brauer (1960) investigated by Jeshar (1964)	Carmen	$\psi = \frac{160}{Re_m} + \frac{3.1}{Re_m^{0.1}}$	$0.4 - 8000$ $20 - 3000$	0.384 – 0.407 0.375 – 0.421	Random	By-pass flow and wall friction in constants
KTA (1980)	Carmen	$\psi = \frac{160}{Re_m} + \frac{3}{Re_m^{0.1}}$	$1 - 10^5$	0.366 – 0.43	Random	By-pass flow and wall friction in constants
Reichelt (1972) (As given by Eisfeld & Schnitzlein (2001)	Ergun	$\psi = \frac{A \cdot 154}{Re_m} + \frac{A}{B}$	$0.02 - 7 \cdot 10^4$	0.33 – 0.882	Random	Varying values for friction and by-pass flow
Wentz & Thodos (1963)	Carmen	$\psi = \frac{0.396}{(Re_m)^{0.05}} - 1.2$	$2500 - 6 \cdot 10^4$	0.48 0.354 0.729; 0.882 0.615; 0.728 0.743	Cubic – packed Body centered cubic – packed Cubic - distended Body centered cubic - distended Face-centered cubic - distended	No by-pass flow Wall friction in constants
Erben (1967)	Carmen	$\psi = \frac{3.3615}{(Re_m)^{0.11}}$	$1.5 \cdot 10^4 - 8 \cdot 10^4$	0.476 0.26	Structured: Cubic packed	By-pass flow and wall friction in constants
Sodré and Parise (1998)	Ergun	$\psi = \frac{150 \cdot C}{Re_m} + 1.75 \cdot C^2$	$600 - 2050$	0.399	Annular packed bed - Random	Correction factor for by-pass flow and wall friction

2.4 Investigation of the secondary pressure drop influences

The first part of the literature survey presented the most important zero-dimensional correlations for different types of packed beds over a very wide range of Reynolds numbers. The correlations summarized in the previous section serve as references against which the experimental data can be compared to indicate whether the purposes of the pressure drop tests were realized. To further aid in this evaluation emphasis is now placed on the secondary pressure losses through packed beds, and the phenomena influencing it. This will be done by investigating the literature concerning detailed macroscopic flow models. To understand the complex flow phenomena in packed beds better some theoretical aspects regarding the influence of the walls on the bed geometry and flow characteristics are presented. This section aims to identify possible methods of quantifying the influence of the walls for further evaluation of the experimental results.

2.4.1 Radial porosity variation

The impact of spatial constraints on the packing arrangement of particles in a packed bed is significant. It has been argued by various authors (Daszkowski and Eigenberger, 1992; Lerou and Froment, 1977; Papageorgiou and Froment, 1995) that the porosity variation should be taken into account when studying the pressure drop, flow and heat transfer characteristics of packed beds. As an introduction to the quantification of the influence of the walls an overview is given regarding the most important approximations of the variation of the porosity in the radial direction (radial porosity variation).

The variation in porosity has been investigated experimentally by Roblee *et al.* (1958), Ridgeway and Turbuck (1968), Benenati and Brosilow (1962) and others for cylindrical packed beds. Their results indicated that the porosity in a cylindrical packed bed oscillates in a damped manner from unity at the walls to that of an infinite packed bed in the centre. For large bed-to-particle diameter ratios the oscillation damps out in about four to five particle diameters (Mueller, 1991). Some methods have been proposed to approximate these oscillations. Martin (1977) used a quadratic approximation for the first half ball diameter from the wall, followed by a damped sinusoidal approximation:

$$\varepsilon(r) = \varepsilon_{min} + (1-\varepsilon_{min}) \cdot z^2, \text{ for } -1 < z < 0$$

$$\varepsilon(r) = \varepsilon_{\infty} + (\varepsilon_{min} - \varepsilon_{\infty}) \cdot e^{-0,25 \cdot z} \cdot \cos\left(\frac{\pi}{0.876 \cdot z}\right), \text{ for } z > 0, \quad (10)$$

$$\text{with } z = 2 \cdot \frac{|\Delta r|}{d_p} - 1.$$

The approximation by Martin (1977) agrees the best agreement with experimental data. The variable $|\Delta r|$ is defined as the distance from the nearest wall.

The approximation of the variation in porosity can be simplified by assuming an exponentially averaged, or smoothed, porosity variation. The equation found to be the most adequate and which represents the porosity the best in the near wall region is that of Hunt and Tien (1990):

$$\varepsilon(r) = \varepsilon_{\infty} \cdot \left[1 + C_1 \cdot e^{-C_2 \cdot \frac{|\Delta r|}{d_p}}\right] \quad (11)$$

with C_1 obtained from equation (11) by letting the porosity equal unity at the walls:

$$C_1 = \frac{1}{\varepsilon_{\infty}} - 1, \quad (12)$$

and C_2 equal to 6. Other values for C_1 and C_2 have been proposed by Vortmeyer and Schuster (1983) and Cheng and Hsu (1986), but do not represent the true nature of the porosity close to the walls.

An equally important averaged porosity approximation is that of White and Tien (1990):

$$\varepsilon(r) = \left\{1 + \left[\frac{1-\varepsilon_{\infty}}{\varepsilon_{\infty}}\right] \cdot \sqrt{1 - e^{\left(-2\frac{|\Delta r|}{d}\right)}}\right\}^{-1} \quad (13)$$

where $|\Delta r|$ is again defined as the distance from the nearest wall.

Figure 2.2 shows the approximations by Martin (1977), Hunt and Tien (1990) and White and Tien (1987) to compare the oscillating and exponentially smoothed approximations for an annular packed bed.

For the calculation of the pressure drop in a discretized model such as Flownex (2006) the average porosity of each control volume must be known. The approximation by White and Tien (1990) was initially used by the M-Tech Industrial Pty (Ltd) design team for the purpose of choosing porosities in the homogeneous porosity test sections. Research by Du Toit (2004)

suggested however that the correlation by Hunt & Tien (1990) is more appropriate and should rather be used.

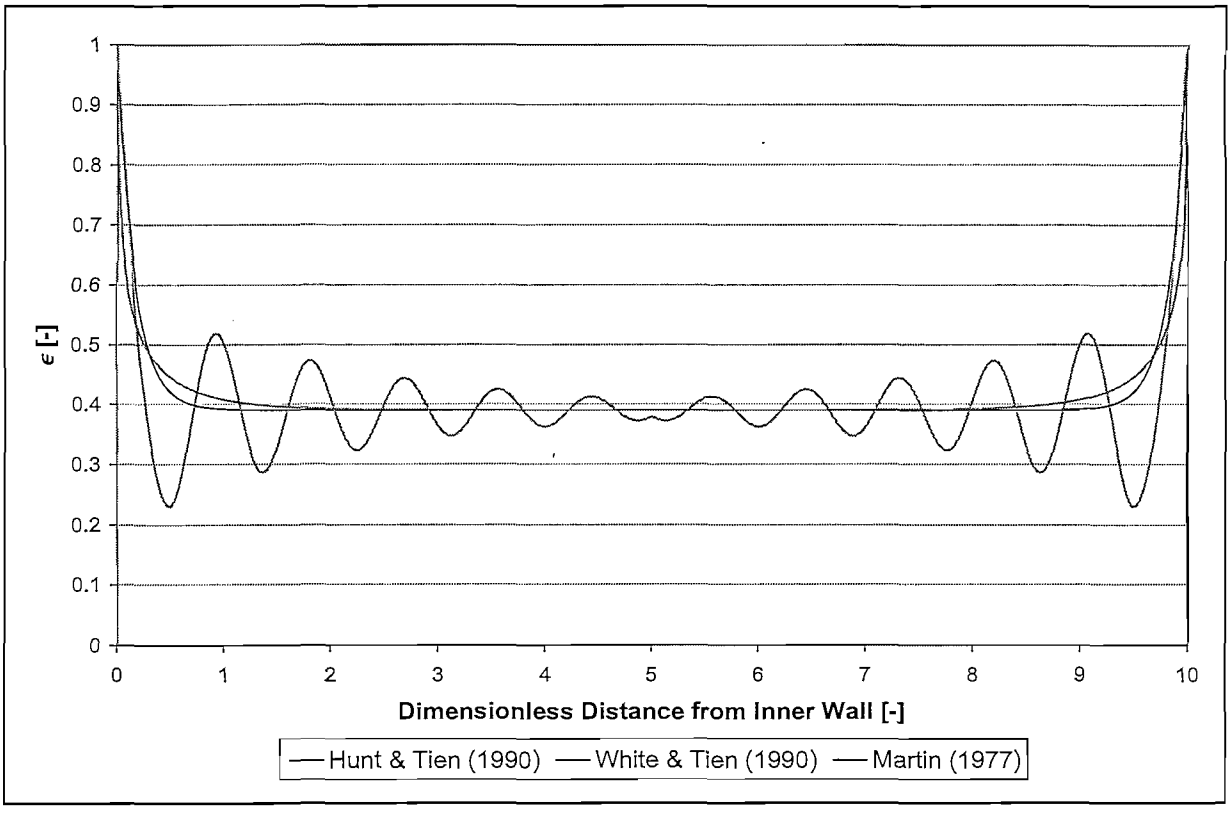

Figure 2.2 *Comparisons between oscillating and exponentially smoothed porosity variation approximations for an annular packed bed.*

2.4.2 The average porosity

In a stationary infinite packed bed the average porosity is approximately 0.36 (Bedenig, 1966). Tests on the THTR have shown that the porosity in a reactor with a MEDUL-type fuel cycle (where fuel balls are regularly added to the top and taken from the bottom) is slightly larger since the balls move very slowly and therefore rearrange continuously. The bed-to-particle diameter ratio of the THTR was 85, which is very large. The average porosity therefore approaches that of an infinite packed bed. The average porosity of the THTR was found to be 0.388 (Bedenig, 1966:9), and the porosity of an infinite packed bed with a MEDUL-type fuel cycle can therefore be taken as 0.388. For design purposes in the PBMR this value for the porosity of an infinite packed bed has been assumed to be valid.

The average porosity can be approximated by integrating the radial porosity variation over the cross-sectional area:

$$\overline{\varepsilon} = \frac{1}{A} \cdot \int_{r_i}^{r_e} \varepsilon(r) \cdot 2 \cdot \pi \cdot r \cdot dr \tag{14}$$

where r_i is the radius of the inner wall, if present, and r_e the radius of the outer wall and A the cross-sectional area of the bed. Care should however be taken using this method since a variation in the porosity in the axial direction exists similar to the radial porosity variation. In the experimental investigation of pressure drop it is ideal to determine the average porosity of the packed bed experimentally in order to compare correlations properly with experimental results.

The sensitivity of the pressure drop on the porosity can easily be pointed out by calculating the error in the prediction of the pressure drop for an error in the true porosity. This is calculated as follows:

$$\frac{d(\Delta p)}{\Delta p} = \frac{\sqrt{\left(\frac{\partial(\Delta p)}{\partial \overline{\varepsilon}}\right)^2 \cdot (d\overline{\varepsilon})^2}}{\Delta p} = \frac{\left(\frac{\partial(\Delta p)}{\partial \overline{\varepsilon}}\right) \cdot (d\overline{\varepsilon})}{\Delta p}. \tag{15}$$

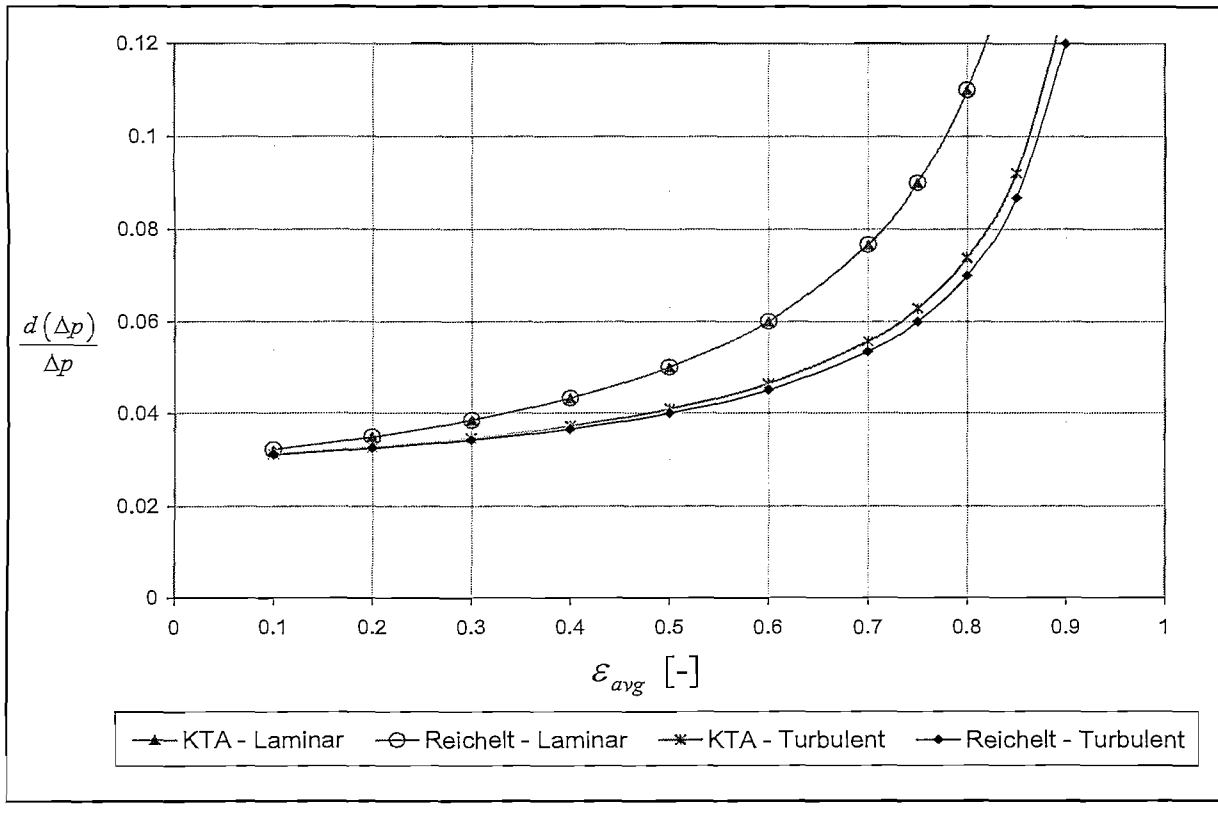

Figure 2.3 *The sensitivity of the pressure drop in laminar and turbulent flow*

Equation (15) can be evaluated numerically or analytically and gives the error in the prediction of the pressure drop at the correct average porosity for a given error in the average porosity. Figure 2.3 illustrates the error in the predicted pressure drop per 1% error in the average porosity if the correlations proposed by Brauer (1960) and Reichelt (1972) are assumed to be representative of the friction factor. The same argument can be followed to show the importance of the accurate estimation of the porosity if the friction factor is to be determined from pressure drop measurements. This will be discussed in the data processing methodology chapter.

2.4.3 Hydraulic diameter modifications

As mentioned, the correlations discussed in the literature survey are zero-dimensional and empirical and cannot describe the complex flow phenomena inside packed beds. The correlation originally proposed by Reichelt (1972) can however predict to a certain extent the influence of the walls on the pressure drop for various bed-to-particle diameter ratios.
The hydraulic radius is defined as the ratio of the cross-sectional area presented to the flow to the perimeter wetted by the flow. In the case of packed beds the cross-sectional area and wetted perimeter are defined on a volumetric basis in terms of the porosity. This implies that the hydraulic radius in any axial position is equal. If the wetted area of a cylinder is added, as proposed by Metha and Hawley (1969), the following relation for the hydraulic radius is obtained:

$$R_h = \frac{\dfrac{\text{Volume of Voids}}{\text{Volume of bed}}}{\dfrac{\text{Wetted surface of spheres}}{\text{Volume of bed}} + \dfrac{\text{wetted surface of wall}}{\text{Volume of bed}}} \tag{16}$$

or when written in terms of the average porosity $\bar{\varepsilon}$, particle diameter d_p and bed diameter D:

$$R_h = \frac{\bar{\varepsilon} \cdot d_p}{6 \cdot (1-\bar{\varepsilon}) \cdot M}, \tag{17}$$

with

$$M = 1 + \frac{4 \cdot d_p}{6 \cdot D \cdot (1-\bar{\varepsilon})} \tag{18}$$

The variable M acts as a modification parameter to the original hydraulic radius proposed by Blake (1922). If the bed-to-particle diameter ratio goes to infinity, the value of M approaches

unity and the original hydraulic radius is obtained. It was proposed by Metha and Hawley (1969) that this modification should be made to the original Ergun equation, yielding

$$\Psi = \frac{\Delta p}{\rho U_o^{\,2}} \cdot \frac{d_p}{L} \cdot \frac{(\bar{\varepsilon})^3}{(1-\bar{\varepsilon})} = \frac{150 \cdot M^2}{\frac{\mathrm{Re}_{dp}}{(1-\bar{\varepsilon})}} + 1.75 \cdot M \tag{19}$$

This equation showed some success in the laminar flow regime ($Re_{dp} < 10$). When applied at higher Reynolds numbers however, it fails to predict experimental data accurately.

This can be mainly attributed to the fact that the original values for A and B as proposed by Ergun (1952) were used, where the value of B should vary according to the bed-to-particle diameter ratio (Reichelt, 1972). Reichelt (1972) correlated the value of B to the bed-to-particle diameter ratio, using data from various authors for different bed-to-particle diameter ratios. By doing so equation (19) was modified as follows:

$$\Psi = \frac{\Delta p}{\rho U_o^{\,2}} \cdot \frac{d_p}{L} \cdot \frac{(\bar{\varepsilon})^3}{(1-\bar{\varepsilon})} = \frac{A}{\frac{\mathrm{Re}_{dp}}{(1-\bar{\varepsilon})}} \cdot M^2 + \frac{1.75}{B_w} \cdot M \tag{20}$$

with

$$B_w = \left[k_1 \cdot \left(\frac{d_p}{D} \right)^2 + k_2 \right]^2 . \tag{21}$$

The values of k_1 and k_2 was originally proposed by Reichelt (1972) to be 1.5 and 0.88 respectively, while keeping the value of A equal to 150 in the case of spheres. Eisfeld and Schnitzlein (2001) followed the same approach of correlating the value of B to the bed-to-particle diameter ratio, using a much larger data set. Their study resulted in values of k_1 and k_2 were equal to 1.15 and 0.87 respectively, and a value for A equal to 154 for spheres.

These values improved the relative root mean square deviation for spherical particles from 0.1684 when Reichelt's correlation is tested with the original values, to 0.1613 with the values calculated by Eisfeld and Schnitzlein (2001:4325).

What makes this method especially valuable is that the pressure drop through a packed bed without walls can also be predicted. This is simply done by letting the bed-to-particle diameter ratio in equations (18) and (21) approach infinity. By doing so the value of M in equation (18) becomes 1 and the value of B_w in equation (21) becomes 0.7569. This allows for the comparison between the pressure drop for an infinite packed bed and a packed bed with the influence of the walls included. Figure 2.4 shows the ratio between the pressure drop for beds with walls and infinite packed beds. The average porosity for each bed-to-particle

diameter ratio was calculated by integrating equation (11) over the cross-sectional area of the bed and assuming the bulk porosity ε_∞ to be 0.39. The average porosity is included as reference for each bed-to-particle diameter ratio.

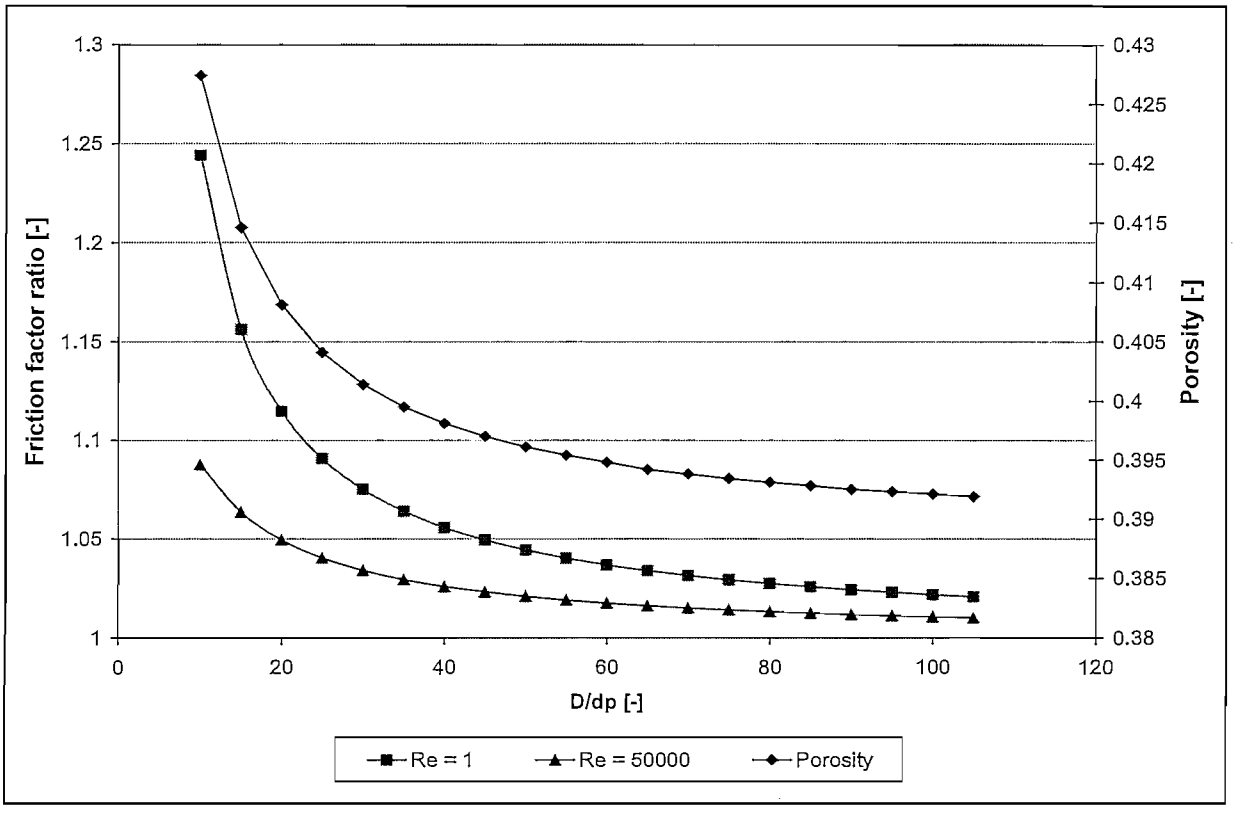

Figure 2.4 *The ratio between the pressure drop predicted for beds with walls and infinite packed beds for the extreme cases of laminar flow (Re_{dp} = 1) and turbulent flow (Re_{dp} = 50000).*

From this prediction it follows that the wall influence is more significant for laminar flow and for low bed-to-particle diameter ratios. Furthermore, it is predicted that the pressure drop is larger due to the wall friction, and does not decrease because of the larger average porosity and channelling effect close to the walls. Figure 2.5 shows the predicted pressure drop ratios for different Reynolds numbers and bed-to-particle diameter ratios. This method of evaluating the influence of the walls is based on experiments for various bed-to-particle diameter ratios. Even though the method may seem crude and very simple, it shows that the influence of the walls is indeed important. The correlation is restricted to cylindrical packed beds, since only experimental data from cylindrical packed beds were used. A more detailed analysis of the flow phenomena is therefore required for the investigation of the wall influence in annular packed beds.

2.4.4 Pseudo-homogeneous models

As pointed out earlier, the advantage of correlating the pressure drop to a friction factor that is dependant on the porosity is that the flow can be modelled macroscopically in more detail by assuming a variation in the radial porosity.

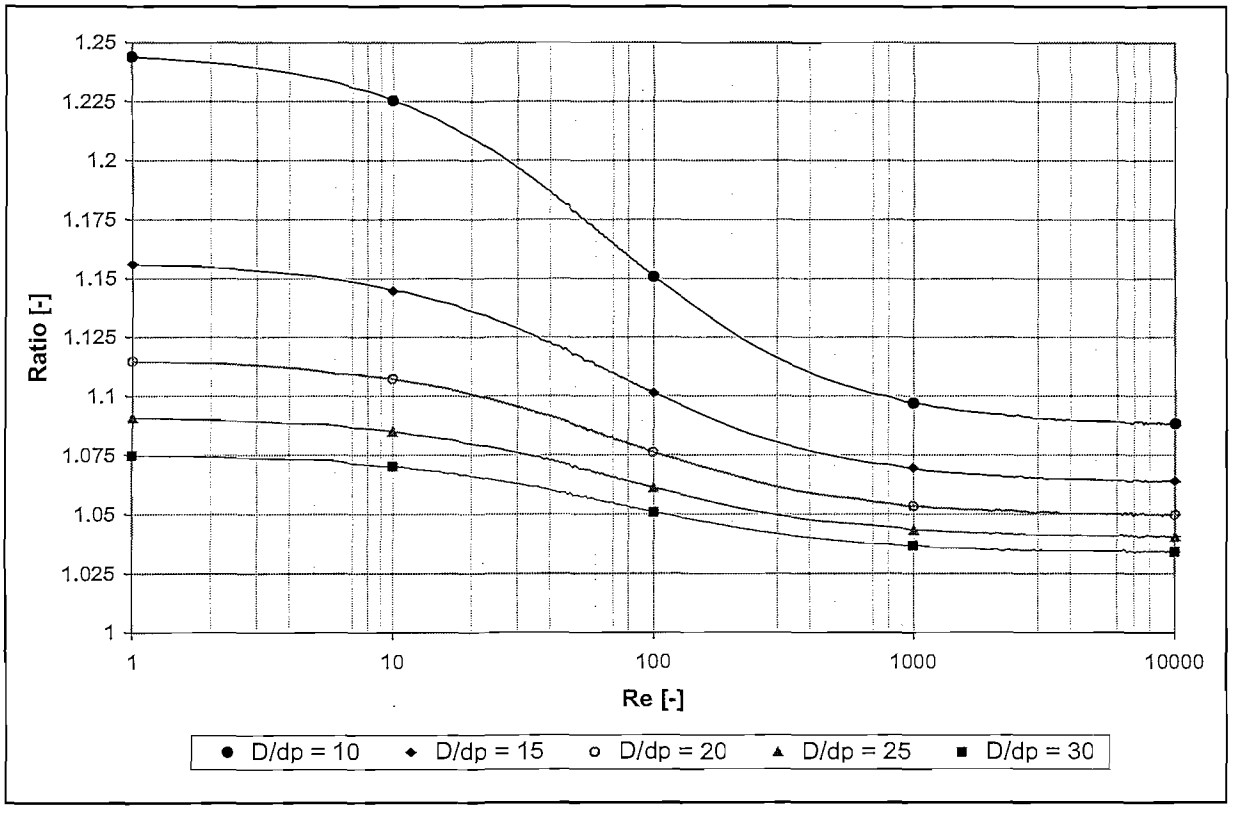

Figure 2.5 *Ratio between the pressure drop predicted for finite and infinite packed beds in laminar, transitional and turbulent flow.*

If a packed bed is considered as a pseudo-homogeneous continuum (i.e. the porosity is assumed to vary continuously in the radial and axial directions) the pressure drop caused by particle-fluid interaction can be added to the Navier-Stokes equations and be used to solve the subsequent continuous variation of the fluid velocity in the bed. If fully developed steady-state flow is assumed, this addition of the particle-fluid pressure loss in the Navier-Stokes equations reduces to the so-called extended Brinkman equation as suggested by Chandrasekhara and Vortmeyer (Vortmeyer and Schuster, 1983):

$$\frac{dp}{dz} = -A \cdot \frac{\left(1-\varepsilon(r)\right)^2}{\varepsilon(r)^3} \cdot \frac{\mu}{d_p^{\,2}} \cdot U_{z0}(r) - B \cdot \frac{\left(1-\varepsilon(r)\right)}{\varepsilon(r)^3} \cdot \frac{1}{\left(\mathrm{Re}_{d_p}/\left(1-\varepsilon(r)\right)\right)^n} \cdot \frac{\rho}{d_p} \cdot \left|U_{z0}(r)\right| \cdot U_{z0}(r) + \frac{\mu}{r}\frac{d}{dr}\left[r \cdot \frac{dU_{z0}(r)}{dr}\right] \tag{22}$$

where $\varepsilon(r)$ is given by a suitable approximation for the porosity at any radial position , r, and U_{z0} the axial superficial velocity. Note that the particle Reynolds number is also calculated from the superficial velocity at the radial position.

The extended Brinkman equation correlates the pressure gradient through the bed to the particle pressure loss and wall friction contribution at each radial position and corresponding porosity. The first two terms on the right hand side is recognized as the particle friction pressure loss terms, and the third as the wall friction pressure loss term.

Any correlation can be used to describe the fluid-particle pressure loss, bearing in mind that the correlation must be valid over the whole range of porosities. It is evident that in order to solve the velocity profile the pressure gradient must be known. This can either be provided from experimental results or can be predicted with the correlations previously discussed for a given mass flow rate. Figure 2.6 shows velocity profiles obtained for different Reynolds numbers. The total pressure gradient was predicted with Reichelt's equation to include the influence of the walls. To predict the particle friction pressure loss at each radial point Reichelt's equation was again used but with the values of M and B_w equal to 1 and 0.7569 respectively to exclude the walls, as previously mentioned. To approximate the porosity variation equation (11) was used. Figure 2.6 shows that the dimensionless velocity becomes higher in the near wall region as the Reynolds number increases, and that the peak shifts closer to the walls. Experimental investigation of the axial velocity profile in packed beds includes various methods of measuring the velocities. In most cases reported in the literature investigators relied on measuring the axial velocity at some distance beyond the flow exit of the bed. Morales *et al.* (1951), Schwartz and Smith (1953) and Schertz and Bischoff (1969) for example measured the axial velocity profile with hotwire anemometers beyond the bed. This simple method allows for the flow to slightly redistribute beyond the packed bed, and is therefore not entirely representative of the velocity inside the bed. Price (1968) and Bey and Eigenberger (1998) were more successful by trying to preserve the velocity profile up to a measuring plane by placing a honeycomb structure beyond the packed bed.

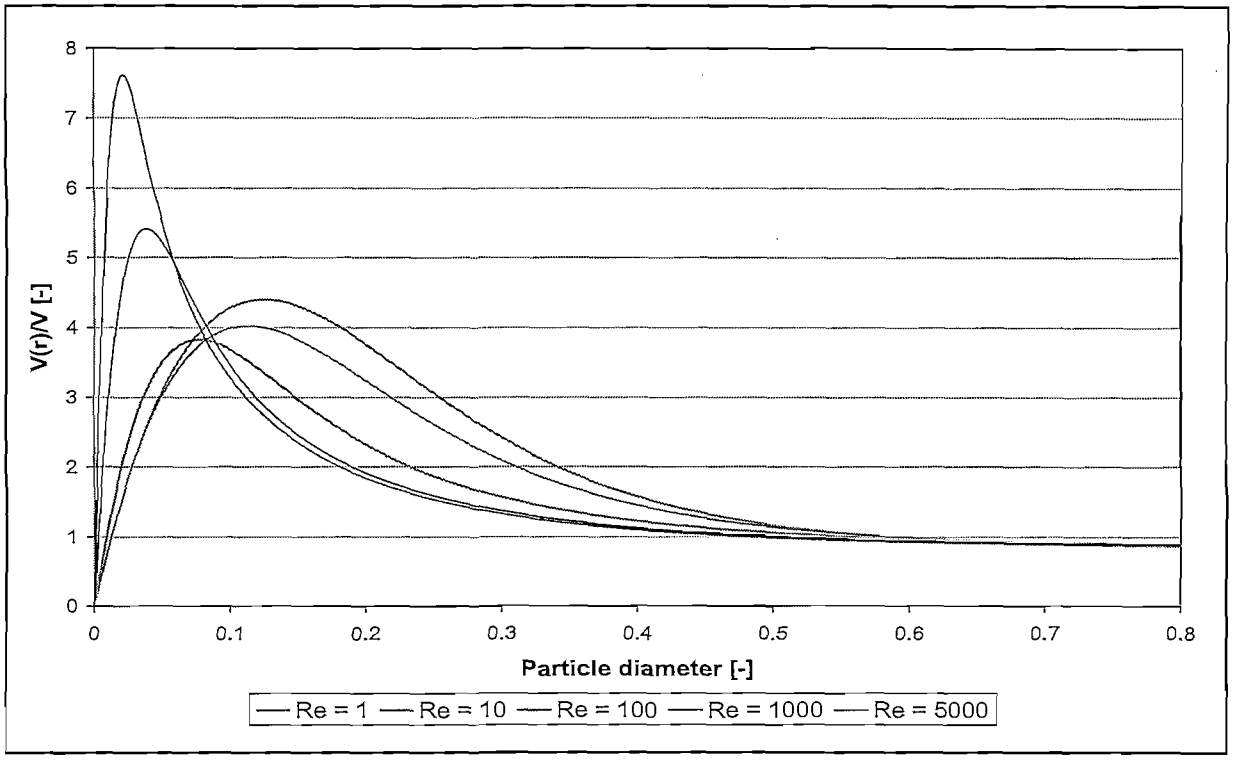

Figure 2.6 *Predicted velocity profiles*

Measurements of the interstitial axial velocities were successfully obtained by Giese *et al.* (1998) using Laser Doppler Anemometry for Reynolds numbers in the range $4 < Re_{dp} < 532$ for spheres.

In general the experimental results from measurements both inside and outside the bed indicate that there is a definite increase in the axial velocity in the near wall region. The results from measurements outside the bed show a tendency for the peak values of the dimensionless velocity in the near wall region to be independent of the Reynolds number (Schwartz and Smith, 1953; Bey and Eigenberger, 1996). The results from the measurements of Price (1968:10) at high Reynolds numbers ($879 < Re_{dp} < 2601$) confirms this for the turbulent flow regime, and therefore show that the dimensionless velocity does not increase at high Reynolds numbers as predicted in Figure 2.6. A quantitative comparison reveals that the predicted average dimensionless velocity within a quarter of a ball diameter from the wall is almost twice as large as the measured values by Price (1968) for a Reynolds number of 2600. Such a comparison with results from physical experiments clearly shows that the prediction of the velocity profile by equation (22) is not entirely correct. Equation (22) predicts that the influence of the porosity in the near wall region will dominate, while the experimental results show a very large influence of the walls, as predicted by the correlation of Reichelt (1972).

Since there is a definitive increase of the flow velocity in the near wall region the velocity gradient will also increase, resulting in an increase in the shear stress at the walls. The correlation of Reichelt (1972) therefore predicts that this increase in shear stress results in a higher total pressure drop. It is however clear from applying equation (22) that the velocity gradient close to walls needs to increase far too high to obtain this noticed increase in the pressure drop. It can there for be concluded from the results of the velocity measurements of Giese *et al.* (1998) and others that the mechanism resulting in the increase in pressure drop due to shear stress at the walls and the increase porosity cannot be predicted using a dynamic viscosity alone in equation (22).

2.4.5 The effective viscosity

The deviations between the axial velocity predictions from pseudo-homogenous models and experimental results have led various researchers to investigate the possibility of the use of an effective viscosity instead of the dynamic molecular viscosity. As of yet no conclusive mathematical model exist to predict such an effective viscosity. The experimental investigations of Bey and Eigenberger (1996) and Giese *et al.* (1997) have shown that the use of an effective viscosity is indeed a plausible model to describe the radial variation of the axial velocity correctly in a pseudo-homogenous model. Of the two investigations the experiment by Giese *et al.* (1997) is of greater value since the actual interstitial velocities were directly measured. From the physical measurements of the axial velocity an effective viscosity was empirically correlated to the Reynolds number so that equation (20) represented the correct velocity distribution for different Reynolds numbers. The correlation determined by Giese *et al.* (1997) is given as:

$$\frac{\mu_{eff}}{\mu_{dyn}} = 2 \cdot e^{0.0035 \cdot \mathrm{Re}_{dp}} \tag{23}$$

with μ_{eff} the effective viscosity, and μ_{dyn} the dynamic viscosity. Equation (23) is restricted to low Reynolds numbers (< 532) for a single bed-to-particle diameter ratio. Bey and Eigenberger (1996) showed that the effective viscosity is also a function of the bed-to-particle diameter ratio. Application of both empirical correlations at high Reynolds numbers (>1000) predicts a velocity profile similar to that of laminar flow in pipes, therefore predicting a very thick boundary layer. This is inconsistent with experimental results.

Even though the use of the empirical correlation for the effective viscosity given by Giese *et al.* (1997) is very restricted, a novel idea by Winterberg and Tsotsas (2000) was to use this effective viscosity to investigate the influence of the walls on the pressure drop. Equation (22) was solved for different mass flow rates (particle Reynolds numbers) while using equation (23) for the effective viscosity and a suitable approximation for the radial variation of the porosity such as equations (11) or (13). For the friction factors the Ergun constants were used. The pressure drop calculated by solving equation (22) can then be compared with the pressure drop calculated using the Ergun equation for a constant average porosity. The constant average porosity used is calculated using equation(14). The ratio of the two calculated pressure drops gives the ratio of the pressure drop including the combined effect of the walls and the pressure drop excluding the walls.

This method can be modified to investigate the influence of the walls more appropriately for packed beds of spherical particles. The constants calculated for an infinite packed bed from equations (18) and (21) are for instance more appropriate for spherical particles since it does not include any influence of the walls. The same constants along with the average porosity can be used to calculate the total pressure drop without the wall friction. It is assumed in this analysis that the effective viscosity proposed by Giese *et al.* (1997) can be applied to various bed-to-particle diameter ratios.

Results from this method are shown in Figure 2.7 and is compared with the predictions from Reichelt's correlation. The correlation of Reichelt (1972) clearly predicts a larger dependency of the pressure drop on the walls.

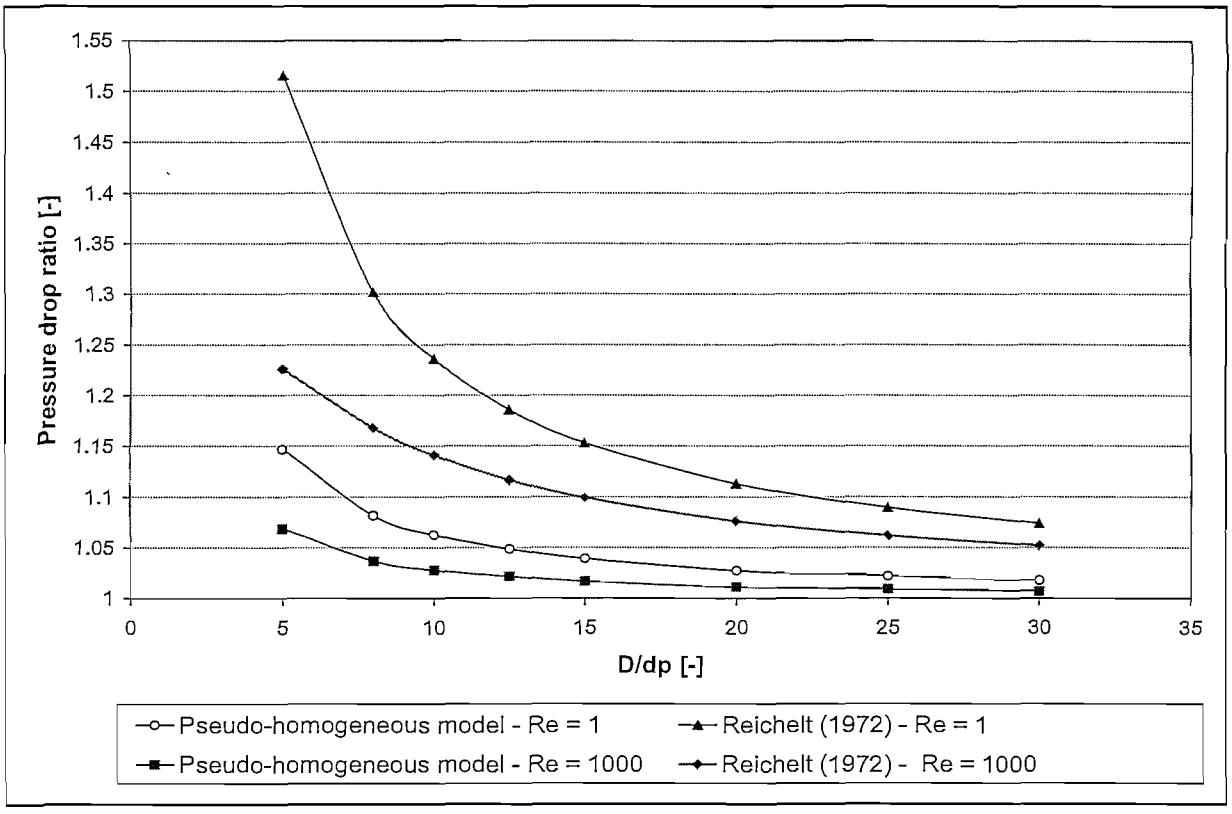

Figure 2.7 *Comparison between different predictions of the wall influence*

The importance of the sensitivity of the predicted pressure drop on the average porosity should be kept in mind, as well as the restrictions of the effective viscosity correlation. The qualitative dependency of the pressure drop on the walls is however reflected in both the models, i.e. the more detailed one-dimensional model and the simple prediction based on empirical data.

2.4.6 Methods of estimating the effective viscosity

Reichelt's method is very simple but seems to qualitatively predict the influence of the walls correctly. Van der Walt and Du Toit (2006) showed that the characteristics of Reichelt's equation can be used to predict the effective viscosity. By assuming Reichelt's correlation to be correct, the total pressure drop in equation (22) can be predicted with the bed-to-particle diameter ratio and average porosity of the actual bed in equations (18) and (21). To exclude the walls in the friction factor in equation (22) Reichelt's constants for an infinite packed bed

can be used. Equation (22) is then solved with the viscosity adjusted so the pressure gradient or mass flow rate is matched.

Effective viscosities calculated using this method agrees qualitatively well with the empirical correlations proposed by Giese *et al.* (1997) and Bey and Eigenberger (1996), as shown in Figure 2.8.

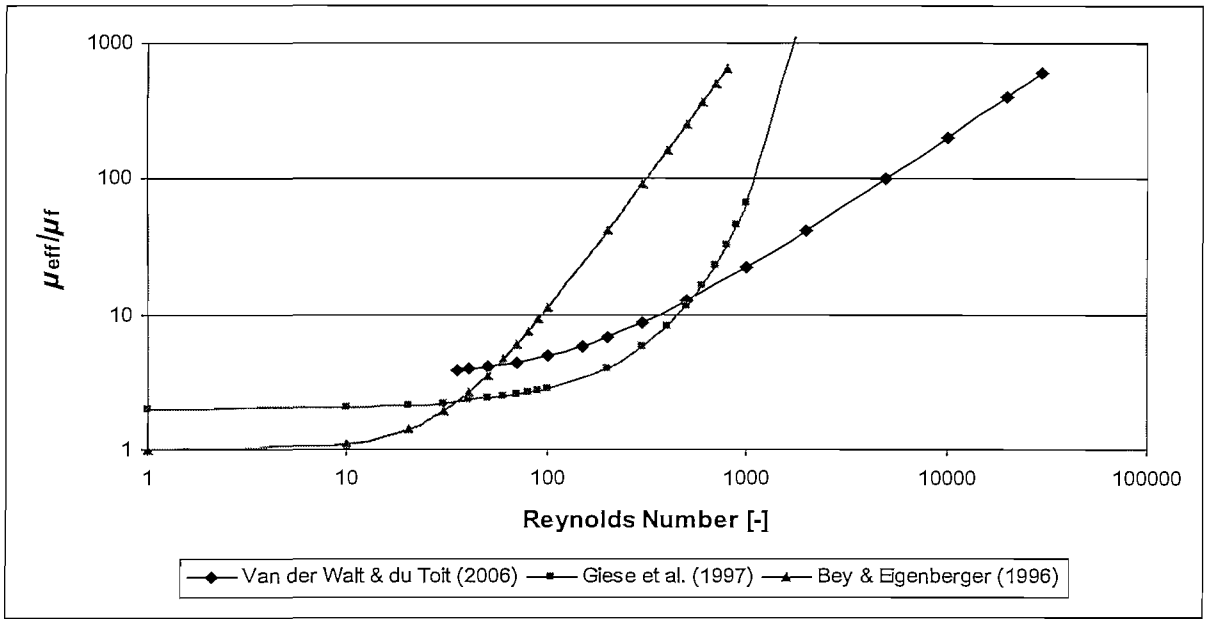

Figure 2.8 *Comparison between empirically calculated and predicted effective viscosities*

The method seems to hold at higher Reynolds numbers and qualitatively predicts the independence of the dimensionless velocity on the Reynolds number in the turbulent flow regime. Figure 2.9 shows velocity profiles calculated from equation (22) with the effective viscosities predicted by the method of Van der Walt and Du Toit (2006).

2.4.7 Physical interpretation of the influence of the walls

The comparison between Reichelt's correlation (1972) as modified by Eisfeld and Schnitzlein (2001) and the application of an effective viscosity in the one-dimensional pseudo-homogeneous model has shown a definite dependency of the pressure drop on the walls. The main purpose of the theoretical background was to establish to what extent walls influence the pressure drop, and not necessarily to give a complete mathematical model or explanation for the complex fluid phenomena. A short physical explanation is however important.

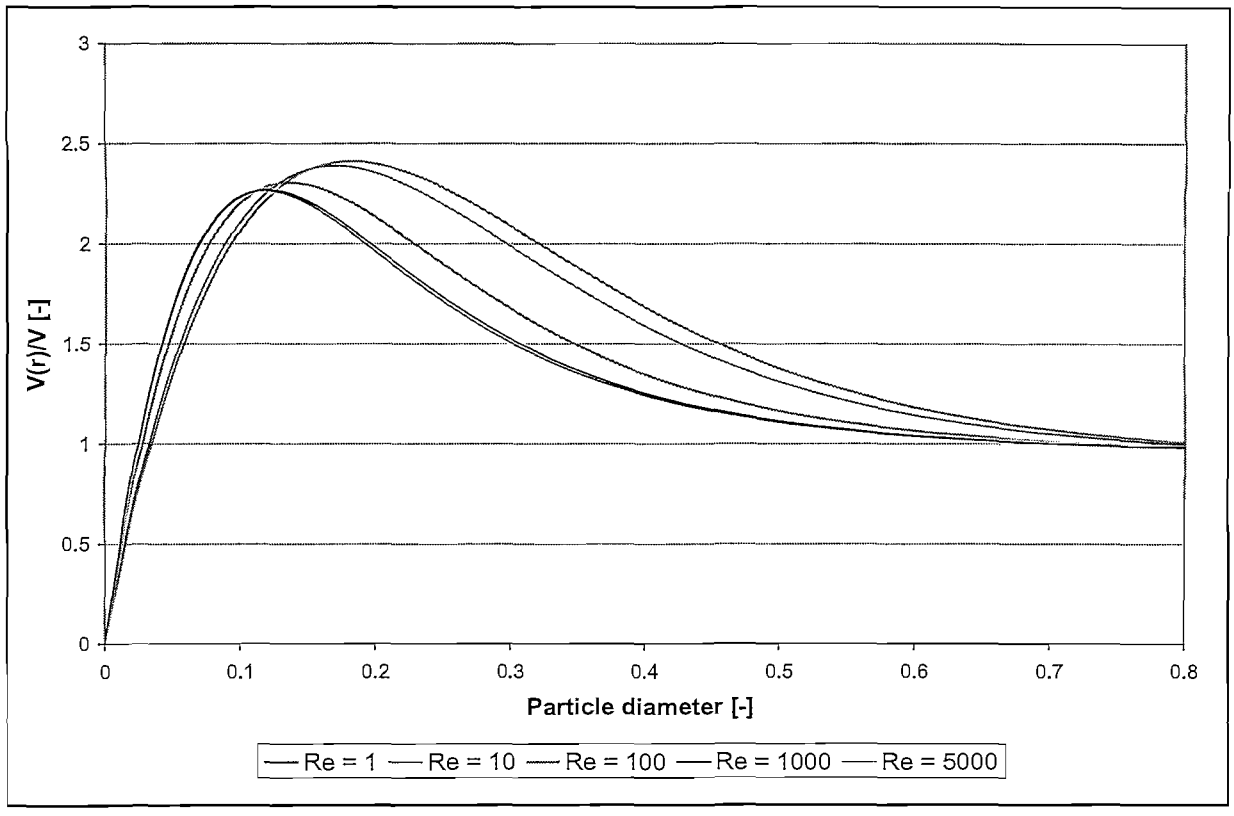

Figure 2.9 *Velocity profiles calculated with the effective viscosities calculated with the method of Van der Walt and Du Toit (2006)*

Since the average porosity is increased by the presence of the walls, a decrease in the pressure drop could initially be expected. The very large velocity gradients in the near wall region will however result in larger shear stresses at the walls. From the use of the dynamic viscosity in equation (22) this is clearly not the only reason for the dominant influence of the wall friction. A high degree of mixing can be expected for flow through the pebbles at the centre of the bed. Since the flow velocity increases in the near wall region the mixing should also be enhanced. According to a boundary layer theory for packed beds developed by Eisfeld (Eisfeld & Schnitzlein, 2001), the boundary layer in the laminar flow regime is very thick and penetrates deep into the packing, while a much thinner boundary layer exists in the turbulent flow regime. Because of the larger velocity near the wall and the enhanced mixing, radial flow in and out of the boundary layer and enhanced contact of fluid particles with the walls can be expected. The drag resulting from the boundary layer at the walls could further apply to a larger area than the actual wall surface since a part the surface area of particles touching the walls are within the boundary layer.

2.5 Conclusion

The survey has presented the most important correlations found in the literature that could possible be used as references against which the experimental data can be compared. Most of the correlations discussed are well-established and tested and are therefore suitable to compare with experimental results.

The literature survey has further succeeded in identifying a tool to investigate the influence of the walls. The combination of the correlations identified and the pseudo-homogeneous one-dimensional representation of the pressure drop can be used to evaluate the experimental data.

Following the literature survey the experimental facility will be discussed to give an overview of the concepts and instruments involved in obtaining the raw data.

3 EXPERIMENTAL SETUP

3.1 Introduction

Throughout the previous chapters reference was made to the experimental facility developed by M-Tech Industrial Pty (Ltd) for the investigation of various flow and heat transfer phenomena encountered in the PBMR core. In the introduction this facility, known as the Heat Transfer Test Facility (HTTF), was introduced as a very important contributor to the PBMR safety case. A distinction was made between the High Pressure Test Unit (HPTU) and the High Temperature Test Unit (HTTU), followed by a short overview of the types of tests to be performed on the HPTU.

This study aims to contribute to the experimental investigation of the pressure drop through packed beds by establishing the data processing methodology and tools to analyze the data obtained. For the sake of completeness a general description of the HPTU plant is firstly given as background while the individual pressure drop test sections are further discussed in more detail.

Since the quality of the experimental data is of utmost importance, the instrumentation involved in the pressure drop measurements and the calibration thereof are also discussed. The data processing methodology will then follow this overview of the test facility.

Before commencing with this chapter it is important to emphasize that the experimental facility was developed be M-Tech Industrial Pty (Ltd), and that the author did not take part in any stage of the design. The author was however directly involved in the calibration and installation of the instrumentation on the HPTU plant, as well as the test phase.

3.2 General description of the plant

Before the test sections involved in the pressure drop tests are discussed, a general description of the HPTU plant is given as background. See Appendix A for schematic layout of plant. The purpose of the HPTU test facility is firstly rearticulated to provide the context. The plant layout and purpose of the main components are then shortly discussed, as well as the design philosophy to obtain the very wide range of Reynolds numbers.

3.2.1 Purpose of the HPTU plant and the tests conducted

As mentioned in the introduction the HPTU plant has a twofold purpose. Various thermal-fluid phenomena are firstly investigated separately. These tests are known as the separate effects tests (SETs), and are accomplished with various homogeneous porosity test sections. The purpose of the separate effects tests is to validate correlations used by PBMR for the whole range of porosities and Reynolds numbers. The correlations tested are specifically for the use in thermal-fluid codes such as Flownex (2006), and the porosities of the test sections are therefore the representative porosities of the typical control volumes encountered in the PBMR core.

Secondly, some tests are performed to investigate the integrated effect of the variation in porosity and the wall friction on specific thermal-fluid phenomena. These tests are known as the integrated effects tests (IETs). The purpose of the integrated effects tests is to generate data that can be used to validate integrated simulations of the PBMR core. The tests conducted on the HTTF and the purpose of the tests and are discussed in detail in the Heat Transfer Test Facility Test Specification report by Rousseau (2005a).

The flow phenomena investigated in the HPTU plant are the following:

- Investigation of the pressure drop through packed beds, i.e. investigating the Euler number for packed beds.
- Investigation of the heat transfer coefficient between the pebbles and the fluid, i.e. investigating the Nusselt number for pebble-to-fluid heat transfer in packed beds.
- Investigation of the heat transfer coefficient between the reactor reflector and the fluid, i.e. investigating the Nusselt number for wall-to-fluid heat transfer in packed beds;
- Investigation of the turbulent mixing phenomena, or the so-called braiding effect encountered in packed beds, i.e. investigating the effective fluid conductivity in packed beds due to turbulent mixing.

Of the phenomena mentioned above the pressure drop and turbulent mixing will be investigated for both homogeneous porosities and randomly packed beds. For both the pressure drop and braiding effects tests three homogenous porosity test sections will be used. Both phenomena will also be investigated for a cylindrical randomly packed bed and an annular randomly packed bed. The cylindrical and annular packed bed test sections contribute to the integrated effects tests. The annular packed beds are downscaled models of the actual

proposed PBMR core. Tests on a cylindrical packed bed are also investigated in each case to establish a basis for comparison with correlations from the literature. The test sections involved in the pressure drop tests are discussed in more detail further in this chapter.

For the calculation of the pebble to fluid heat transfer coefficient a single pebble needs to be heated. The only cost-effective and practical way to do this is through an electrical heater inside a pebble. The surface temperature of the heated pebble is measured at various positions to determine the temperature difference between the pebble surface and the gas stream for a measured electrical power. To heat the ball and measure the surface temperatures a number of thermocouple wires and electrical cables must reach the pebble through the packed bed. The calculation of the pebble to fluid heat transfer coefficient is therefore not easy in randomly packed beds without disturbing the packing structure close to the heated pebble. For this reason only homogeneous porosity test sections are used in the investigation of the pebble-to-fluid heat transfer coefficient. As in the case of the pressure drop and braiding effects tests, three homogeneous porosity test sections will be used for the pebble-to-fluid convection heat transfer coefficient tests. Wall-to-fluid heat transfer only takes place at very high porosities close to the wall. Only one test section involves the calculation of the wall-to-fluid heat transfer coefficient at a porosity representative of the packing structure close to the walls. The tests to be conducted on the HPTU plant are summarized in Table 3.1.

3.2.2 Pressure variation Reynolds number control

The HPTU plant must be able to deliver the whole range of important particle Reynolds numbers expected in the PBMR core, i.e. from 1000 up to 50000. To obtain the range of Reynolds numbers either the flow velocity or the density must be varied accordingly. A single off-the-shelf blower is however not available to deliver the range of mass flow rates required in the HPTU plant flow. Higher flow velocities also imply higher secondary losses (Labuschagne, 2005a). By varying the system pressure at a constant volume flow rate the Reynolds numbers can however be obtained with off-the-shelf blowers. The HPTU plant is therefore subjected to various pressures ranging from 1 to 50 bars, while two positive displacement blowers deliver near constant volume flow rates at each pressure interval for given rotational speeds. The system is supplied with the required pressure from high pressure nitrogen banks in an auxiliary bay. The working fluid for all the tests is high purity nitrogen.

The quality of the gas as well as the properties can be better determined by using nitrogen instead of air, since the nitrogen is supplied with a certain guaranteed purity.

Table 3.1: Summary of the tests to be performed on the HPTU plant

Type	Test Name and acronym	Phenomena	Number of Test Sections	Porosities Tested
Separate Effects Test	Pressure Drop Test Section (PDTS)	Pressure drop	3	0.36, 0.39, 0.45
	Convection Coefficient Test Section (CCTS)	Pebble-to-fluid heat transfer	3	0.36, 0.39, 0.45
	Braiding Effects Test Section (BETS)	Effective fluid conductivity due to turbulent mixing	3	0.36, 0.39, 0.45
	Near Wall Test Section (NWTS)	Wall-to-fluid heat transfer	1	0.45
Integrated Effects Test	Small Annular Packed Bed pressure drop test (SAPB dP)	Pressure drop	1	Random
	Small Cylindrical Packed Bed pressure drop test (SCPB dP)	Pressure drop	1	Random
	Small Annular Packed Bed braiding effects test (SAPB BETS)	Effective fluid conductivity due to turbulent mixing	1	Random
	Small Cylindrical Packed Bed braiding effects test (SCPB BETS)	Effective fluid conductivity due to turbulent mixing	1	Random

3.2.3 Plant layout and component description

A short description of the layout and most important components of the HPTU plant with their respective functions will now follow. The description of the plant is done according to the schematic layout of the plant given in Appendix A from the Test Plan by Labuschagne (2005c). A detail description of each component can be found in the Thermal Fluid Design Report (Labuschagne, 2005a).

Main loop components

The mass flow rate through the system is supplied by two Sutorbilt positive displacement blowers (HPTU BL) driven by a single 35 kW motor. The pressure rise over each of the blowers will not exceed 1 bar. The whole motor-blower assembly is housed within a pressure vessel. From the blower vessel the gas flows through a heat exchanger (HPTU HX) that is connected to a secondary cycle with a cooling tower (HPTU CT). The purpose of the heat exchanger is to remove heat added by the blowers and heaters and to cool the gas to a meaningful temperature after which the system temperature can be effectively controlled by the main inline heater (HPTU GH). The heat exchanger is of the shell-and-tube type with a maximum heat transfer capability of 34 kW (Labuschagne, 2005a).

After the heat exchanger the main inline heater controls the system temperature. The main inline heater has a heating capability of 20 kW, and controls the system temperature a few degrees above the ambient temperature. By controlling the system temperature just above the ambient temperature, steady-state conditions can be obtained relatively quickly.

From the main heater the gas flows through two orifice stations (HPTU FM). Each orifice station can measure the gas flow rate accurately between pipe Reynolds number of 5000 and10^6. Above the maximum Reynolds number of 10^6, which roughly corresponds to 1.444 kg/s, both orifice stations must be open. It follows that the maximum mass flow rate through the system is restricted to approximately 2.888 kg/s. After each orifice station a sensing hand valve is located to direct the flow through the desired orifice station.

At this point in the cycle the flow can split to go either directly to the test section pressure vessel or through the braiding line, if the braiding effect tests are under consideration. The main loop flow simply enters the test section pressure vessel (HPTU TS) at the side of the bottom part of the test section pressure vessel. The test section pressure vessel consists of a

bottom and a top part, with the test section interface plate fixed between the bottom and top parts of the vessel. Each test section has an interface plate around the test section, with the plate and test section fixed and sealed in such a way that the flow can only pass from the bottom of the pressure vessel through the test section to the outlet at the top of the pressure vessel.

There are two inlets to the pressure vessel at the bottom part. One inlet is for the main loop gas flow, which is always open, and the other for the hot gas stream of the braiding loop. In the case of the braiding effects tests the test section is connected directly to the entrance at the bottom of the test section pressure vessel where the hot gas stream can enter directly into the test section. In the case of the SAPB and SCPB braiding effects tests, hot gas enters from the side into the test section via a number of smaller pipes which can be closed for other tests.

A number of pressure relief valves are also situated at various positions in the plant and vent to outside the building in the case of overpressure.

Braiding Loop

A control valve (HPTU CV) is located in the main loop just after the inlet to the braiding loop. The control valve controls the amount of flow through the braiding line by adding flow resistance in the main loop. A sensing hand valve is located in the braiding line to shut the line from the system if the braiding effects tests are not taking place. Mass flow measurement in the braiding line is done with a thermal mass flow meter (HPTU BFM). Downstream from the mass flow meter the braiding inline heater (HPTU BGH) heats the gas that will enter the test section for the braiding effects tests. In the case of the homogeneous porosity test sections the hot gas stream simply enters from the bottom directly into the test section. As mentioned above, for the SAPB and SCPB braiding effects tests the hot gas enters from the side into the test sections via a number of smaller pipes. In each of the lines hand valves are located to direct the flow path.

Auxiliary systems

Two auxiliary systems exist – one to supply and extract nitrogen to and from the system, and the other to cool the system gas temperature so that the inline heater can effectively control the system temperature.

The nitrogen supply system consists of high pressure nitrogen banks, a number of control valves and a vacuum pump to purge the system. Before each test takes place a number of purge cycles are performed. The purge cycle is initiated by using the vacuum pump to lower the system pressure to approximately 35 kPa. The gas in the system is evacuated from the test section pressure vessel to the atmosphere, and high purity nitrogen is injected into the test section pressure vessel from the nitrogen banks until atmospheric pressure is reached. After each test it is also required to purge the system in a similar way to remove all the nitrogen and fill the system with air.

The heat exchanger cooling water system is the second auxiliary system. The secondary cycle consists of a pump (HPTU HX PMP), a cooling tower (HPTU CT) and a three-way control valve (HPTU HX CV). The control valve is used to control the amount of water flowing though the cooling tower, which in turn controls the gas temperature at the outlet of the heat exchanger.

Control System

The control system consists of an operational control system (OCS) and an equipment protection system (EPS). The OCS is used to control the plant throughout the operating conditions, while the EPS ensures safety of the HPTU plant under operating conditions. The OCS consists of two Programmable Automation Controllers (PACs) positioned on the plant floor and two personnel computers in the control room. The PACs are programmed in Labview Realtime and the personal computers (PC's) use Labview 7.1 as user interface.

Data are sent to the SCADA (Supervisory Control and Data Acquisition) on the PC in the control room from the PACs every half second while the operator supplies the PACs with commands and set points through the SCADA. A detail report on the HPTU control systems is presented in the HPTU Detail Control Design Report (Prinsloo, 2006).

3.3 Pressure drop test sections

3.3.1 Homogeneous porosity test sections

All the homogeneous porosity test sections consist of spherical particles held in specific positions in square columns by tensioned steel strings and spacers on the strings between the

spheres. In the case of the PDTS the particles are translucent acrylic spheres with a diameter of 1.125 inch, or 28.575 mm. The position of each string and the length of the spacers are chosen so that a specific average porosity is obtained. The average porosities of the test sections are chosen to present the average porosities of one particle diameter wide control volumes at different radial positions in a PBMR core. Average porosities were obtained from the exponentially smoothed approximation of the variation in the porosity by White and Tien (1987). The annular width of the PBMR core is approximately 14 sphere diameters. If the reactor is considered as axial-symmetric, the control volumes are annular slits with a certain height. For control volumes of one sphere diameter in width it follows that there are 14 control volumes in the radial direction.. From the porosity variation by White and Tien (1987) the average porosity in each control volume is obtained by calculation of the point value at the centre of the control volume from equation (13). The calculated average porosities for each control volume are shown in Table 3.2.

Table 3.2:Average porosities associated with control volumes at different particle diameters from the inner wall

Distance from inner wall (as function of the particle diameter)	Average Porosity
1,14	0.446
2,13	0.396
3,12	0.391
4,5,6,7,8,9,10,11	0.390

Table 3.2 shows that for most of the control volumes the average porosity is approximately 0.39. Rousseau (2005a) argued that for this reason it is very important to verify the pressure drop correlation for a porosity of 0.39. The dependence or sensitivity of the pressure drop on the average porosity was emphasized in the theoretical background. The error in the pressure drop calculated for a control volume next to the wall at the bulk porosity will be significant, since a 14% error is made in the average porosity. The resultant error in the Euler number was calculated by Rousseau (2005a) to be 42%. Following this result it was suggested that the pressure drop must be investigated for an average porosity of approximately 0.45. From Table 2.1 it is also noted that the KTA equation is not valid for porosities as high as 0.45. This further motivates the investigation of the pressure drop at such high porosities. Rousseau

(2005a) also argued that it would be better to investigate at least three porosities to establish useful trends. For this reason a porosity of 0.36 was also selected.

There is thus three different homogeneous porosity test sections for the pressure drop test. They are referred to as PDTS 036 for the 0.36 porosity test section, and likewise for the 0.39 and 0.45 porosities the tests are labelled PDTS 039 and PDTS 045 respectively. These porosities are also used in the CCTS and BETS test sections. In the case of the CCTS tests the test sections are referred to as CCTS 036, CCTS 039 and CCTS 045, and likewise for the BETS BETS 036, BETS 039 and BETS 045. The BETS test sections use the same particle size as the PDTS test sections. The CCTS test section use 60 mm diameter balls, as well as the NWTS test section.

To obtain the specific values of porosities distended structured beds are used. A tetrahedral packing structure was chosen as the base packing structure in test sections with a square cross-section. To ensure that the desired porosities were obtained the beds were constructed to very strict tolerances. There are however drawbacks to the concept of placing the particles on strings. It is for instance not entirely clear how the strings and spacers will influence the pressure drop, and whether or not to take the volume of the spacers into account in the calculation of the average porosities. Even though the length of the strings is in the direction of the flow, some flow across the strings will take place. It is also not entirely clear whether the flow over the balls could possibly cause vibrations of the strings and whether this would influence the pressure drop. The average porosities are shown for both including and excluding the volume of the spacers in Table 3.3. Even though the spacers contribute significantly to the average porosity, their effect on the pressure drop is not proportional to the reduction in the porosity as predicted for spheres. For this reason it will be assumed in the discussion of the results that the porosity without the spacers must be used in the correlations for comparison purposes.

Table 3.3: PDTS test section information

Test Section	D1 [mm]	D2 [mm]	D3 [mm]	ε_{avg} with spacers [-]	ε_{avg} without spacers [-]	Approximate number of particles
PDTS 036	741.1	300	300	0.352	0.369	3445
PDTS 039	756.46	300	300	0.389	0.407	3307
PDTS 045	781.7	300	300	0.448	0.465	3080

From the literature survey it was shown that the influence of the walls can be significant in packed beds with small bed-to-particle diameter ratios. Correlations used for control volumes at the centre of the packed bed must not include the influence of the walls, as this could possibly result in an incorrect pressure drop prediction. In the design of the test sections it is therefore important to exclude the influence of the walls. For this to be the case a uniform porosity distribution must be maintained up to the container walls so that there is no by-pass flow or wall-channelling. Particles were cut and fixed to the walls in such a way that the porosity is uniform at any axial position up to the container walls. Theoretically the influence of the container walls will then be negligible and the measured pressure drop will only be the result of the resistance of the pebbles. The as-built test section dimensions and information are given in Table 3.3 with reference to Figure 3.1 where the parameters are defined. An example of a homogeneous porosity test section is shown in Figure 3.2 from the Detail Design Report (Lindeboom, 2005), showing the interface plate, strings and pressure impulse lines.

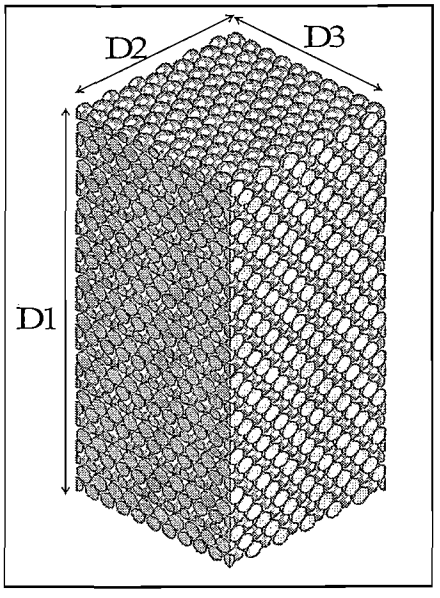

Figure 3.1 *Definition of the parameters for the PDTS test section information*

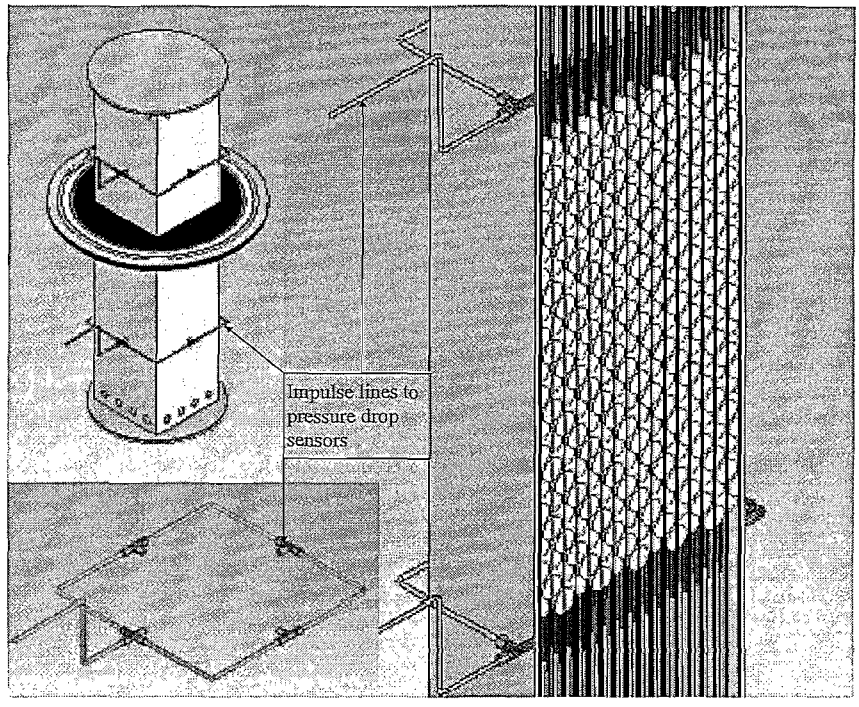

Figure 3.2 *Example of a homogeneous porosity test section*

3.3.2 Small annular and small cylindrical packed beds

The small cylindrical and small annular packed beds are used for the investigation of the integrated effects of the walls and porosity variation on the pressure drop. Spherical particles are randomly dumped into the test section. The dimensions of the annular packed beds were chosen in such a way that the radial dimensions of the bed are an exact scale model of the proposed PBMR core. The inner diameter of the outer reflector of the PBMR core is 3.7 m, and outer diameter of the centre reflector is 2 m. The PBMR fuel pebbles to be used have a diameter of 60 mm whereby the annular width-to-particle diameter ratio is approximately 14. By scaling the real PBMR dimensions down ten fold the dimensions of the small annular packed bed are 370 mm outer diameter and 200 mm inner diameter. 6 mm ball bearings are used as particles. The height of the bed was chosen to be 30 particle diameters, whereby possible entrance and exit effects will be negligible. The height is therefore approximately 180 mm.

The small cylindrical packed bed uses the same outer cylinder as the small annular packed bed. The centre column is removed and 6mm ball bearings are once again used as particles.

The bed-to-particle diameter ratio of the cylindrical packed bed is therefore approximately 62. For such a large bed-to-particle diameter ratio the influence of the wall should be negligible according to both the predictions of both the pseudo-homogeneous model with an effective viscosity and the correlation of Reichelt (1972). Table 3.4 summarizes the as-built test section information for the SAPB and SCPB test sections, with reference to Figure 3.3 for the definition of the parameters.

Table 3.4: Summary of the as-built dimensions of the SAPB and SCPB test sections

Test Section	D_1 [mm]	D_2 [mm]	h [mm]	Approximate number of particles for an average porosity of 0.39	Average porosity calculated from Equation (9)
SAPB	368.9	200	179.4	73900	0.405
SCPB	368.9	[-]	178.2	104400	0.393

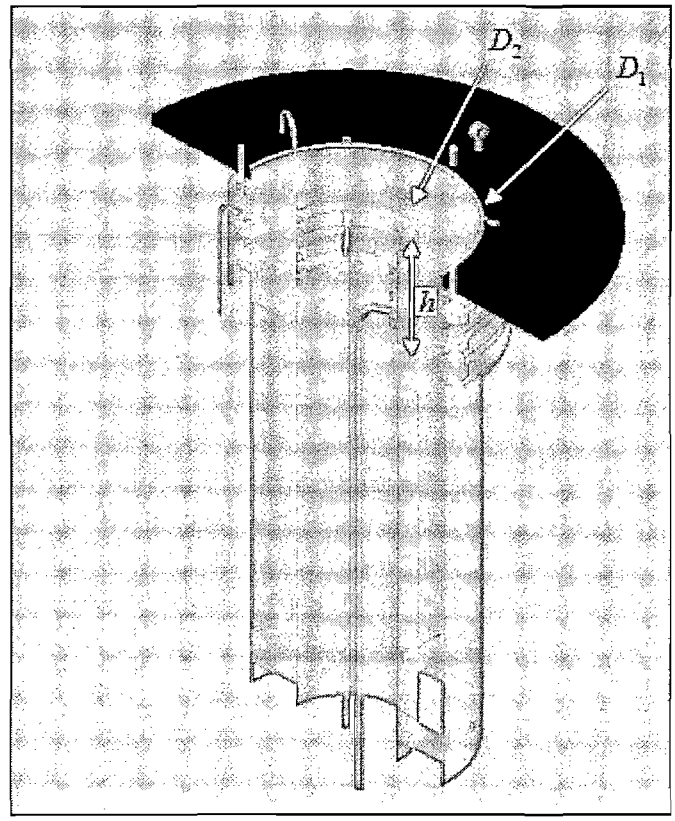

Figure 3.3 *Cut though the SAPB test section*

In the case of the SCPB the centre column is removed. A relatively long upstream section is provided to ensure fully developed flow before the bed. The pipes in the centre column are for the braiding effects tests and transport the hot gas to the inside of the packed bed. In the calculation of the average porosities the as-built heights must be used with caution, since the pebbles are not necessarily level with the specific height. The heights should rather be used as guidelines in the estimation of the average porosity.

3.4 Instrumentation and calibration

One of the main reasons why some correlations must be validated is because of a lack of knowledge regarding the quality control associated with the experiments used to develop the correlations obtained from the literature. To ensure the quality of the measurements taken on the HPTU plant a Calibration Plan was compiled by Van Niekerk (2006) in which the documentation and procedures regarding the instrument calibration are stipulated. It is very important that the instruments are calibrated at regular intervals. An uncertainty calculation for each measurement is also very important to indicate the quality of the measurements.
Instruments are divided by Van Niekerk (2006) into general instruments and test specific instruments. Most of the instruments mentioned in this chapter are general instruments with the exception of the pressure drop instruments for the test section pressure drop. Instruments are further divided by Van Niekerk (2006) into category A, B and C instruments. Category A instruments involve instruments used to obtain results in each test, and are calibrated on a regular basis according to the Calibration Plan (Van Niekerk, 2006). Category B instruments are for control or indication purposes only and are calibrated once before the operation of the HPTU plant commences. Category C instruments are not calibrated at all. Only category A instruments are mentioned in this chapter.

3.4.1 Mass flow rate measurement

Mass flow rate measurement on the HPTU plant is done with two orifice measuring stations. Each of the orifice measuring stations must be manufactured and installed according to ISO 5167 (2003a and b) standards. A full review of the installation requirements and the installed

orifice stations are given by Van der Walt (2006a). The mass flow rate through an orifice plate is correlated to the pressure drop over the plate according to ISO 5167 (2003b) as:

$$\dot{m} = \frac{C \cdot \varepsilon}{\sqrt{1-\beta^4}} \frac{\pi}{4} d_{or}^2 \sqrt{2 \cdot \rho \cdot \Delta p_{or}} \tag{24}$$

with the variables defined in Table 3.5.

Table 3.5: Explanation of the variables in equation (24)

Variable	Description	Unit
$\dot{m}$	Mass flow rate	[kg/s]
C	Discharge Coefficient	[-]
d_{or}	Orifice throat diameter	[m]
D	Pipe diameter	[m]
β	Diameter ratio - d/D	[-]
ε	Expansion coefficient	[-]
Δp_{or}	Differential pressure	[Pa]
ρ	Fluid density	[kg/m^3]

The equations for the discharge coefficient and expansion coefficient are given in Appendix B. The uncertainty associated with the use of equation (24) is given by ISO 5167 (2003b) as:

$$\frac{\Delta(\dot{m})}{\dot{m}} = \sqrt{\left(\frac{\Delta(C)}{C}\right)^2 + \left(\frac{\Delta(\varepsilon)}{\varepsilon}\right)^2 + \left(\frac{2\beta^4}{1-\beta^4}\right)^2 \cdot \left(\frac{\Delta(D)}{D}\right)^2 + \left(\frac{2}{1-\beta^4}\right)^2 \left(\frac{\Delta(d_{or})}{d_{or}}\right)^2 + \frac{1}{4}\left(\frac{\Delta(\Delta p)}{\Delta p}\right)^2 + \frac{1}{4}\left(\frac{\Delta(\rho)}{\rho}\right)^2} \tag{25}$$

The different uncertainties used in equation (25) are explained in Appendix B, along with the relevant values used to calculate the mass flow rate for each orifice station.

3.4.2 Pressure and temperature instruments

Absolute pressure measurements are made upstream of both orifice stations and at the inlet of the test section pressure vessel. The pressure measurements are mainly used along with the temperature measurements for the calculation of the density at the relevant positions. At each

pressure measurement position two different WIKA pressure transducers are used for two different ranges.

Temperature measurements are made downstream of each orifice measurement station with PT100 sensors for the calculation of the density. Upstream of the inlet to the test section pressure vessel the temperature is measured with two PT100 sensors.

Differential pressure measurements are made for the pressure drop at each orifice measurement station and for the pressure drop through the test section in the case of the pressure drop tests. Three Endress and Hauser differential pressure transducers are used for three ranges at each point.

Table 3.6 summarizes the instruments and their ranges along with the supplier instrument uncertainties (un-calibrated uncertainty).

Table 3.6: Summary of the category A instruments used on the HPTU plant

Type of instrument	Range	Unit	Un-calibrated uncertainty	Unit
Pressure	$100 < P < 1600$	[kPa]	±1.5	[kPa]
	$1600 < P < 5000$	[kPa]	±30	[kPa]
Temperature	$0 < T < 100$	[°C]	±0.25	[°C]
Differential pressure	$0 < \Delta p < 1$	[kPa]	±0.0015	[kPa]
	$1 < \Delta p < 10$	[kPa]	±0.005	[kPa]
	$3.5 < \Delta p < 50$	[kPa]	±0.025	[kPa]

3.4.3 Preliminary uncertainty analysis

An uncertainty analysis was performed by Rousseau (2005b) to investigate the influence of the un-calibrated uncertainty of each instrument on the Euler number calculation. In HPTU Test Specification (Rousseau, 2005a) it was required that the Euler number must be determinable within ±6.5% of the true value with a 95% confidence interval. The uncertainty analysis aided in determining whether the proposed instruments could deliver the required accuracy. Since the un-calibrated uncertainties are used in the uncertainty analysis it seems realistic that the actual uncertainty in the Euler number from calibrated instruments could be even lower.

The largest uncertainty in the Euler number predicted by Rousseau (2005b) is in the order of 4.5%, which is well within the required 6.5%. This will be compared with the actual uncertainty in the Euler number from the test data, as will be discussed in more detail in the next chapter.

3.4.4 Calibration of instruments

The calibration of the instruments is mainly performed on-site with the aid of a suitable secondary standard. The secondary standard used for each instrument is typically a high quality instrument with a higher resolution than the instrument to be calibrated. All the secondary standards are calibrated at SANAS (South African National Accreditation System) accredited laboratories. This ensures traceability of the measurements to national standards. The secondary standard certificate for each instrument is contained in the technical file HTTF001 (2006) on the HPTU plant. For each type of instrument (pressure, differential pressure and temperature) a work instruction exists, describing the calibration procedure in detail, as required by the Calibration Plan (Van Niekerk, 2006). A calibration log is kept on the HPTU plant, indicating when each instrument was last calibrated, what type of calibration took place and when it is due for the next calibration.

The ranges and uncertainties of the secondary standards used are given in Table 3.7. Note that the calibration of the differential pressure transducers were not done on-site with a secondary standard, but in a SANAS accredited laboratory. The uncertainty of each instrument is obtained from the calibration certificates supplied by the SANAS accredited laboratory that did the calibration. The use of the standard and general uncertainties will be discussed in more detail in the following chapter.

Table 3.7: Ranges and uncertainties of the secondary standards

Type of instrument	Range	General Uncertainty ($2 \cdot \sigma_m$)	Standard Uncertainty (σ_m)	Unit
Pressure	0 – 400	1	0.5	[kPa]
	400 - 5000	2	1	[kPa]
Temperature	0 – 150	0.1	0.05	[°C]
Differential Pressure	0 – 50 [kPa]	0.4 % of value	0.2% of value	[-]

3.5 Test sequence and procedure

The pressure drop tests were performed first. The sequence in which the tests took place is as follows:

- PDTS 036
- PDTS 039
- PDTS 045
- SAPB pressure drop test
- SCPB pressure drop test

To investigate the repeatability of the experiment, each test is performed twice at almost exactly the same conditions (particle Reynolds numbers). The first test run is performed while the system pressure is increased in a stepwise manner from the minimum pressure to the maximum pressure, obtaining various predetermined Reynolds numbers at different intermediate pressures. The second test run is preformed likewise by blowing the system pressure down in a stepwise manner. Tests are performed according to the Test Procedure (Labuschagne, 2005b). The predetermined Reynolds numbers and associated pressures are given in the Test Plan (Labuschagne, 2005c). Each action performed on the HPTU plant during a test is logged in an operations procedure checklist. Table 3.8 lists the Reynolds numbers to be investigated in the SET and IET pressure drop tests, along with the required system pressure as outlined in the Test Plan (Labuschagne, 2005c). It follows that 14 Reynolds numbers will be investigated in the SET pressure drop tests and 5 in the IET pressure drop tests.

Throughout the following chapter in the discussion of the results, tests will be referred to by the test section number, the set point number and the test run number. For example PDTS045-011-02 refers to the 0.45 porosity test section, set point number 11 (as shown in Table 3.8) and test run number 2.

3.6 Conclusion

In this chapter the basic components of the HPTU plant were introduced and discussed according to the layout shown in Appendix A. The purpose of the HPTU plant was revisited and elaborated. Each test section was discussed and the relevant dimensions were given. The

instruments used for the measurement of the pressure drop and the calculation of the Euler number were summarized along with the uncertainties of each instrument. The ranges and uncertainties of the secondary standards were also shown. With this knowledge of the HPTU plant the preliminary results of the pressure drop tests can be discussed in a meaningful manner. The following chapter is devoted to the processing procedure, the criteria set for the calculation of steady-state conditions and the uncertainty analysis performed to investigate the quality of the data.

Table 3.8: Reynolds numbers to be investigated with the associated pressures

Set point number.	Reynolds number [-]	System Pressure [kPa]	
		SETs: PDTS 036 PDTS 039 PDTS 045	IETs: SAPB pressure drop tests SCPB pressure drop tests
001	1000	100	309
002	2000	200	618
003	3000	300	928
004	4000	400	1239
005	5000	500	1552
006	6000	600	[-]
007	7000	700	[-]
008	8000	800	[-]
009	9000	900	[-]
010	10000	1000	[-]
011	20000	2000	[-]
012	30000	3000	[-]
013	40000	4000	[-]
014	50000	5000	[-]

4 DATA PROCESSING METHODOLOGY

Following the discussion of the HPTU plant layout, components and instrumentation in the previous chapter, this chapter will proceed to explain how the raw data obtained from the experiments are processed into meaningful results. This will include the criteria developed to predict steady-state conditions, the uncertainty analysis for the calculation of the uncertainty in the Euler and Reynolds numbers and comparison between important variables calculated in Labview and Excel. Repeatability of measurements will be investigated by comparison of the test runs.

4.1 Determination of steady-state conditions

During the first test (PDTS 036) no guidelines were available regarding the time involved for the system to reach steady-state conditions. Possible criteria for steady-state conditions could only be investigated after sufficient experimental results were available. The first test run was therefore carried out without any criteria and the HPTU test team judged whether the steady-state conditions were obtained. Conservatively long times were waited to ensure that steady-state conditions were indeed obtained and that the test had not to be repeated. After the first test the data was investigated and the important variables for steady-state criteria were identified. The important variables are the following:

- The test section inlet temperature for the calculation of the density;
- The test section inlet pressure for the calculation of the density;
- The test section pressure drop;
- The particle Reynolds number.

All the variables listed above are used in the calculation of the Euler and Reynolds numbers. For steady-state conditions al the measured variables listed above must have reached a steady state. It was decided that five minutes duration of steady-state data must be used for further calculations. This amounts to 600 data points for each Reynolds number which is more than sufficient for the meaningful calculation of averages and standard deviations. After completion of the processing of all the pressure drop experimental data a simple test was performed where the standard deviation and average of different amounts of data points was calculated after steady state has been reached. It was found that after 120 data points an

insignificant change in the average values and standard deviation took place, and that 120 data points would have been sufficient for further processing of the results. A larger number of data point decreases the error in the calculation of the standard deviation (Squires, 1976), and the results presented is therefore based on 600 data points, rather than 120 data points.
As a first attempt an exponential approximation valid for first-order systems was used to predict steady-state conditions. This approach worked well for the test section inlet temperature, but not quite as well for the particle Reynolds number or test section pressure drop. This is due to the fact that the change in the Reynolds number and pressure drop is approximately linear and not exponential, except for the last part of the change up to steady-state conditions. Visible steady-state conditions could in some cases not be predicted by the exponential approach without various attempts. The desired criteria had to be programmed into the control system so that the prediction of steady-state conditions did not only depend on operator judgment, which could results in biased interpretations or unnecessarily long waiting periods. This was not entirely possible with the exponential approach for the reasons mentioned above. Two steady-state criteria were therefore developed by the HPTU test team that could predict steady-state conditions for all the important variables over the whole applicable range for each. All the calculations were done using Excel spreadsheets.

The first criterion is based on the amount the variable changed relative to certain maximum and minimum values. At the time that the system pressure is changed to obtain the next desired Reynolds number the test for steady-state conditions is initiated. For each time step from the change in the system pressure the difference between the one minute running average and the five minute running average is calculated. The one minute running average is calculated after the 120 data points are available, and the five minute running average after 600 data points are available. This difference between the running averages is therefore calculated from the 600^{th} data point. This difference is then normalized by the difference between the maximum and minimum values of the variable over the elapsed time (over five minutes). The purpose of the one minute running average is to smooth out the noise in the measurements. The five minute running average provides a history of the change in the variable against which the more current change in the variable (the one minute running average) can be evaluated. The difference between the minimum and maximum values serves as a means by which the comparison in the change of the variable can be normalized independent of the variable investigated. To ensure that the difference between the one minute and five minute running average does not change significantly for a period of time the

normalized difference between the running averages is averaged over five minutes. This final running average must be smaller that 5. The tolerance of 5 was observed by the test team to be sufficient and conservative for all the variables tested. The criterion is mathematically expressed as:

$$C_1(k)=\frac{1}{n}\cdot\sum_{i=k-n}^{k} abs\left[\frac{\frac{1}{m}\sum_{j=i-m}^{i}P(j)-\frac{1}{n}\sum_{j=i-n}^{i}P(j)}{P_{\max}(i)-P_{\min}(i)}\right]<5 \tag{26}$$

where $m=120$, $n=600$ and $C_1(k)$ is the criterium evaluated at the k_{th} measured value from the initiation of the test for steady state. P represents any of the variables required for the steady-state calculation.

The first criterion can however be satisfied under non-steady-state conditions if the slope between the one minute running average and the five minute running average doesn't change while the actual values are still changing. A second criterion was therefore introduced to test the variation of the slope of the variable.

In the second criterion a slope between the value of the one minute running average at a specific time and a value of the one minute running average a minute earlier is calculated. This slope is then expressed as a percentage of the average of the two one minute running average values. To ensure that this normalized slope remains below a certain value the five minute running average is once again calculated. This calculation was implemented on all the variables selected for all the measurement points of the PDTS 036 test. It was found that the five minute running average of the normalized slope must be below 0.004 in all parameters. The criterion is mathematically expressed as:

$$C_2(k)=\frac{1}{n}\sum_{i=k-n}^{k}\left[\frac{P_{1\min avg}(i)-P_{1\min avg}(i-m)}{\left[t(i)-t(i-m)\right]}\cdot\frac{100}{\left[\frac{P_{1\min avg}(i)-P_{1\min avg}(i-m)}{2}\right]}\right]<0.004 \tag{27}$$

where $P_{1\min avg}$ represents the average of the parameter over a minute and $P_{5\min avg}$ the average of the parameter over five minutes.

For steady-state conditions to exist both the criteria must be satisfied. To obtain five minutes duration of steady-state data both criteria for all the important variables must be satisfied uninterrupted for five minutes. These criteria were implemented after the first test (PDTS 036), and were evaluated after the second test (PDTS 039). Each time before the pressure is adjusted for the next measurement point the running average calculations and maximum and minimum values are reset. The user interface allows the operator to see how the criteria behave. Before any data are logged both test engineers on site must agree that steady-state conditions have been reached.

An example of the criteria used to determine steady-state of the inlet test section vessel temperature is shown in Figure 4.1. The steady-state temperature predicted by the exponential approximation is also included, and corresponds to the 100% curve. The 99% and 101% curves are 99% and 101% of the steady-state temperature. Steady-state conditions are accurately predicted by the two criteria to begin after the temperature has approached the steady-state temperature. Note that the difference between the maximum and minimum temperatures is approximately 0.3°C, which is very small. For such small changes the second criterion predicts that the temperature is steady state. The variation at the beginning of the transient must obviously not be included. The two criteria are therefore very useful together and no cases were observed for the PDTS036 tests where steady-state conditions were predicted during a transient.

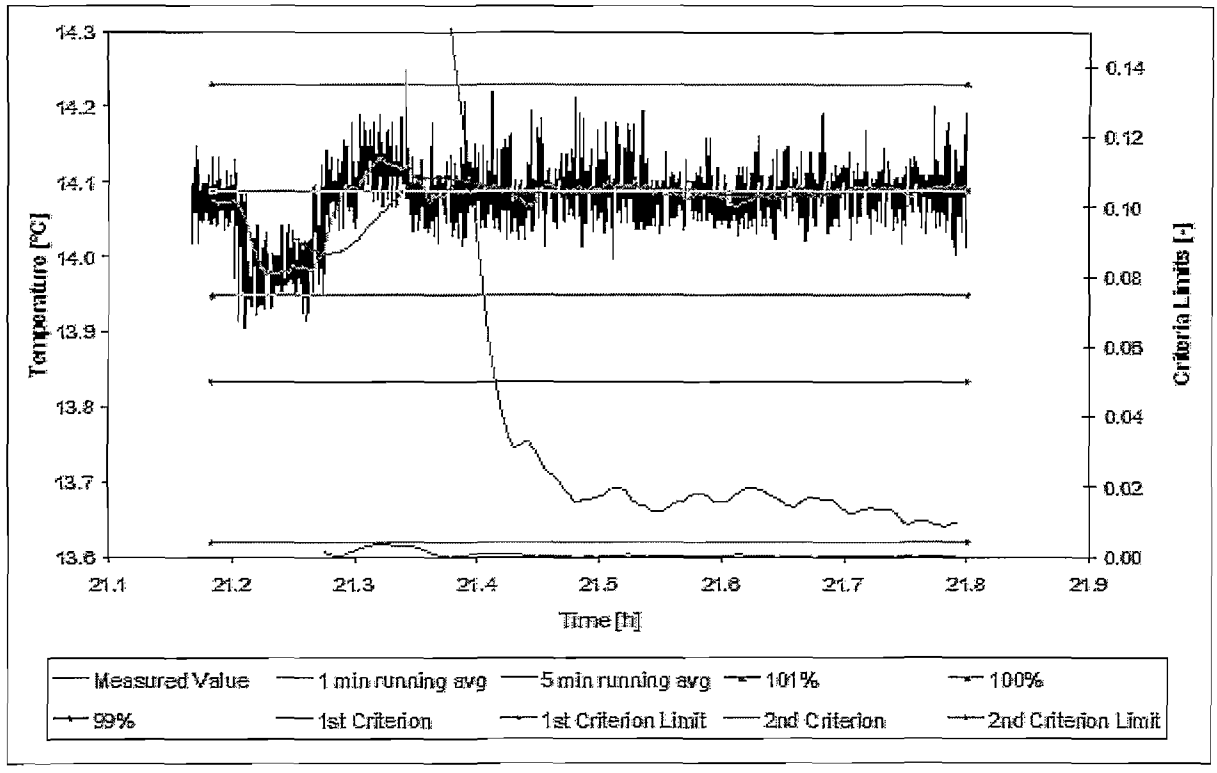

Figure 4.1 *Example of the implemented steady-state criteria*

The criteria were implemented into Labview for automatic prediction of steady-state conditions during testing. In the PDTS039 test the criteria were tested and worked well. To ensure that the calculations were indeed being performed correctly in Labview two set points were randomly selected in each test to compare the initial time predicted for steady-state conditions by Labview and Excel. The data calculated for the criteria in Labview were copied to an Excel file with the raw data in which the criteria were also calculated. The steady-state criteria are compared with a simple logical test where a one indicates steady-state for all the important parameters and zero not. An example is shown in Figure 4.2 for the SCPB-002-02 measurements. The initial time for steady-state is clearly identical. Other comparisons showed a very small deviation in the order of 10 seconds. This is due to the calculation procedure followed in Labview that results in a small time delay. The Labview predicted steady-state conditions are however always more conservative. The implementation of the steady-state criteria is therefore also correct.

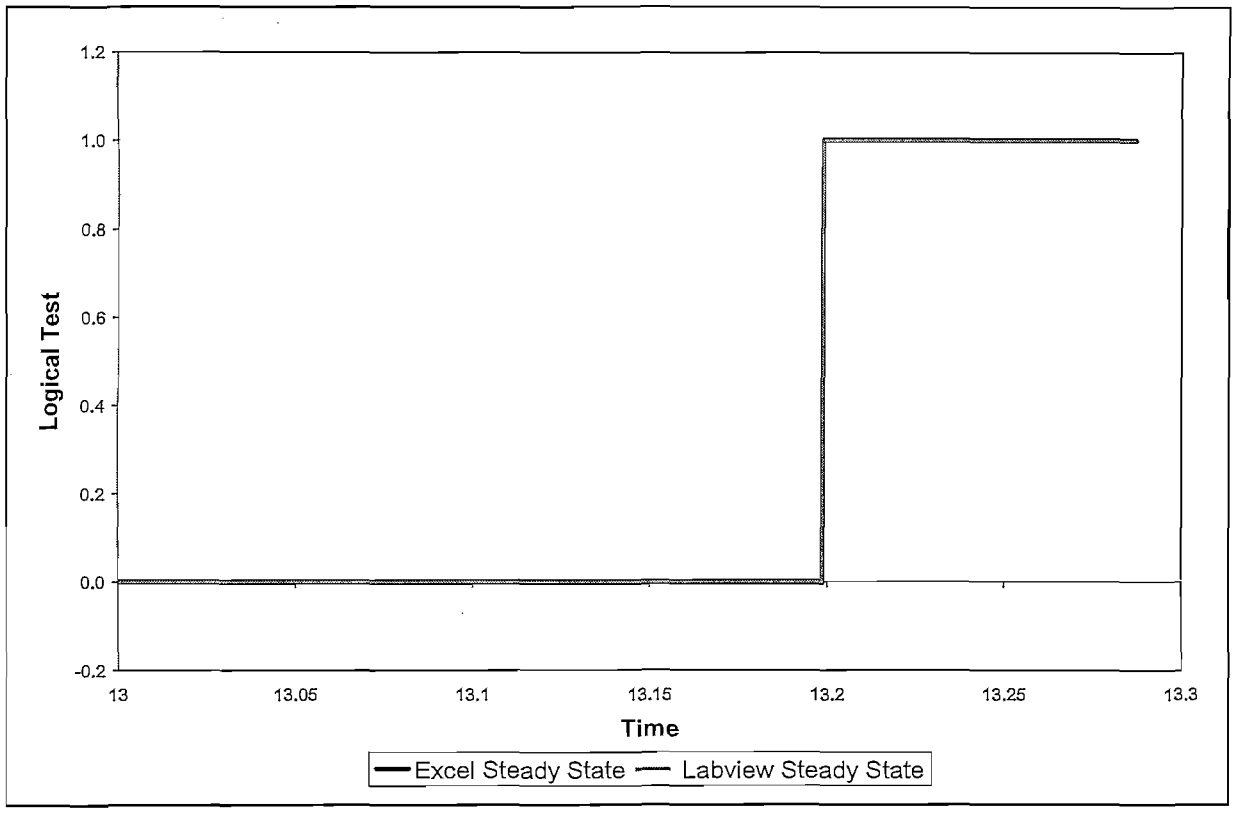

Figure 4.2 *Steady-state comparison for Labview and Excel calculations*

The calculations performed in Labview were also compared to the calculations from the raw data in Excel. This is necessary to ensure that the data from calculations during the test are reliable. A critical variable is the mass flow rate, since iteration of equation (24) is required. Before the tests all dimensions were verified to be correctly implemented in Labview. The mass flow rate calculation was also verified with dummy input values. The calculation throughout the tests are compared in Table 4.1 showing two cases for Reynolds numbers calculated from Excel and Labview. A very small difference between the calculated values exists, below 1%. The difference is almost insignificant in the calculation of the rest of the variables. The calculations from Excel will however be used throughout to ensure the quality of the processed data. The calculations in Excel are more accessible and can be controlled throughout.

Table 4.1: Comparison between Reynolds numbers calculated from Excel and Labview

Test Run	Average Reynolds number [-]		Percentage difference [%]	Standard Deviation [-]	
	Excel	Labview		Excel	Labview
HPTU002-TST-SCPDdP-001-01SS_unc.xls	1006.03	999.20	0.6784	0.8704	0.8878
HPTU002-TST-SCPBdP-005-02SS_unc.xls	5041.01	5000.41	0.8053	4.981	4.846

4.2 Uncertainty Analysis

The criteria for determining steady-state conditions have been explained. This section will now proceed to discuss the uncertainty analysis performed on the 600 data points to evaluate the total uncertainty of the Euler number. The uncertainty of a variable is given by a range which is likely to include the variable. The uncertainty as such does not imply doubt in the measurement of a variable, but rather adds confidence in the validity of the measured results.

4.2.1 Introduction

If the measurement of a variable is repeated enough times, a good estimate of the standard deviation can be obtained. The standard deviation, σ, then represents the uncertainty of a single measurement, and has the same units as the variable measured. The standard error in the average can then readily be obtained as

$$\sigma_m = \frac{\sigma}{\sqrt{n}} \tag{28}$$

Note that σ_m is precisely correlated to σ. The value of σ, as calculated from standard functions, is however only an estimate of the standard deviation. By using enough data points the error in the estimate is significantly reduced. 600 data points were therefore selected as a reasonable and manageable number of measurements. If the standard deviation in equation (28) is used to represent the uncertainty in the measurement, a confidence interval of

approximately 68.3% is associated with the uncertainty (Squires, 1976). Such an uncertainty is known as the standard uncertainty, and is denoted $u_s(\phi)$ in this study.

The standard deviation therefore states that 68.3% of the measured values will fall within $\pm\sigma_m$ from the actual value. The confidence in the uncertainty can however be increased by multiplying σ_m with an appropriate coverage factor, k. For a coverage factor of $k=2$, the confidence interval is increased to approximately 95%, and for a coverage factor of $k=3$ the confidence interval is increased to approximately 99.7%. The uncertainty associated with a specific confidence interval is known as the general uncertainty, and is denoted $u_g(\phi)$. It should now be clear why the uncertainty analysis adds confidence in the measured results, rather than placing doubt on the measurements. In this uncertainty analysis a general uncertainty of the Euler number and the Reynolds number will be reported with a 95% confidence interval. All the uncertainties used in the calculation of the uncertainty in the Euler number must be converted to a standard uncertainty with coverage factor $k=1$.

The standard deviation discussed above represents the random errors in the measurements. In the uncertainty analysis the standard deviation calculated from the measurements will replace the un-calibrated uncertainties of the instruments given in Table 3.7, which were used to calculate the predicted uncertainty in the Uncertainty Analysis Report (Rousseau, 2005b). Additional to this the uncertainty existing in the calibration of the instruments must be investigated, which is a systematic error. Any systematic errors in the measurement should be significantly reduced after calibration. The uncertainty of the secondary standard will be used as the general uncertainty existing in the calibration, as given in Table 3.7 for each secondary standard. Both the general uncertainties and standard uncertainties are specified in Table 3.7. The general uncertainties were obtained from the calibration certificate of the instrument. In all the cases the general uncertainties are reported with a 95% confidence interval by the SANAS accredited laboratories. To be able to use the uncertainties of the secondary standards the general uncertainties specified by on the calibration certificate were converted to standard uncertainties. This is simply done by dividing the reported uncertainties by the coverage factor of $k=2$ for the 95% confidence interval.

Throughout the uncertainty analysis only the largest of the standard uncertainties calculated for a variable is used. If an uncertainty is given without a confidence interval, it will be assumed that a rectangular distribution of the variable is valid, in which extreme values of the variable is as likely to occur as values close to the average. This is the case for uncertainties

obtained from as-built drawings. For a rectangular distribution the standard uncertainty is related to the general uncertainty as follows:

$$u_g(\phi) = \sqrt{3} \cdot u_s(\phi) \tag{29}$$

All general uncertainties are reported with a 95% confidence interval, unless otherwise stated.

Uncertainties are combined using a general method reported by Squires (1976). For a variable ϕ as a function of two variables α and β, the error in ϕ due to the errors in its constituent variables is given as

$$\left(u_s(\phi)\right)^2 = \left(\Delta\phi_\alpha\right)^2 + \left(\Delta\phi_\beta\right)^2 \tag{30}$$

with $\Delta\phi_\alpha$ the error in ϕ due to an error $\Delta\alpha$ in α given by $\Delta\phi_\alpha = \frac{\partial\phi}{\partial\alpha} \cdot \Delta\alpha$. Likewise for the error in β, $\Delta\phi_\beta = \frac{\partial\phi}{\partial\beta} \cdot \Delta\beta$. To calculate the standard uncertainty in a variable the standard uncertainties of the constituent variables must be used throughout, therefore all uncertainties are first converted to standard uncertainties.

While using uncertainties to indicate the confidence associated with a measurement, it is very important to understand the importance of the average or base value of a measurement. Throughout the background given it is assumed that the distribution of the measurements of a particular variable will follow a Gaussian or normal distribution. For a Gaussian distribution the mean value of a set of measurements is defined as the value which maximizes the probability of getting a particular set of measured values (Squires, 1976). The mean of a set of values is therefore the value that is most likely to occur. This is important when comparing results where the uncertainties in the results overlap. If the friction factor is for example determined from experimental values with a particular uncertainty and is compared to the KTA predicted friction factor with a specific uncertainty, these uncertainties could overlap. The possibility therefore exists that the KTA equation predicts the precise same value as calculated, if one measurement is made. The probability of this to occur is however less likely if the mean values are further apart. To state that the measured and predicted values are the same if the uncertainties overlap is therefore not correct.

4.2.2 Euler number uncertainty

The Euler number is defined as

$$Eu = \frac{\Delta p}{\rho U_0^{\,2}} \tag{31}$$

Substitution of the equation (31) into equation (5) leads to the following definition of the Euler number in terms of the friction factor:

$$Eu = \psi \cdot \frac{1-\bar{\varepsilon}}{\bar{\varepsilon}^3} \frac{L}{d_p} \tag{32}$$

Equation (31) is used to calculate the Euler number from the experimental data, and equation (32) is used to predict the Euler number from the correlations. Equation (31) can be re-written in a more useable form in terms of the mass flow rate as:

$$Eu = \frac{\Delta p \cdot A^2 \cdot \rho}{\dot{m}^2} \tag{33}$$

with A the cross-sectional area of the test section.

The standard uncertainty of the Euler number can be expressed as the combination of the errors of its constituent variables in the following way:

$$u_s(Eu) = \sqrt{\left(\frac{\partial(Eu)}{\partial\rho}\cdot u_s(\rho)\right)^2 + \left(\frac{\partial(Eu)}{\partial\dot{m}}\cdot u_s(\dot{m})\right)^2 + \left(\frac{\partial(Eu)}{\partial A}\cdot u_s(A)\right)^2 + \left(\frac{\partial(Eu)}{\partial(\Delta p)}\cdot u_s(\Delta p)\right)^2} \tag{34}$$

The partial derivatives in equation (34) are easily calculated. The standard uncertainties in the components of equation(33), $u_s(\rho)$, $u_s(\dot{m})$, $u_s(A)$ and $u_s(\Delta p)$ is left to be determined.

The general uncertainty in the Euler number is reported as $u_g(Eu) = k \cdot u_s(Eu) = 2 \cdot u_s(Eu)$, implying a 95% confidence interval.

4.2.3 Reynolds number uncertainty

The particle Reynolds number can be re-written in terms of the mass flow rate as follows:

$$\mathrm{Re}_{d_p} = \frac{\dot{m} \cdot d_p}{A \cdot \mu} \tag{35}$$

The general uncertainty in the particle Reynolds number can then be expressed in the same way as done for the Euler number as:

$$u_s\left(\mathrm{Re}_{d_p}\right)=\sqrt{\left(\frac{\partial\left(\mathrm{Re}_{d_p}\right)}{\partial\mu}\cdot u_s\left(\mu\right)\right)^2+\left(\frac{\partial\left(\mathrm{Re}_{d_p}\right)}{\partial\dot{m}}\cdot u_s\left(\dot{m}\right)\right)^2+\left(\frac{\partial\left(\mathrm{Re}_{d_p}\right)}{\partial A}\cdot u_s\left(A\right)\right)^2+\left(\frac{\partial\left(\mathrm{Re}_{d_p}\right)}{\partial d_p}\cdot u_s\left(d_p\right)\right)^2} \tag{36}$$

The standard uncertainty in the particle Reynolds number is reported as $u_g\left(\mathrm{Re}_{d_p}\right)=k\cdot u_s\left(\mathrm{Re}_{d_p}\right)=2\cdot u_s\left(\mathrm{Re}_{d_p}\right)$, implying a 95% confidence interval. The partial derivatives are once again easy to calculate, leaving the general uncertainties of the constituent variables, $u_s\left(\mu\right)$, $u_s\left(\dot{m}\right)$, $u_s\left(A\right)$ and $u_s\left(d_p\right)$ to be determined.

4.2.4 Uncertainties in the Euler- and Reynolds number uncertainties

Uncertainty in the density and viscosity

Densities and viscosities for nitrogen were calculated from curves fitted to REFPROP (Reference Fluid Thermodynamic and Transport Properties) data obtained from NIST Standard Reference database 23, Version 7, as explained in the PDTS036 test report (van der Merwe, 2006). The functions for the density and viscosity are given in Appendix C.

The standard uncertainties in the density and viscosity are calculated as:

$$u_s\left(\rho\right)=\sqrt{\left(\frac{\partial\rho}{\partial T}\cdot u_s\left(T\right)\right)^2+\left(\frac{\partial\rho}{\partial p}\cdot u_s\left(p\right)\right)^2} \tag{37}$$

and

$$u_s\left(\mu\right)=\sqrt{\left(\frac{\partial\mu}{\partial T}\cdot u_s\left(T\right)\right)^2+\left(\frac{\partial\mu}{\partial p}\cdot u_s\left(p\right)\right)^2} \tag{38}$$

The partial derivatives in equations (37) and (38) can be calculated either analytically or numerically.

The uncertainties resulting from the calibration of the temperature and pressure sensors are shown in Table 3.7. In the case of the test section density, two temperature measurements are made of which the average is used for the calculation of the density. The standard uncertainty of the test section inlet temperature is therefore:

$$u_s\left(T_{avg}\right)=\sqrt{\left(\frac{1}{2}\cdot u_s\left(T_1\right)\right)^2+\left(\frac{1}{2}\cdot u_s\left(T_2\right)\right)^2} \tag{39}$$

were the partial derivative of the average temperature for either of the temperatures is 0.5. The largest value between the calibration standard uncertainty and the standard deviation from the measurements is used in each case for the standard uncertainty of the pressures, $u_s\left(p\right)$ and the temperatures $u_s\left(T\right)$, respectively.

Uncertainty in the cross-sectional area

The uncertainties in the cross-sectional areas were obtained from the tolerances specified in the as-built test section drawings for each test section. The tolerances are used as the general uncertainties without a confidence level. Equation (29) was used to calculate the standard uncertainty of each dimension. The standard uncertainties in the cross-sectional area are given in Table 4.2 as obtained from the test reports. The references to the test reports of the various tests are included in Table 4.2.

Table 4.2: Summary of the cross-sectional area uncertainties

Test Section	Standard Uncertainty in the cross-sectional area [% of area]	Reference
PDTS 036 PDTS 039 PDTS 045	0.0118	PDTS 036 Test Report (van der Merwe, 2006) PDTS 039 Test Report (Hoogenboezem, 2006a) PDTS 045 Test Report (Van der Walt, 2006b)
SAPB	0.483	SAPB Test Report (Hoogenboezem, 2006b)
SCPB	0.313	SCPB Test Report (Van der Walt, 2006c)

Uncertainty in the particle diameter

In the case of the homogeneous porosity test sections the pebbles are assumed to be machined to within 50μm. The general uncertainty in the pebble diameter is therefore assumed to be

50μm. This value is given without a confidence level, and a rectangular distribution is therefore assumed. Using equation (29) the standard uncertainty is calculated as $u_s(d_p) = \frac{0.00005}{\sqrt{3}} = 0.000028m$.

A sample of 100 particles was measured for the SAPB and SCPB pressure drop tests. The average value of a single particle was determined to be 0.006002m, with a standard deviation of 0.000005607m. The standard uncertainty is therefore $u_s(d_p) = 0.000005607\text{m}$.

Uncertainty in pressure drop and mass flow rate

The uncertainty in the pressure drop through the test section is simply taken as the largest of the standard deviation and the calibrated instrument uncertainty given in Table 3.7 for each measurement. The uncertainty in the mass flow rate is presented in Appendix B according to the specification of the ISO 5167 (2003b) standard.

4.2.5 Uncertainty in the average porosity

As indicated in the literature survey an accurate estimation of the average porosity is very important for the calculation of the friction factor. In the case of the homogenous porosity test sections the average porosity is obtained from the program used to design the packing arrangement. The tolerances specified in the manufacturing were very strict. Since the position of each ball is known, the number of balls in each test section is exactly determined as specified in Table 3.3.

In the case of the SAPB and SCPB the average porosity must be estimated in some way. This is done by estimating the number of balls in the test section and by calculating the total volume of the balls. To calculate the average weight of one ball a Sartorius digital scale with a resolution of 0.0001g were used to weigh fifty samples. A digital scale with a resolution of 1g was used to weigh small buckets of balls thrown into the test section. Neither of the scales were calibrated. To test how accurate the number of balls in a single bucket could be estimated, a thousand balls were counted and weighed. It was found that the balls could be estimated exactly from the measurements of the two scales. This was repeated twice for two different samples of a 1000 balls each and for 2000 balls at once. For a sample of 2000 balls

the uncertainty in the number of balls was one per 2000. As long as the weight of the bucket did not exceed the weight of 2000 balls, the error in the estimate of the number of balls per bucket would not be more than 1 per bucket. To be conservative the error per bucket mass was assumed to be the mass of 2 balls.

The average diameter of a ball was determined from the measurement of 100 balls with a micrometer with a resolution of 0.005mm. From the average diameter of the balls the average volume could be calculated, which could in turn be used along with the estimated number of balls to calculate the total volume of the balls. From the as-built test section drawings the empty volume of the cylinder in the SCPB and the annulus in the SAPB could be determined. The error in the cross-sectional areas of the test section is given in Table 4.2. It is assumed that each bed can be packed to within 1mm of the height given in Table 3.4. This is then the standard error given without a confidence interval, and is converted to a general interval using equation (29). The average porosity could thus be determined along with a general error. Table 4.3 summarizes the measurements for the calculation of the average porosity.

Table 4.3: Variables for the calculation of the average porosity and the error

Variable	Average	Unit	Standard uncertainty $u_s(\phi)$	Unit
Weight of ball	0.8856	[g]	0.002278	[g]
Diameter of ball	0.006002	[m]	0.000005607	[m]
Number of balls in the SCPB (n)	101486	[-]	100	[-]
Number of balls in the SAPB (n)	72151	[-]	100	[-]
Height of the SCPB	0.1782	[m]	$0.001/\sqrt{3}$	[m]
Height of the SAPB	0.1788	[m]	$0.001/\sqrt{3}$	[m]

The average porosity is calculated as

$$\overline{\varepsilon} = 1 - \frac{V_{balls}}{V_{bed}} \tag{40}$$

with V_{balls} the total volume of the balls and V_{bed} the empty volume of the column or annulus. Therefore the error in the porosity is calculated as:

$$u_s(\bar{\varepsilon}) = \sqrt{\left(\frac{\partial \bar{\varepsilon}}{\partial V_{balls}} \cdot u_s(V_{balls})\right)^2 + \left(\frac{\partial \bar{\varepsilon}}{\partial V_{bed}} \cdot u_s(V_{bed})\right)^2} \quad (41)$$

with

$$\frac{\partial \bar{\varepsilon}}{\partial V_{balls}} = \frac{-1}{V_{bed}} \quad (42)$$

and

$$\frac{\partial \bar{\varepsilon}}{\partial V_{bed}} = \frac{V_{balls}}{V_{bed}^2} \quad (43)$$

The uncertainty in the volume of the balls is

$$u_s(V_{balls}) = \sqrt{\left(\frac{\partial V_{balls}}{\partial d_p} \cdot u_s(d_p)\right)^2 + \left(\frac{\partial V_{balls}}{\partial n} \cdot u_s(n)\right)^2} \quad (44)$$

with

$$\frac{\partial V_{balls}}{\partial d_p} = n \cdot \frac{1}{2} \cdot \pi \cdot d_p^2 \quad (45)$$

and

$$\frac{\partial V_{balls}}{\partial n} = \frac{1}{6} \cdot \pi \cdot d_p^3 \quad (46)$$

d_p is the average diameter of a single ball, and n the total number of balls per test section. The uncertainties in the diameter of the balls and the number of balls are given in Table 4.3. The uncertainty in the empty volume of the bed is

$$u_s(V_{bed}) = \sqrt{\left(\frac{\partial V_{bed}}{\partial A_{bed}} \cdot u_s(A_{bed})\right)^2 + \left(\frac{\partial V_{bed}}{\partial L_{bed}} \cdot u_s(L_{bed})\right)^2} \quad (47)$$

with $u_s(A_{bed})$ given in Table 4.2 and $u_s(L_{bed})$ in Table 4.3. The errors in the estimated average porosities for the SCPB and the SAPB are shown in Table 4.4.

Table 4.4: Average porosities and estimated errors in the average porosity of the IET test sections

Test Section	Average Porosity	Error	Percentage
SCPB	0.3967	0.008485	2.14
SAPB	0.3946	0.004223	1.07

In the case of the homogeneous porosity test sections the uncertainty in the number of balls is zero. The uncertainty in the sphere diameter is given as $u_s(d_p)=\frac{0.00005}{\sqrt{3}}=0.000028m$. The uncertainty in the volume of the balls are therefore estimated by equation (45). The uncertainty in the cross-sectional area of the test section is given in Table 4.2. The uncertainty in the length of the bed can be calculated from the total number of spheres and spacers on a string. The number balls and spacers on a string are the same for all the test sections and are equal to 10 balls and 9 spacers (Van der Walt, 2006b). The distance between the outer edges of two balls at the top and bottom of a string is thus calculated as

$$L=n\cdot d_p+j\cdot s \tag{48}$$

with n the number of spheres on the string, j the number of spacers and s the length of the spacers. The uncertainty in the bed length is therefore;

$$u(L_{bed})=\sqrt{\left(n\cdot u(d_p)\right)^2+\left(j\cdot u(s)\right)^2} \tag{49}$$

since $\frac{\partial L_{bed}}{\partial d_p}=n$ and $\frac{\partial L_{bed}}{\partial s}=j$. The spacers are machined accurately to within 50 μm (Van der Walt, 2006b). It is assumed that since the uncertainty is given without an associated confidence level that the extreme values are just as likely to occur as those close to the actual measured value. Therefore a rectangular distribution is assumed, with a standard uncertainty of:

$$u(s)=\frac{0.00005}{\sqrt{3}}=0.000028m$$

Given this, the uncertainty in the length of each of the beds is 0.0003884m. Combined with the uncertainty in the cross-sectional area the uncertainty in the porosity could be estimated for each homogenous porosity test section. The uncertainties are summarized in Table 4.5.

Table 4.5: Average porosities and estimated errors in the average porosity of the SET test sections

Test Section	Average Porosity	Error	Percentage
PDTS 036	0.369	0.00194	0.526
PDTS 039	0.407	0.00182	0.448
PDTS 045	0.465	0.00164	0.353

4.2.6 Uncertainty in the friction factor

The uncertainty in the friction factor can be calculated as follows:

$$u_s(\psi)=\sqrt{\left(\frac{\partial(\psi)}{\partial Eu}\cdot u_s(Eu)\right)^2+\left(\frac{\partial(\psi)}{\partial L_{bed}}\cdot u_s(L_{bed})\right)^2+\left(\frac{\partial(\psi)}{\partial d_p}\cdot u_s(d_p)\right)^2+\left(\frac{\partial(\psi)}{\partial(\bar{\varepsilon})}\cdot u_s(\bar{\varepsilon})\right)^2} \quad (50)$$

The respective partial derivatives are calculated from equation (32) as:

$$\frac{\partial(\psi)}{\partial Eu}=\frac{\bar{\varepsilon}^3}{1-\bar{\varepsilon}}\frac{d_p}{L_{bed}} \quad (51)$$

$$\frac{\partial(\psi)}{\partial d_p}=Eu\frac{\bar{\varepsilon}^3}{1-\bar{\varepsilon}}\frac{1}{L_{bed}} \quad (52)$$

$$\frac{\partial(\psi)}{\partial L_{bed}}=-Eu\frac{\bar{\varepsilon}^3}{1-\bar{\varepsilon}}\frac{d_p}{L_{bed}^2} \quad (53)$$

and

$$\frac{\partial(\psi)}{\partial\bar{\varepsilon}}=Eu\frac{d_p}{L_{bed}^2}\left[\frac{3\cdot\bar{\varepsilon}^2}{1-\bar{\varepsilon}}+\frac{\bar{\varepsilon}^3}{(1-\bar{\varepsilon})^2}\right] \quad (54)$$

with the uncertainties in each of the variables as previously defined.

4.3 Data processing results

A number of cases will be presented showing the uncertainties calculated for different variables and tests. Following the results of the uncertainty analysis a number of comparisons between test runs are presented to show the repeatability of the measurements. The results pertaining to the repeatability that are not included in this section are shown in Appendix D.

4.3.1 Results from the uncertainty analysis

The uncertainties in the calculated density of the PDTS045 test run 1 are shown in Figure 4.3 as an example for each set point in the test run. It is clear that the uncertainty in the density resulting from the pressure and temperature measurements is very small, with the maximum standard uncertainty equal to 0.036 kg/m^3 or 0.04% of the calculated density. The maximum standard deviation in the measured pressure for the PDTS045 test is 4988 ±3.18 kPa, and the maximum standard deviation in the measured temperatures for the PDTS045 test is 20°C ±0.06°C. These results show that reliable instruments were selected for temperature and pressure measurements. It also shows that the temperatures and pressures don't change

significantly over time, supporting that the steady-state criteria predict steady-state conditions successfully.

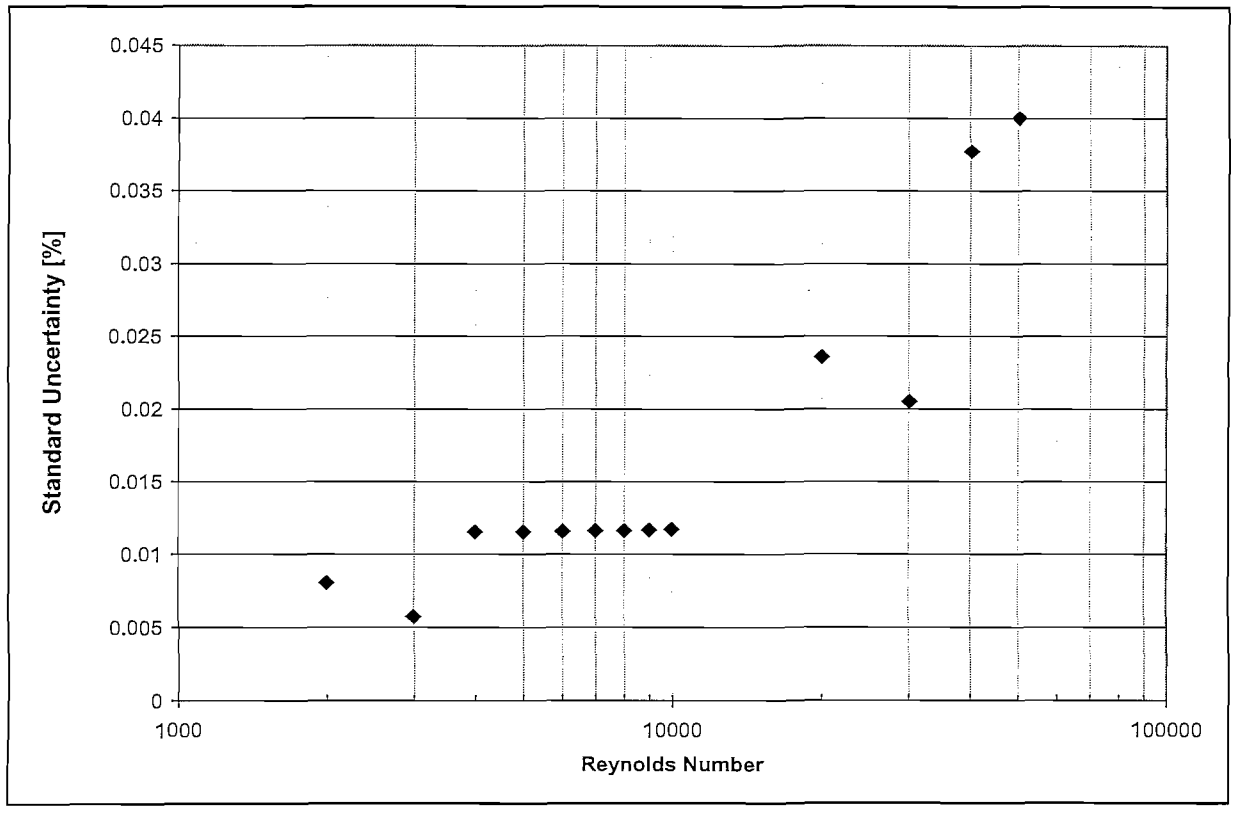

Figure 4.3 *Standard uncertainties of the test section density for PDTS045, test run 1*

Figure 4.4 shows the calculated standard uncertainty for the test section pressure drop, along with the measured pressure drops. It can be seen that the standard deviation of the measurements is in all cases larger than the standard uncertainty of 0.2% existing from the calibration. The maximum standard deviation is ±5.75 Pa at 0.683 kPa. The lowest pressure drop measured in all the pressure drop tests is 0.054 ±0.00033kPa from the PDTS045-001-02 test. Figure 4.4 indicates that the accuracy of the measuring instrument decreases at lower pressure drops, but is still more than sufficient. It can therefore be concluded that the selection and calibration of the pressure drop instruments are successful, even for the extremely low pressure drops measured.

Figure 4.5 shows the general uncertainty of the Reynolds number, with a confidence interval of 95% and the standard uncertainty of the mass flow rate. Since the standard uncertainty in the cross-sectional area and particle diameter remains constant throughout each test, the uncertainty in the mass flow rate is reflected in the Reynolds number uncertainty. The

contribution of the uncertainty in the viscosity, cross-sectional area and particle diameter to the total uncertainty in the Reynolds number is very small compared to the contribution of the mass flow rate uncertainty. The step in the Reynolds number and mass flow rate uncertainty

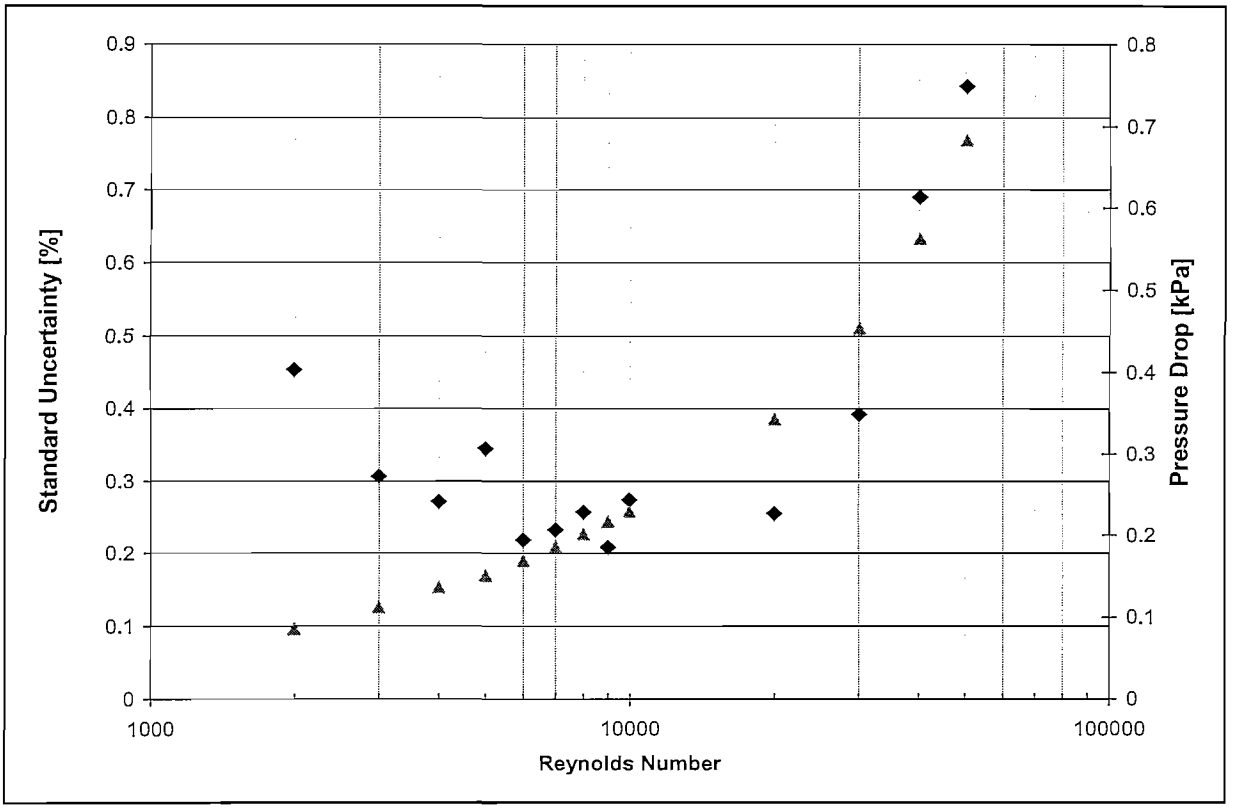

Figure 4.4 *Standard uncertainties for the pressure drop measurement in PDTS045 test run 1*

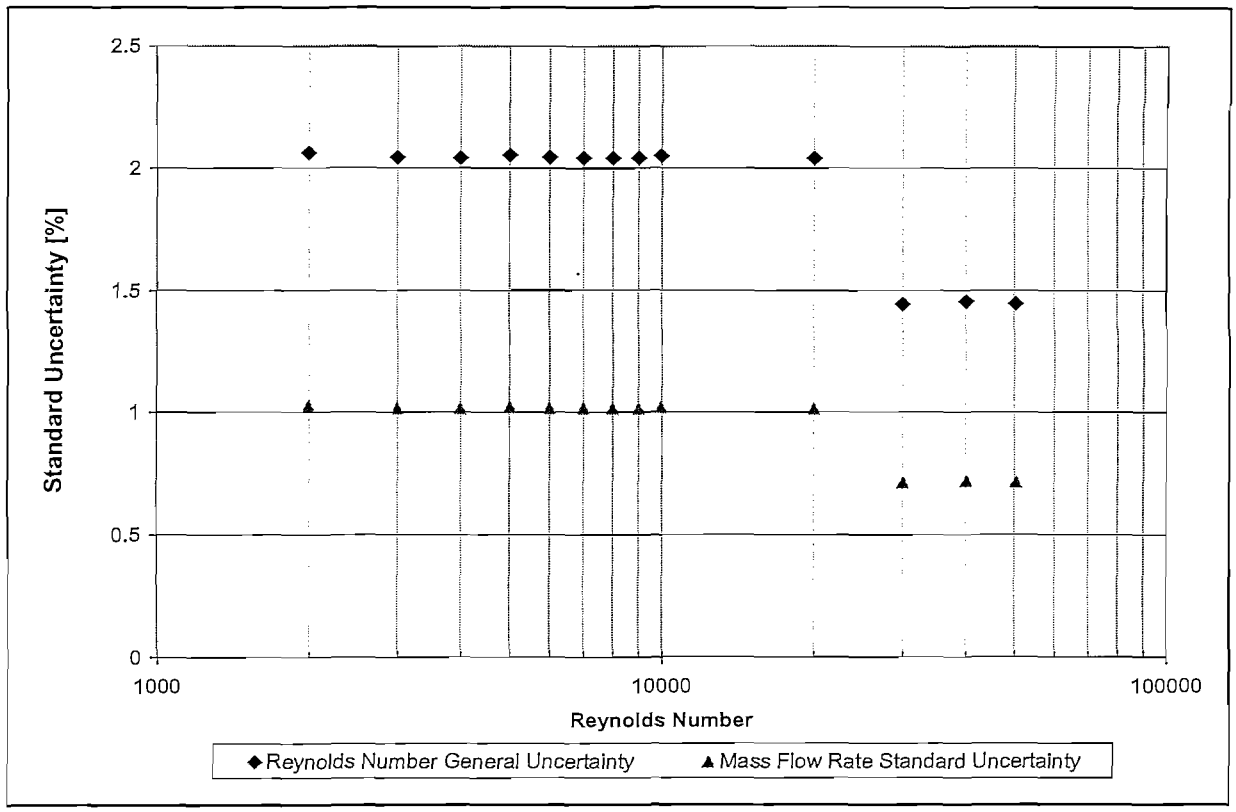

Figure 4.5 *Mass flow rate and Reynolds number standard uncertainty, PDTS045 test run 1*

at a Reynolds number of 30000 is due to the fact that both orifice stations are used above Reynolds numbers of 20000, and that the combined uncertainty is smaller than the uncertainty of a single orifice station.

The main contributor to the uncertainty in the mass flow rate is the uncertainty of the discharge coefficient, which is 1% of the calculated discharge coefficient. The successful installation of the orifice stations to reduce the uncertainty in the discharge coefficient is therefore evident.

The general uncertainties in the calculated Euler number from the PDTS045 test run 1 measurements are shown in Figure 4.6. The influence of the mass flow rate uncertainty in the Euler number is once again evident and even more pronounced. The step at a Reynolds number of 30000 is once again attributed to the use of both orifice stations. The maximum general uncertainty in the Euler number with a confidence interval of 95% is 4.62% for the PDTS045 test run 1 measurements. This is lower than the initially required 6.5% specified by Rousseau (2005a). The uncertainties in the Euler numbers of all the measurements are given in Table D.. The maximum Euler uncertainty from all the tests is 4.63% of the calculated value. From the uncertainty analysis it can therefore be concluded that the instrumentation

were correctly selected, installed and calibrated to obtain the desired level of confidence of 95% in the Euler number measurement for an uncertainty below 4.63%. The uncertainty analysis also showed that the criteria set for the determination of steady-state conditions were sufficient and that the change in the value of a variable during the time which the values were logged did not influence the uncertainty significantly.

The uncertainty in the friction factor was not predicted before the test in the Uncertainty Analysis Report (Rousseau, 2005b). The uncertainty in the friction factors of the homogeneous porosity test sections is much lower than the friction factors of the SAPB and the SCPB pressure drop tests. This is mainly due to the lower uncertainty in the average porosity of the homogeneous porosity test sections, which is more difficult to obtain in randomly packed beds. The maximum uncertainty in the homogeneous porosity test section friction factors is 5.89%, and 17.9% for the randomly packed beds. This uncertainty is for a confidence interval of 95%. The uncertainty in the Euler numbers and the friction factors are tabulated in Appendix D for each test.

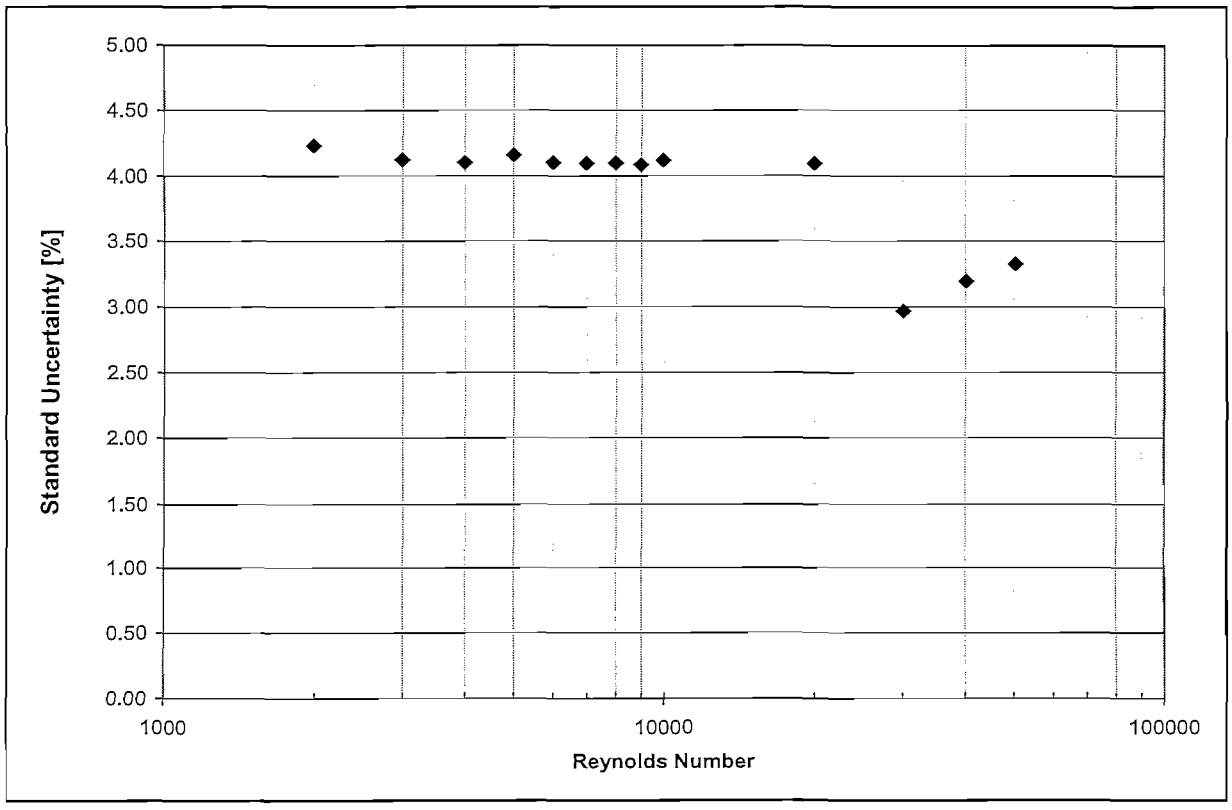

Figure 4.6 *Euler number uncertainty in for the PDTS045 test run 1 measurements*

4.4 Repeatability

As examples of the repeatability of an IET and a SET pressure drop test the Euler number calculated for both test runs of the PDTS045 and SCPB pressure drop tests are compared in Figure 4.7 and Figure 4.8. Both the comparisons indicate that excellent repeatability was obtained during the test runs. These results provide confidence in the measurements and the calculation procedures. The results also show that the Reynolds number could be controlled effectively to obtain a specific Euler number.

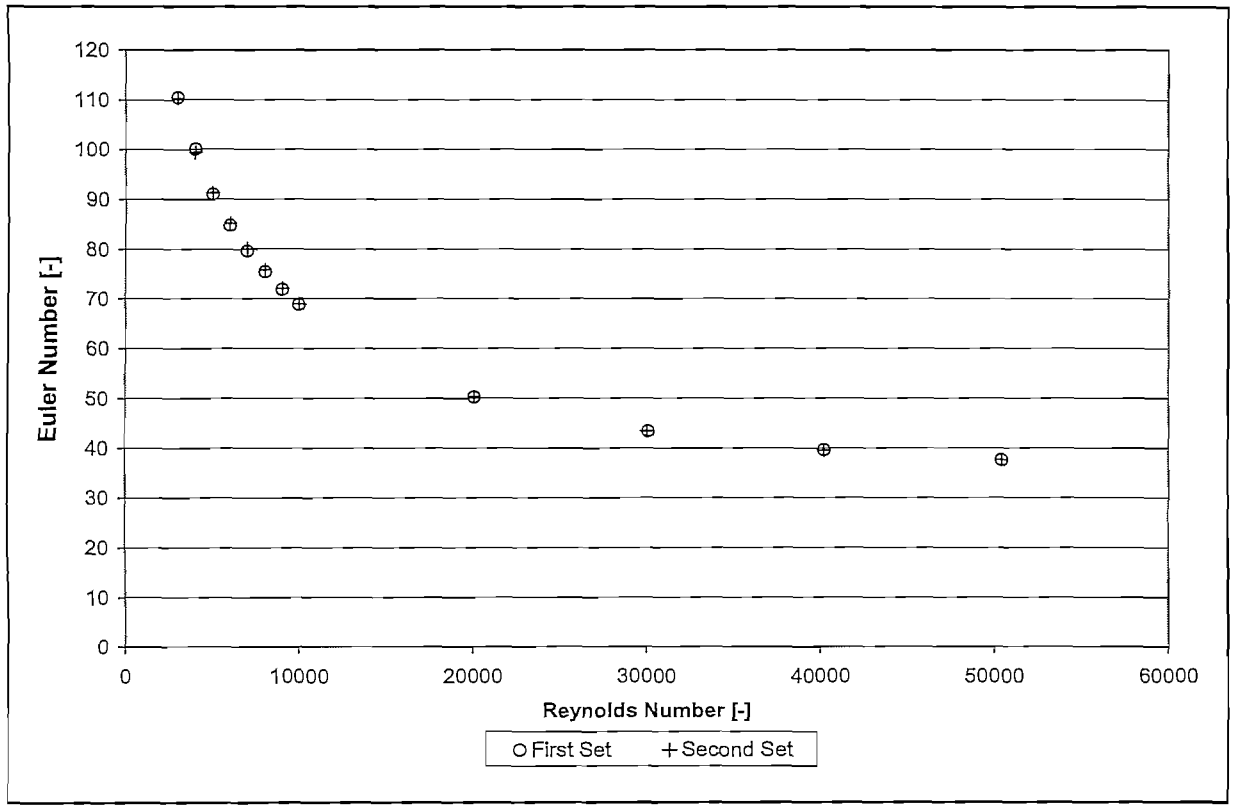

Figure 4.7 *Comparison between the Euler numbers of the two test runs of the PDTS045 test*

The percentage deviation between the first and second test run of each test is shown in Appendix D. The maximum deviation between the Euler numbers of two test runs at a specific set point is 1.79% of the average of the two Euler numbers. All other deviations are below 1%, and therefore within the estimated Euler number uncertainty. The repeatability of the PDTS036, PDTS039 and SAPB pressure drop tests are provided in graphical form in Appendix D. From the uncertainty analysis and repeatability results it can be concluded that

the measurements and the processed data are both reliable and of high quality. The processed results can now be compared with correlations found in the literature survey.

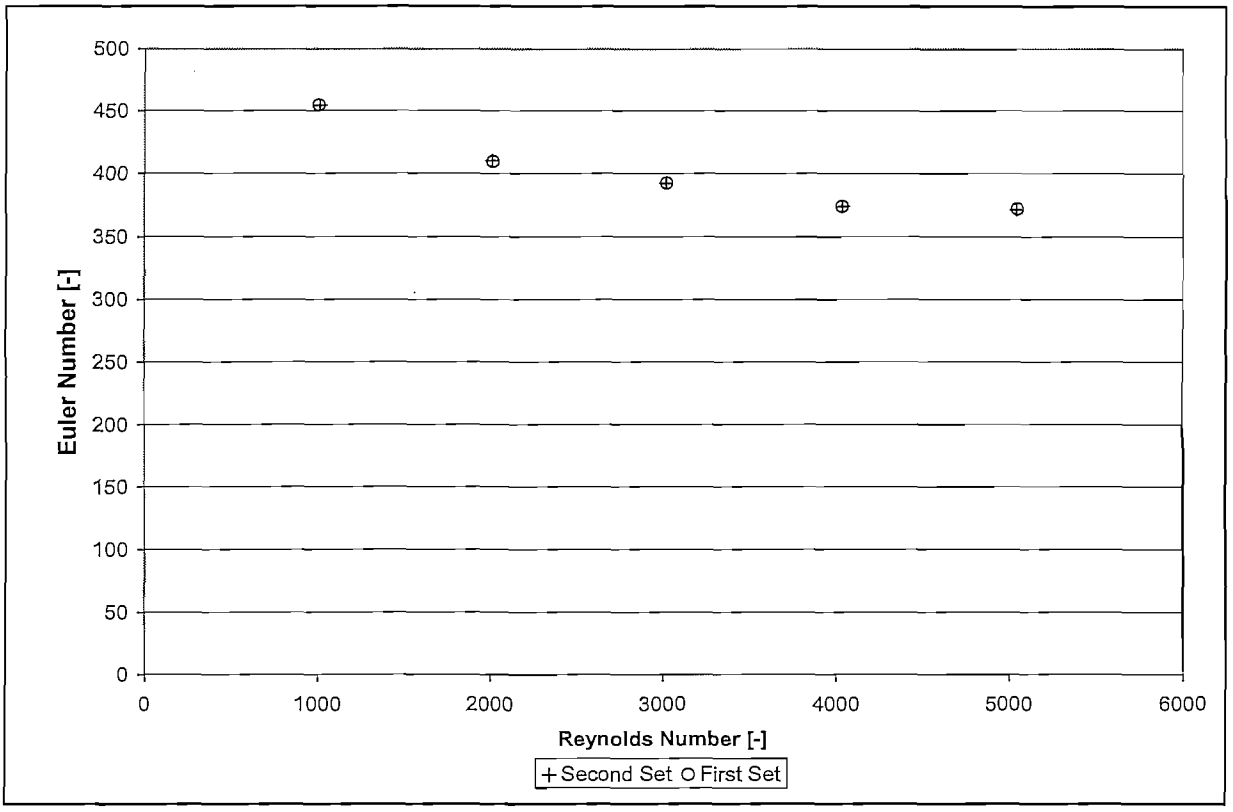

Figure 4.8 *Comparison between the Euler numbers of the two test runs of the SCPB test*

5 RESULTS AND DISCUSSION

In the previous chapter the integrity and quality of the data were investigated, and were shown to be within the specifications originally desired. In this chapter the results will be evaluated further to indicate whether the purpose of the tests as originally intended is fulfilled. This is done by comparing the results with correlations. In the case where the experimental results deviate from the correlations, possible reasons will be speculated. Note that the purpose of this chapter is not to give a verdict regarding the correlation used by PBMR or to give an exact explanation for deviations. The comparisons should firstly show from a qualitative point of view whether the results from the SETs can be used to verify the KTA equation and possibly derive new more reliable correlations for the use in coarsely discretized thermal-fluid simulation models such as Flownex (2006). Likewise in the case of the IETs the comparison must show qualitatively whether the data can be used for verification of the KTA equation for the prediction of the total pressure drop. Secondly, if deviations occur, possibilities for the differences will be investigated with the knowledge obtained from the literature survey to show whether the differences are of primary or secondary importance.

5.1 SET pressure drop results and discussion

The results of the SETs are first compared with correlations from the literature. The KTA equation is used as first reference, since it is the correlation currently used by PBMR. The repeatability of the experiment was proven and only the results from the first test run are used for comparisons in Figure 5.1 to Figure 5.4. Also included is the Euler number predicted by the correlation of Wentz and Thodos (1963), since their experiments with distended beds resemble the homogeneous porosity test sections more closely It can be seen from the comparison of the results with the correlations that the Euler number is considerable over predicted by the KTA equation and the Wentz and Thodos correlation, even though it seems as though the same type of curve is obtained.

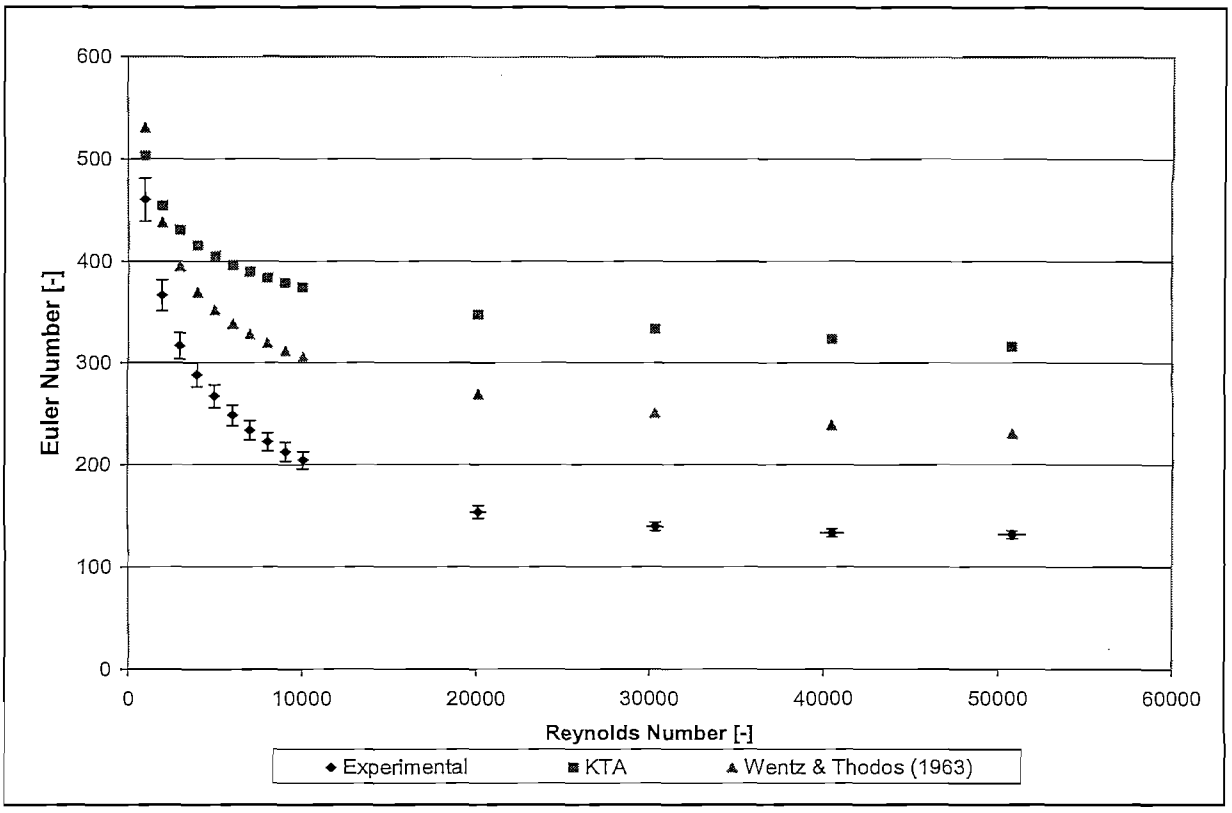

Figure 5.1 *Comparison of the experimental and expected Euler numbers: PDTS036-01*

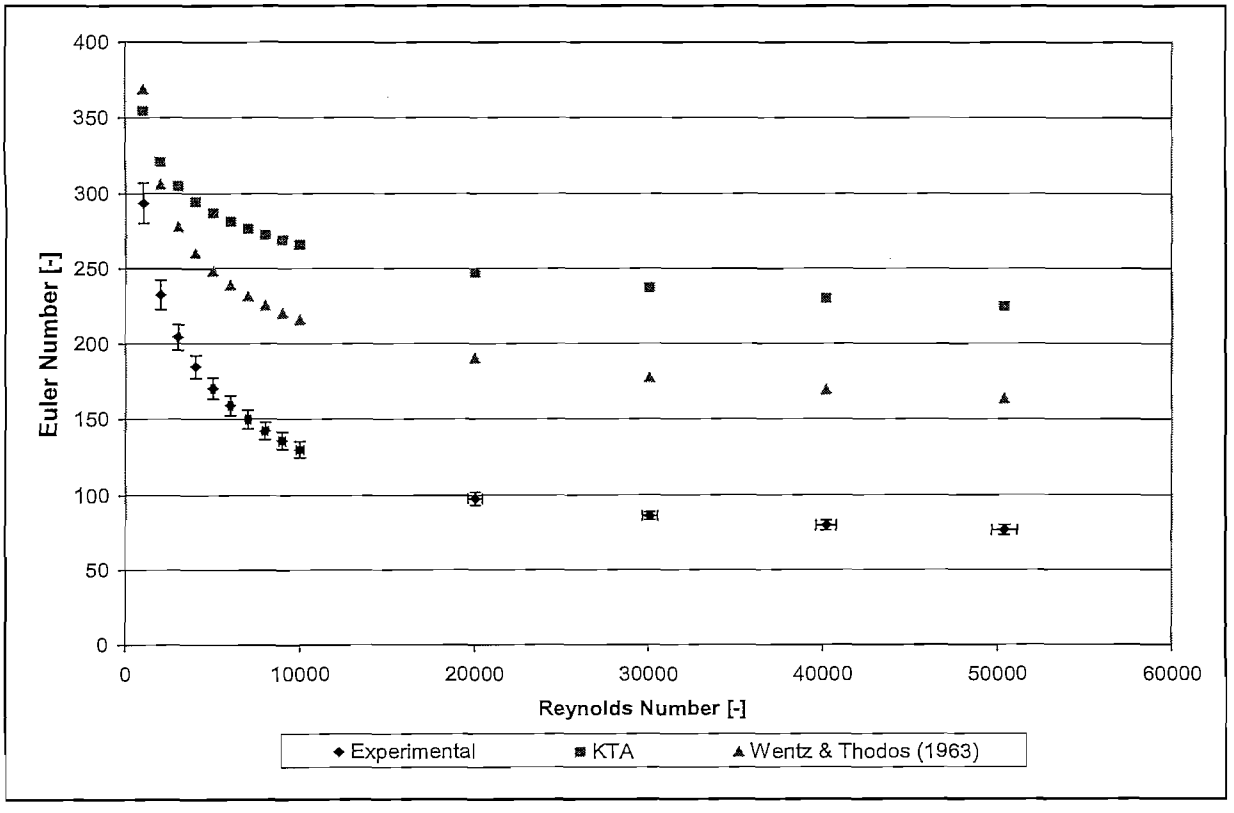

Figure 5.2 *Comparison of the experimental and expected Euler numbers: PDTS039-01*

From the three graphs comparing the experimental and predicted Euler numbers it can be seen that the PDTS036 Euler numbers are better predicted, with the errors in the predicted Euler number increasing as the porosity increases. The percentage errors between the predicted and experimental Euler numbers are given in Appendix D for each test. To investigate why the error in the Euler number increases for an increase in the porosity, the results are more appropriately compared by calculating the friction factors for each test section as shown in Figure 5.4. Note that the friction factor is presented as a function of the modified Reynolds number. The error in the experimentally calculated friction factor was not estimated. It can be seen that the friction factor decreases with increasing porosity for the homogeneous porosity test sections. The predicted friction factors from the KTA equation and the correlation by Wentz and Thodos (1963) are less independent on the modified Reynolds number. It could in general be expected that the friction factors calculated from different experiments would differ to some extent since secondary influences are not necessarily included or accounted for, as was shown for the influence of the wall friction and porosity variation in the literature survey. However, for the primary contribution of the pressure drop, i.e. the particle resistance to the flow in both the laminar and turbulent regimes, such a dramatic variation is unexpected.

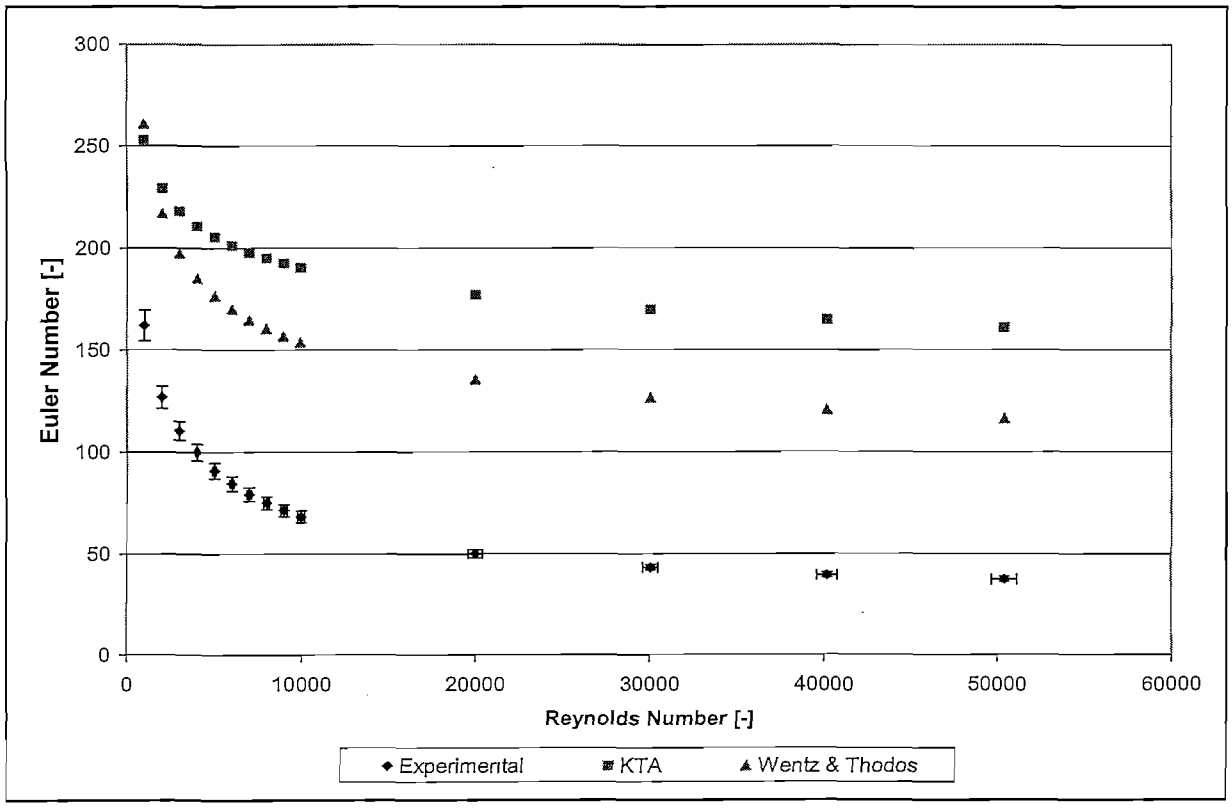

Figure 5.3 *Comparison of the experimental and expected Euler numbers: PDTS045-01*

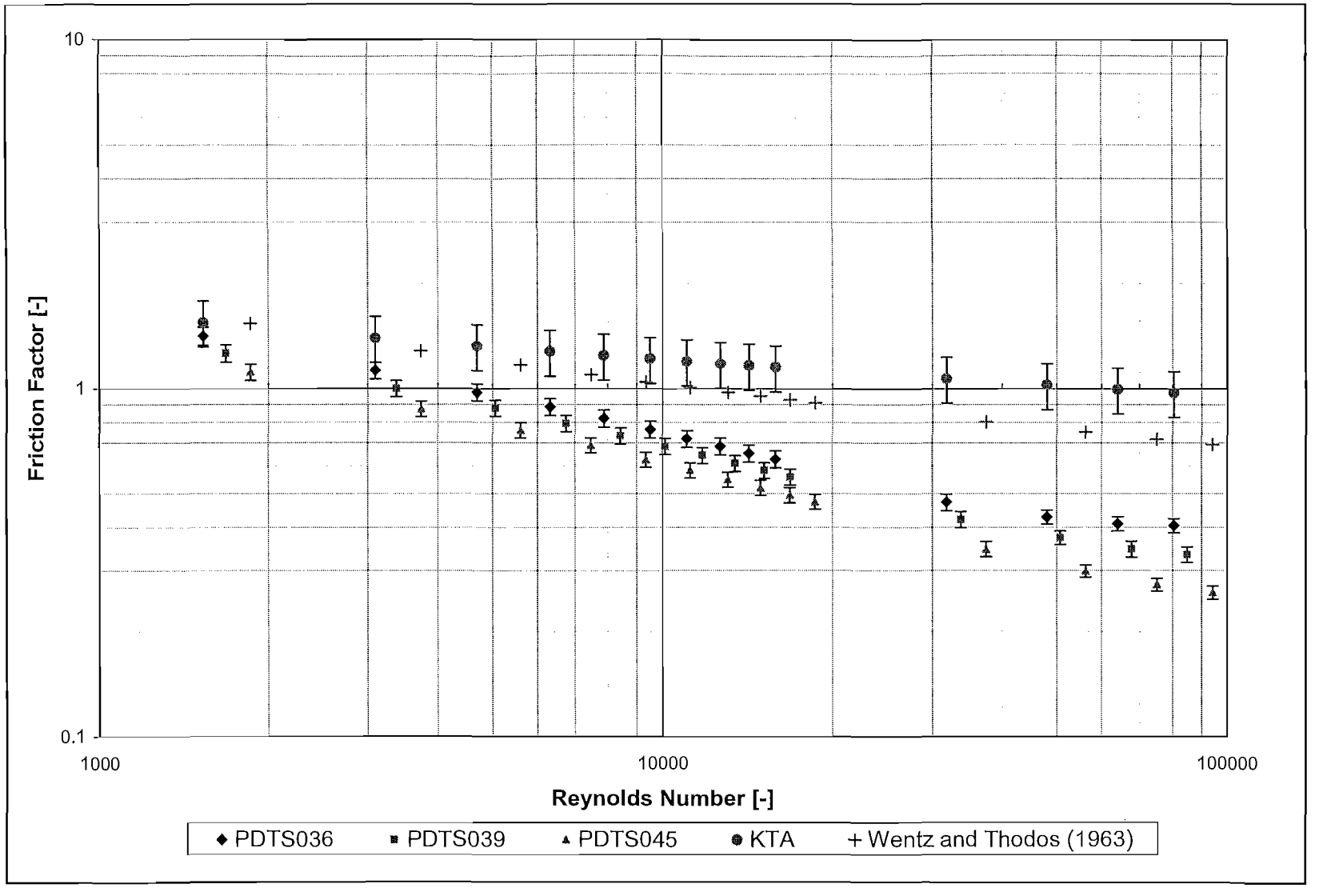

Figure 5.4 *Predicted and calculated friction factors for each homogeneous porosity test section*

Since the purpose of the dimensionless parameters is to enable comparison of the pressure drop for different geometries (porosities and bed-to-particle diameter ratios), mass flow rates, particle sizes etc., it follows from Figure 5.4 that the friction factors calculated for the SETs are not predicted by the general form of the friction factor in equation (5), but has some further dependency on the porosity or other characteristic parameter which are not accounted for.

The correlation by Wentz and Thodos (1963) predicts the friction factor more closely, but does not predict the observed difference of the friction factor for different porosities, even though a very wide range of porosities were investigated. From Figure 2.1 it is noticed that the friction factors correlated for structured beds by Erben (1967) and Barthels (1972) are similar to the KTA correlation, and predicts the same friction factor for structured and randomly packed beds. In the experimental investigation of Wentz and Thodos (1963) the particles adjacent to the walls were cut to obtain a homogeneous porosity throughout the bed. This would eliminate any by-pass flow, whereby the wall friction would also be reduced and also the total pressure drop. This possible reduction in the pressure drop would however be extremely small compared to the total pressure drop, as was shown by Winterberg and Tsotsas (2001), and does not seem to be a sufficient explanation for the lower friction factors predicted by Wentz and Thodos (1963). The cause for the reduction in friction factors calculated from both the correlation of Wentz and Thodos (1963) and the HPTU SETs must therefore lie in the structure of the beds used. The porosities of the SETs in the HPTU experiment were calculated from the total volume of the bed and the total volume of the particles. A desired average porosity is obtained without considering any variation of the porosity in the radial and axial direction. In the case of the HPTU SETs the pebbles are suspended and do not touch. It is therefore possible that voids or regions with higher porosities are connected to form channels or preferred flow paths. Such channels would have the same effect on the pressure drop as the increased porosity close to the walls in a randomly packed bed. The influence of wall friction will however not be present and the pressure drop would be significantly lower, similar to the pressure drop calculated for packed beds with a variation in porosity without using an effective viscosity.

From Figure 5.4 the influence of the particles on the pressure drop is evident, and the friction factor is typical of that calculated for packed beds, only significantly lower. It is possible that the general pressure drop correlations such as the KTA equation is still valid for the prediction of local pressure drop. A pseudo-homogeneous model could therefore be used to

investigate the pressure drop and flow through the bed, if the variation in the porosity is known.

At high modified Reynolds numbers ($Re_m > 50000$) the PDTS036 friction factor is observed to tend to a fixed value of 0.4. If the friction factor becomes independent of the Reynolds number at some point, the possibility exists that preferred flow paths act in a similar way as the channels existing in randomly packed beds close to the walls where the peak value in the normalized velocity becomes independent of the Reynolds number. This would imply that the pebbles surrounding a preferred flow path or channel acts as walls, and that the influence of the viscosity is significant for the pressure drop through the preferred flow path. In the case of the PDTS039 this also seems to take place, but at higher modified Reynolds numbers. The PDTS039 is packed in exactly the same way as the PDTS036, but is expanded to obtain the desired average porosity. The size of preferred flow paths relative to the particle diameter is therefore larger, and the influence of the pebbles surrounding the flow paths will be less significant. This could also apply to the PDTS045, in which the friction factor could become independent of the modified Reynolds number at still higher Reynolds numbers. Such possible explanations must however be confirmed experimentally at higher Reynolds number, especially for the PDTS039 and PDTS045, and should also be investigated through detailed numerical experiments.

The results from the pressure drop SET experiments does not seem to be very useful to develop correlations for specific average porosities in network codes such as Flownex (2006). The dependency of the friction factor on the average porosity was not expected during the design of the test sections, and the deviation in the predicted friction factor from the experimental results cannot be ascribed to secondary influences. It is clear that further investigation of the pressure drop through distended beds is needed, and that the interpretation of the average porosity must be carefully considered. To investigate and develop correlations for coarsely discretized thermal-fluid simulation codes the use of structured packed beds must be investigated.

5.2 IET pressure drop results and discussion

5.2.1 SCPB pressure drop results

The results from the SCPB pressure drop tests are presented first and compared with friction factors predicted by different correlations in Figure 5.5. The general error with a 95% confidence interval was estimated for each calculated friction factor using equation (50). Friction factors are firstly compared with the KTA equation. It is clear that the predicted friction factor is within the general uncertainty of the experimentally calculated and predicted average friction factors. The uncertainties of the predicted KTA friction factors and of the experimentally calculated frictions overlap in each case. The KTA equation underpredicts the average value of the calculated experimental uncertainty. The percentage difference between the calculated and predicted friction factors vary between 3.3% and 4.8%.

The results are secondly compared with the friction factors predicted by the model of Reichelt (1972) with the constants proposed by Eisfeld and Schnitzlein (2001). From this comparison it is clear that the experimentally calculated friction factors are dependant on the modified Reynolds number well into the turbulent flow regime, and follows the Carmen-type prediction with a systematic deviation. It can therefore firstly be concluded that friction factors calculated will be best predicted by a Carmen-type correlation, and not an Ergun-type correlation. The third important comparison to be made is with the correlation by Brauer (1960). This correlation is very similar to the KTA equation, with the constant in the term representing the turbulent pressure loss differing slightly. The correlation by Brauer (1960) gives an even better prediction in the average values, with the percentage difference varying between 0.2% and 1.67%. Since the bed-to-particle diameter ratio is very large ($\approx$62), it seems that the correlation by Brauer (1960) is the most appropriate correlation for the prediction of the pressure loss due to the particles without the influence of the walls. Qualitatively the results from the SCPB compare extremely well with the correlations found in the literature.

To investigate the slight difference with the correlation of Brauer (1960), effective viscosities were calculated from the method outlined by van der Walt and Du Toit (2006), and used in equation (22) to investigate whether this difference is possibly due to the walls. The porosity variation given by Hunt and Tien (1990) in equation (11) was used, with the bulk porosity adjusted so that integration of equation (11) would give the average porosity calculated for the SCPB test section. The total pressure loss in equation (22) was calculated with the correlation

by Reichelt (1972) as modified by Eisfeld and Schnitzlein (2001), while using the same correlation without the influence of the walls as the friction factor due to the pebbles. Equation (22) was then solved, with the effective viscosity optimized to give the same total pressure drop. To investigate how the walls influence the pressure drop, the calculated effective viscosity was used in conjunction with the correlation of Brauer (1960) to predict the total pressure drop. A friction factor was calculated from the predicted total pressure drop and is compared in Figure 5.5. (PHM refers to Psuedo Homogenous Model and Fk to friction factor). Note that the values for the KTA predicted friction factors and the experimentally calculated friction factor are plotted at slightly off-set Reynolds numbers for clarity, and actually coincides with the other Reynolds numbers. The pressure drop predicted with the influence of the walls included is between 1.4% and 1.6% larger than with the correlation of Brauer (1960). The percentage difference between the experimentally calculated friction factors and the predictions are shown in Figure 5.6.

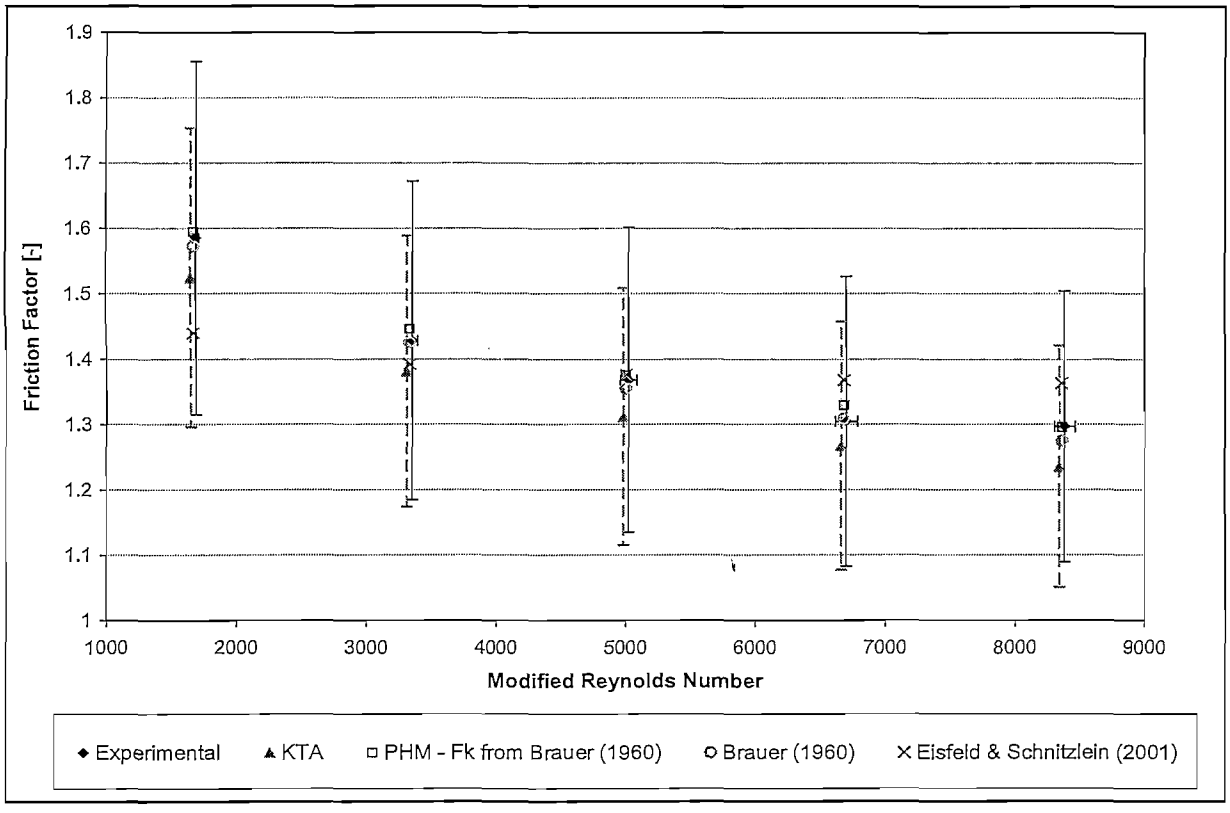

Figure 5.5 ***SCPB friction factor results and comparison***

An improvement is observed in some of the predictions, but not systematically, and in some cases larger deviations occur. An overall improvement can therefore not be claimed showing

that the difference between the experimental and predicted friction factors cannot definitely be attributed to the influence of the walls.

From this comparison with the average values it can however be concluded that the correlation by Brauer (1960) predicts the pressure drop for packed beds with spherical particles at large bed-to-particle diameter ratios fairly accurately and better than the KTA equation. Since it was shown that the influence of the walls should be very small, it can also be concluded that the correlation of Brauer (1960) represents the friction factor for an infinite packed bed fairly well. The SCPB pressure drop test is therefore successful in producing experimental data for Reynolds numbers well into the turbulent flow regime for the pressure drop through a test section where only the particle friction is of importance. The results from the SCPB pressure drop tests can therefore be used with confidence to evaluate or develop correlations to predict the particle friction factor.

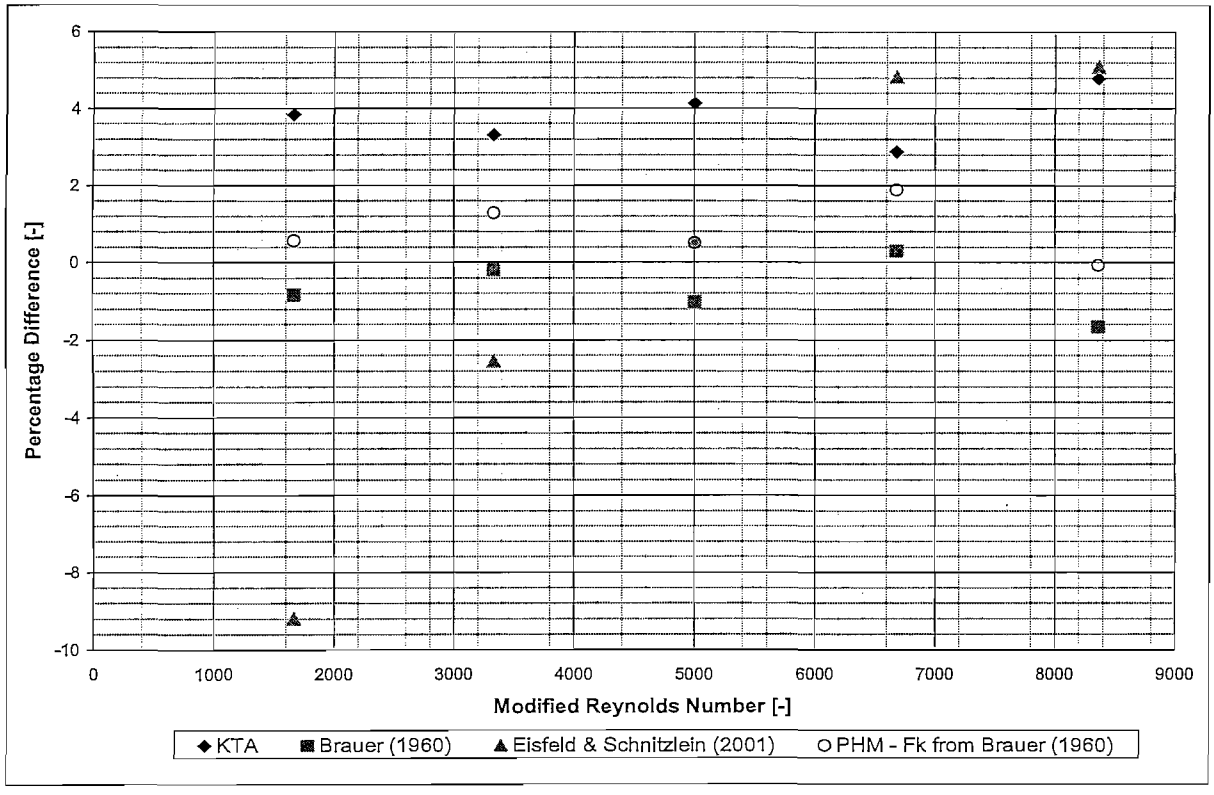

Figure 5.6 *Percentage difference between experimental and predicted friction factors*

5.2.2 SAPB pressure drop results

The SAPB pressure drop test results are presented in the same manner as the SCPB test results. The KTA predicted friction factors are firstly compared to the experimentally calculated friction factors in Figure 5.7. Note once again that the values for the KTA predicted friction factors and the experimentally calculated friction factor are plotted at slightly off-set Reynolds numbers for clarity. The average friction factor calculated from the experimental data includes a general uncertainty with a coverage factor of 1 calculated for the influence of the bed length, average porosity, particle diameter and Euler number uncertainties. The average KTA predicted friction factors deviate systematically from the experimentally calculated friction factors, and falls just within the uncertainty bands of the experimental results. The experimental results are also within the uncertainty of the KTA equation. The KTA predicted friction factors differ from the experimental results between 6.5% and 8.1%. Figure 5.7 also show the predicted friction factors from the correlations by Brauer (1960), which deviate systematically from the experimental results similarly to the KTA equation. The correlation by Brauer (1960) predicts the results slightly better, with the difference between the prediction and the results varying between 3.45% and 5.1%. From these comparisons it can firstly be concluded that the pressure drop through annular packed beds with spherical particles also follows a Carmen-type correlation, and not an Ergun-type correlation because of the dependence on Reynolds number.

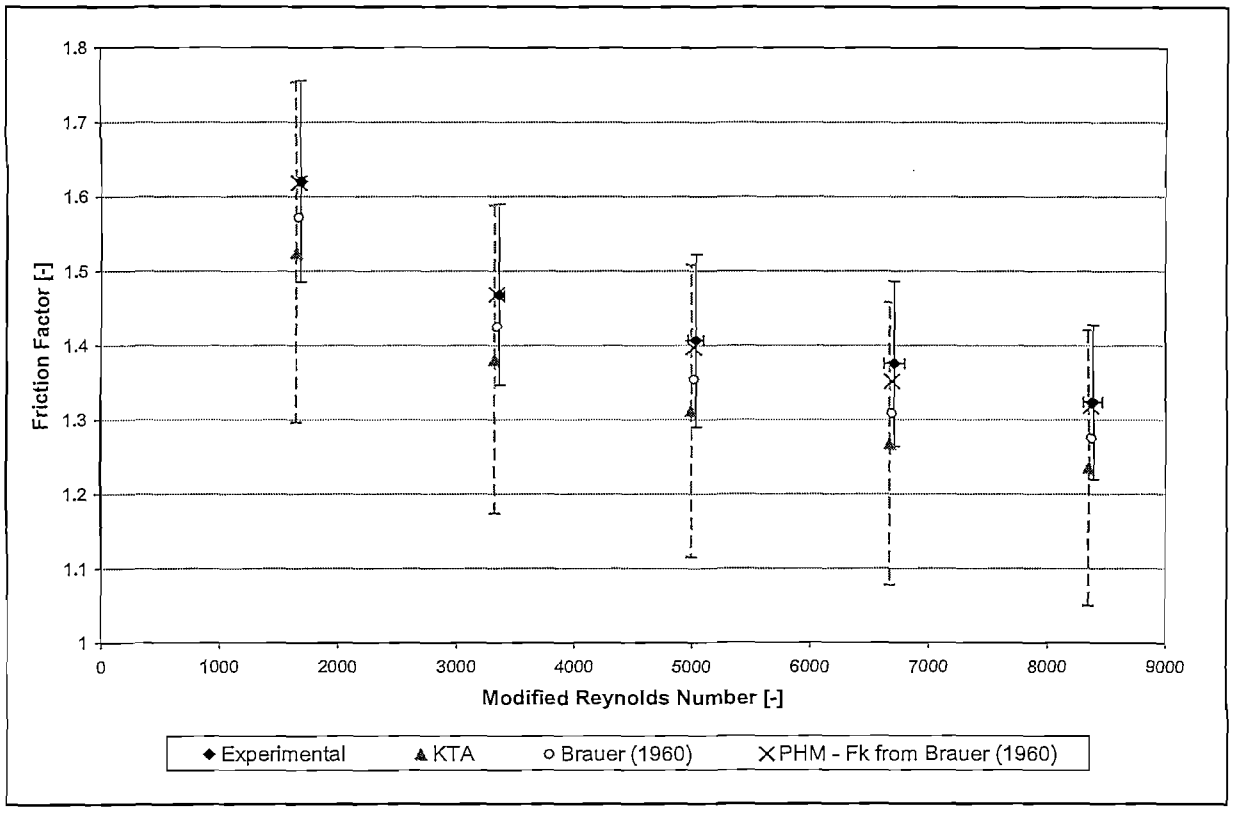

Figure 5.7 *SAPB friction factor results and comparison*

The difference between the results and the predictions are investigated in a similar way as done for the SCPB. From the discussion in the theoretical background it could be expected that the presence of the two walls in an annular bed will influence the pressure drop. There is therefore reason to believe that this difference could be due to the walls. The pseudo-homogeneous model is used to test this, with an effective viscosity obtained from the method by Van der Walt and Du Toit (2006). To obtain an effective viscosity to use in equation (22) a cylindrical packed bed with the same bed-to-particle diameter ratio as the annular width-to-particle diameter ratio of the SAPB is used. The porosity variation by Hunt and Tien (1990) is once again assumed, and the bulk porosity adjusted so that integration of equation (11) gives the same average porosity as calculated for the SAPB. It is then assumed that the effective viscosities calculated for the cylindrical packed bed are applicable to the annular configuration. In each case the exact same values of the density and viscosity were used as calculated for each measurement. Equation (22) is then used for the annular configuration along with the predicted effective viscosities and the friction factor predicted by Brauer (1960). From the results of the SCPB it is assumed that the correlation by Brauer (1960) will predict the friction factor the best without including the wall friction. For each Reynolds

number the pressure drop was calculated to match the mass flow rate, and a friction factor could be determined. The friction factors calculated from this procedure are also shown in Figure 5.7 with *PHM* meaning pseudo homogenous models and F_k referring to the friction factor used. The percentage difference between the results and the different predictions is shown in Figure 5.8. A significant improvement in the prediction of the friction factor is obtained. The percentage difference between the experimental and predicted values ranges between 0.5% and 2%.

The ratio between the effective viscosity and the dynamic viscosity is shown in Figure 5.9 against the modified Reynolds number. The ratio of the effective viscosity to the dynamic viscosity gives a quantitative indication of the degree to which turbulent mixing takes place. Figure 5.9 also shows the ratio between the friction factors calculated using the effective viscosity and the friction factors predicted by Brauer (1960). The ratio between the effective and dynamic viscosity increases linearly with the modified Reynolds number. The ratio between the friction factors increases with the modified Reynolds number, but not linearly. This could suggest that the influence of the wall friction becomes independent of the modified Reynolds number at higher modified Reynolds number.

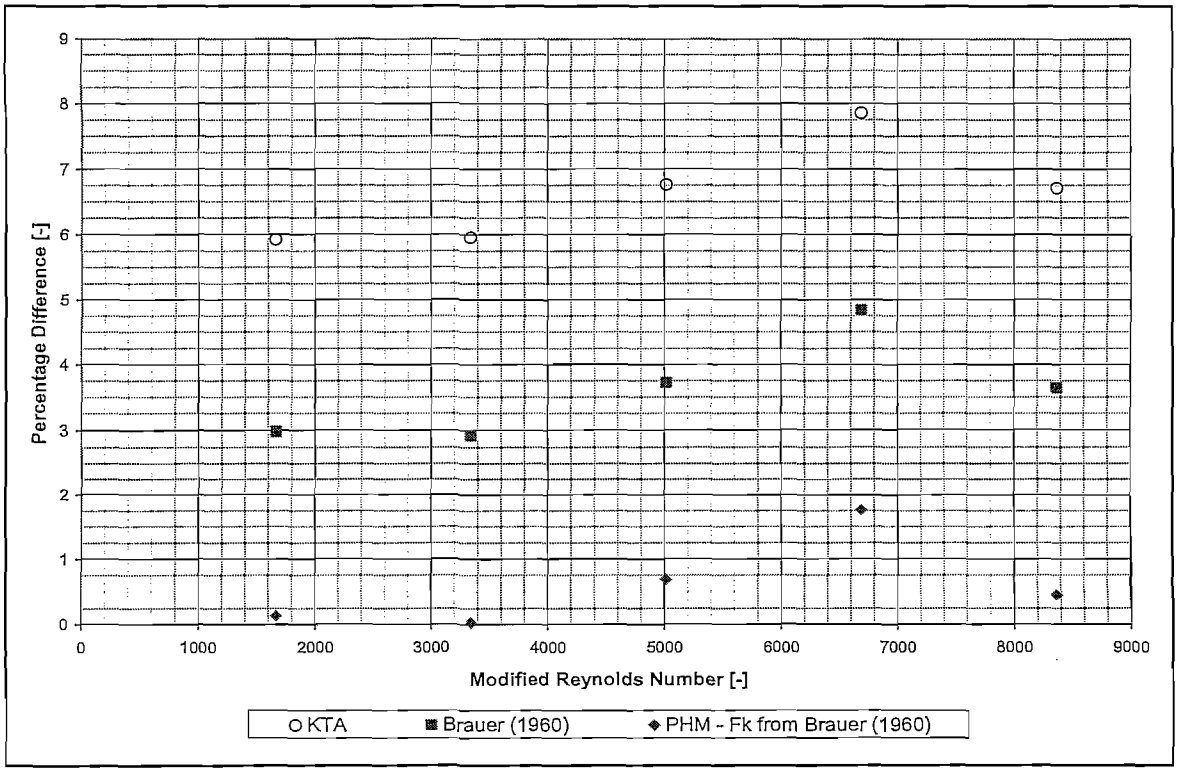

Figure 5.8 *Percentage difference between experimental and predicted friction factors*

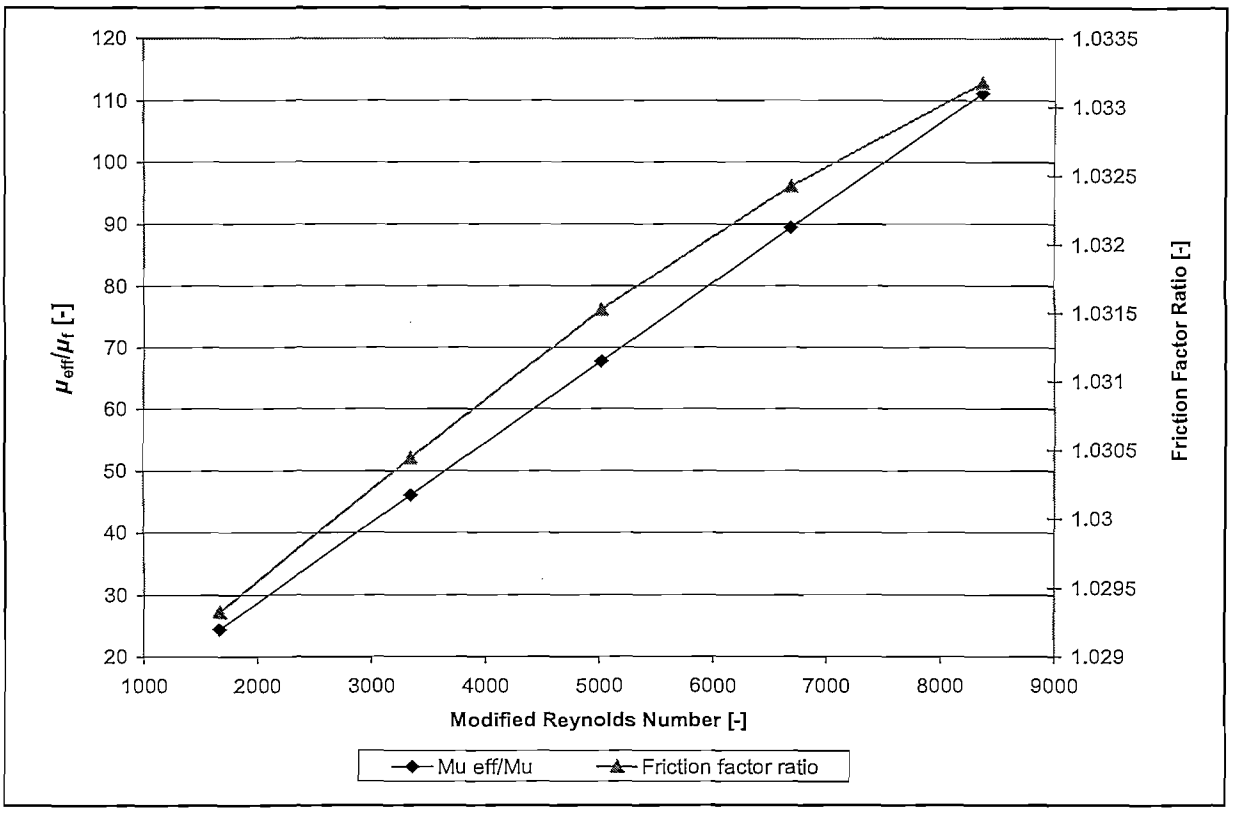

Figure 5.9 *Ratio between the friction factors and the effective and dynamic viscosity*

It must be emphasized that the procedure used to estimate the effective viscosity and the simple one-dimensional model in which it is implemented are not claimed to describe and predict the complex flow phenomena exactly. The model simply indicates that the difference between the experimental friction factors and friction factors from correlations can possibly be ascribed to the influence of the walls. The results from the SCPB pressure drop test motivate the use of the correlation by Brauer (1960) to predict the friction factor due to the particles alone. In both the SAPB and SCPB tests the friction factor calculated at a modified particle Reynolds number of 7000 seems to deviate slightly from the general trend. In neither of the cases the deviation could be attributed to a change in instrumentation.

5.2.3 Comparison between the SAPB and SCPB results

The results of the SAPB and SCPB pressure drop tests are finally compared to quantify the difference between the pressure drop in cylindrical and annular packed beds. Figure 5.10 shows the experimentally calculated friction factors for both the SAPB and SCPB measurements. Note once again that the values for the KTA predicted friction factors and the

experimentally calculated friction factor are plotted at slightly off-set Reynolds numbers for clarity.

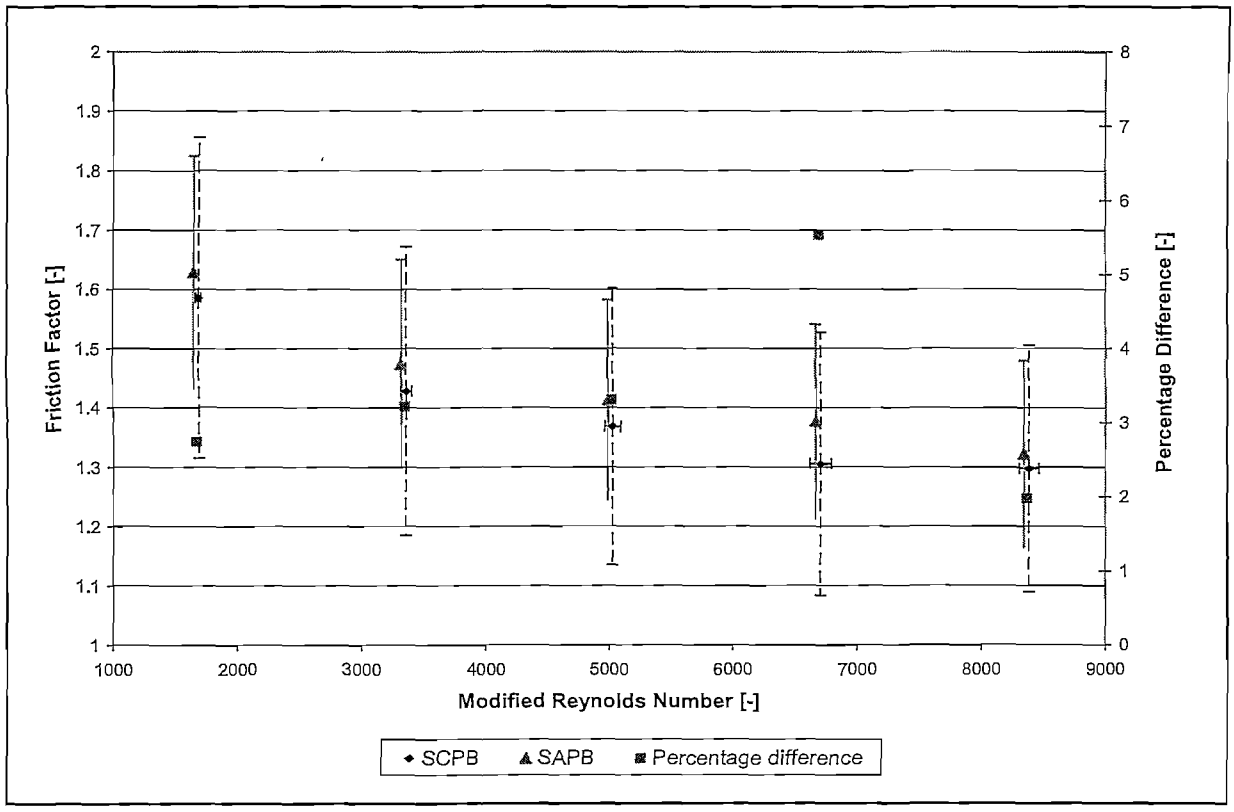

Figure 5.10 *Comparison between the SAPB and SCPB results*

The difference between the friction factors as a percentage of the SCPB friction factor is also included. There does not seem to be any trend in the differences between the results other than that the SAPB friction factor is slightly larger. For each test all the measurements fall within the other test's calculated uncertainty. The difference between the pressure drop measured in annular and cylindrical packed beds is therefore smaller than the uncertainty in the measurement. The difference between the pressure drop in annular and cylindrical packed beds is systematic, but not significant. For smaller bed-to-particle diameter ratios of the cylindrical packed bed it could be that the difference between experimentally calculated friction factors become totally insignificant due to the influence of the walls.

5.3 Conclusions

A qualitative comparison was made between the pressure drop results and the correlations reported in the literature survey for both the separate effects tests (SETs) and the integrated

effects tests (IETs). The comparison of the SET results show that the pressure drop through the homogeneous porosity test sections behaves in a manner not expected. It was shown that the friction factor is extremely dependent on the average porosity and is not predicted by any of the correlations for randomly packed beds, structured packed beds or distended structured packed beds. From the literature survey it does not seem plausible that the deviation from the various correlations tested can be attributed to the influence of the walls. The dependency of the friction factor on the average porosity therefore seems to be an inherent characteristic of the packing design which has not been observed in other experiments. It does not seem meaningful to develop correlations from the experimental data to be used for calculating the pressure drop in thermal-fluid simulation models built from homogeneous porosity control volumes. Further investigation of structured and distended structured packed beds is therefore required.

The qualitative comparison between the IET pressure drop results and the correlations reported in the literature survey shows that the experimentally calculated friction factor follows a Carmen-type correlation the best for both the cylindrical and annular configurations investigated. It was found that the correlation by Brauer (1960) predicts the friction factor the best for the SCPB pressure drop tests, and that the influence of the walls for such a large bed-to-particle diameter ratio is negligible.

The pseudo-homogenous model (equation (22)) reported in the literature survey showed that the deviation between the experimental results of the SAPB and the particle friction factor predicted by Brauer (1960) could possibly be attributed to the influence of the walls. The correlations for the particle friction factor and the models predicting the influence of the wall showed that the results of the IET can be used for the purposes originally intended and that the measurements are successful. The results from the IET further show that the deviation in the SET results is not due to faulty instrumentation i.e. some systematic error. The purpose of the literature survey is therefore also satisfied.

6 CONCLUSIONS AND RECOMMENDATIONS

6.1 Overview of the background and aim of the study

In the Introduction the importance of the development of the PBMR nuclear reactor in South Africa was emphasized for economic and social development to take place on a continuous and sustainable basis. Thermal-fluid simulations play an important part in this development, both for the design of the integrated plant and the prediction of safety characteristics of a pebble bed nuclear reactor. At the hart of fast modelling approaches suggested for simulation of both steady-state and transient operations are thermal-fluid correlations that predict the flow and heat transfer macroscopically for immensely complex phenomena. Such correlations, including pressure drop correlations can only be used if thoroughly investigated through high quality experiments. The best correlations available for the prediction of the pressure drop have not been derived in the adequate quality assurance environment. Experimental investigation of the pressure drop through annular packed beds has furthermore received very little attention in the past, and no conclusive experimental results exist in the literature that can show whether there is indeed a noteworthy difference between the pressure drop through annular and cylindrical packed beds.

For among other purposes the Heat Transfer Test Facility was developed to investigate the pressure drop through a series of homogeneous porosity test sections and randomly packed beds. The High Pressure Test Unit was successfully deployed and was proven during the commissioning phase as capable of delivering the desired Reynolds numbers at which the pressure drop correlations should be verified. An experimental facility that could address the general problems regarding pressure drop correlations was therefore successfully developed.

The aim of this study was to establish a data processing procedure that could be used to convert the raw data into meaningful results. This included the determination of steady-state conditions and an uncertainty analysis that would enable the results to be presented with a certain confidence and investigation of the repeatability. However, a simple presentation of the results would not be enough to show that the experiment results are credible. A thorough comparison with existing correlations was therefore necessary to show that the pressure drop were indeed measured and that both the measurements and the physical test sections used did not include undesirable trends or characteristics. The literature survey performed therefore

had to point out the best correlations to which the experimental could be compared to show that the results are conceivable and realistic. The literature survey also endeavoured to point out possible methods that could quantify the influences not taken into account in the general correlations found in the literature survey, such as the variation in the radial porosity and the wall friction. Such methods would further aid in proving the credibility of the experimental data.

6.2 Summary of the Literature Survey

The literature survey pointed out that there are in general two types of correlations associated with the hydraulic diameter concept, namely the Ergun-type correlations and the Carmen-type correlations. The KTA-correlation is currently assumed to be the most appropriate for predicting the pressure drop through the PBMR core, and is of the Carmen-type. The study by Eisfeld and Schnitzlein (2001) further showed that the correlations by Brauer (1960) and Barthels (1972), which is very similar to the KTA equation is also very good candidates for predicting the pressure drop. The study by Eisfeld and Schnitzlein (2001) also showed that the most promising Ergun-type correlation is that of Reichelt (1972), which include terms to predict the influence of the walls implicitly.

The correlation by Wentz and Thodos (1969) was identified as the most important correlation to predict the pressure drop through distended structured beds. The experiments by Erben (1967) and Barthels (1960) also include measurements of the pressure drop through structured bed, but the correlations derived do not predict the same low friction factor as the correlation from the experiments by Wentz and Thodos (1969).

The correlation by Sodré and Parise (1998) were identified as the only correlation to predict the pressure drop through annular packed beds. The correlation is of the Ergun-type and predicts a much higher friction factor than the KTA-equation.

A method of predicting an effective viscosity can be used in a one-dimensional pseudo-homogeneous model for the prediction of the pressure drop with the variation in the radial porosity and the wall friction included was discussed. This method given by Van der Walt and Du Toit (2006) is based on the correlation of Reichelt (1972) to account for the wall friction and a method outlined by Winterberg and Tsotsas (2001) for investigating the influence of the walls and the porosity variation on the pressure drop.

6.3 Data processing methodology

Two criteria were proposed to predict steady-state conditions on the plant. The criteria were developed from experimental data of the important variables identified and are therefore purely empirical. The criteria were implemented into the control system and predicted steady-state conditions in real time. The criteria were compared with Excel calculations after each test and were shown to predict steady-state conditions sufficiently.

For each set point five continuous minutes of steady-state data were logged for further processing. This amounted to 600 data points per variable, which is sufficient for the calculation of statistical quantities. From the 600 data points for each variable an uncertainty analysis was performed. Systematic errors from the instruments were eliminated as far as possible using appropriate calibrated secondary standards to calibrate the instruments. The random errors due to the measurements and the systematic errors due to calibration of the instruments were included as uncertainties. In the calculation of an uncertainty of a variable the largest of the systematic and random errors were used. The final uncertainty in the Euler number, Reynolds number and friction factors were calculated with a 95% confidence interval. The uncertainties in the calculated Reynolds numbers are in the order of 2%. The largest uncertainty in the Euler number from all the tests was 4.63%, which is well below the initially desired 6.5%. The uncertainty in the friction factor is larger than that of the Euler number, with the largest uncertainty 8.45% for the homogeneous porosity test sections. The largest uncertainty in the friction factor for the integrated effects tests is 17.9%. In the construction of the homogenous porosity test sections the uncertainty in the length of the bed could be reduced by high machining tolerances. This was however not possible for the randomly packed beds, where an uncertainty in the length of the bed were assumed. The uncertainty in the bed length contributed markedly to the uncertainty in the porosity and the friction factor, and results in a larger uncertainty in the friction factor for the randomly packed beds.

The repeatability of the experiments was tested by performing each test twice. The repeatability of the experiments was found to be excellent with the maximum difference in the Euler number from two test runs at a set point is 1.79% from the average between the two values. All other differences are less than 1%. The excellent repeatability greatly increases the confidence in the measuring methods and consequently the results.

It can be concluded that the first aim of investigating the experimental data were very successful. The steady-state criteria prove to be invaluable in reducing testing time. The steady-state criteria also prove to be consistent in the prediction of steady-state conditions, as noticed from the consistently low random uncertainties.

The uncertainty analysis was successfully used to estimate the uncertainty in the Euler number, Reynolds number and friction factor. The uncertainty in the Euler number were lower than the initially desired values, showing that the measuring instruments and the secondary standard used for the calibration were correctly selected. The repeatability shows consistency in the measuring procedure.

In summary it can be concluded that the tests were successfully conducted and that the procedures developed aided in reducing the uncertainty in the measured variables. Raw data were successfully converted according to statistically based methods to average values with an associated uncertainty with a 95% confidence interval. Following the data processing procedure the processed data can be used with confidence in further comparisons.

6.4 Comparison with correlations

The successfully processed data were compared to correlations from the literature to give further credibility to the experimental results. The important correlations reported in the Literature Survey were compared firstly to the Separate Effects Test results. The comparison firstly showed that the KTA equation over predicted the current results in terms of the Euler number and the friction factor. The friction factor from the homogeneous porosity test sections are more dependant on the Reynolds number than the KTA equation, and also shows a high dependency on the average porosity. Higher average porosities resulted in significantly lower friction factors. The correlation by Wentz and Thodos (1963) predicts the experimentally calculated friction factors the closest, but does not predict the dependency of the friction factor on the average porosity. The explanation for the low experimental friction factors does not seem to be mainly ascribed to the wall friction, but rather to the characteristics of the packing arrangement. At high Reynolds numbers the friction factor for the 0.36 homogeneous porosity test section becomes less dependant on the Reynolds number and appears to approach a constant value, which suggests that the friction factor could become independent of the Reynolds number at very high Reynolds numbers. The same tendency seems to take place in the friction factor calculated for the 0.39 homogeneous

porosity test section. At the lower Reynolds numbers the experimentally calculated friction factor approach the correlations of both Wentz and Thodos (1963) and the KTA equation.

The integrated effects tests for a cylindrical-packed bed (SCPB) were firstly compared to the correlation by Reichelt (1972) as modified by Eisfeld and Schnitzlein (2001) and the KTA equation to show whether an Ergun-type or Carmen-type correlation would predict the pressure drop best. From the comparison friction factors from both the cylindrical and annular configurations are best predicted by a Carmen-type correlation, with the KTA equation predicting the friction factor systematically lower in both cases. The correlation of Brauer (1960) predicts the experimental results from the cylindrical configuration the best from all the correlations presented in the Literature Survey. It was shown by the use of the pseudo-homogeneous model (equation (22)) that the influence of the walls seem to be negligible. Considering the uncertainty in the calculation of the friction factors from the experimental results the correlation by Brauer (1960) predicts the average value of the friction factor fairly well with a maximum deviation of 1.67%.

For annular-packed beds (SAPB) the experimental friction factors were compared to the KTA equation and the correlation by Brauer (1960). Both correlations predict the friction factor systematically lower, with the correlation by Brauer (1960) giving a slightly better prediction. The results from the comparison of the correlation by Brauer (1960) and the SCPB friction factors suggests that the correlation by Brauer (1960) should be used as the friction factor in the pseudo-homogeneous model (equation (22)) to investigate the influence of the walls in the annular configuration. Effective viscosities were calculated following the method by Van der Walt and Du Toit (2006) and were used in equation (22) to predict the pressure drop with the wall friction and porosity variation included. A better prediction is obtained with a maximum difference in the frictions of 2%. This suggests that the influence of the walls could be significant in the prediction of the friction factor for annular packed beds. The average friction factors from the SAPB and SCPB pressure drop experiments differ with the SAPB results being slightly larger.

6.5 Conclusions regarding the success of the study

A data processing methodology was successfully established and implemented. Raw data from the pressure drop tests performed on the HPTU were processed into meaningful results.

The uncertainty in the experimental results were reduced by minimizing the systematic errors in the measurements through calibration and by establishing criteria to predict steady-state conditions to minimize systematic change in the measured variables during testing. An uncertainty analysis was performed and showed that the uncertainties were lower than the initially expected uncertainties. The repeatability of the experiments was proven by comparison of the test runs in each experiment. The good agreement adds confidence in the measured values. It can therefore be concluded that the process followed to reduce the data and ensure that unnecessary uncertainties were not included were successful. The pressure drop experiments were therefore successfully completed and produced credible and reliable results.

The Literature Survey provided important correlations regarding different types of packed beds, as well as possible methods of evaluating the influence of the walls. The correlations proved to be useful in evaluating the characteristics of the beds and the influence of the walls qualitatively. It was especially shown that the influence of the walls in annular backed beds could be important, and that this should investigated further. It was also shown that the pressure drop through the SET test sections does not behave as expected, and cannot be predicted by correlations thus far obtained from the literature. The literature presented in this study indicated possible aspects to be considered for the successful prediction of the pressure drop through different types of packed beds.

It can be concluded that the outcomes set in the aim of the study were successfully met. The processed experimental results can now be used with confidence to evaluate the correlation currently used for the prediction of the pressure drop through the PBMR core (the KTA equation). The experimental results can also be used to derive new correlations and aid in understanding the phenomena influencing the pressure drop in annular packed beds, such as the PBMR core.

6.6 Recommendations

Even though the pressure drop through the homogeneous porosity test sections behaved unexpectedly, and does not seem to provide useful data for the purpose originally intended, it is still very important that the characteristics resulting in this behavior are thoroughly

investigated. For this reason it is suggested that the SETs should be conducted at lower and higher Reynolds numbers than investigate in this study. This could indicate whether the flow behavior is different in the laminar flow regime, and whether the friction factor becomes independent of the Reynolds number at higher Reynolds numbers. The literature must further be investigated find similar experiments. The results by Erben (1967) and Wentz and Thodos (1963) must also be critically evaluated, as well as the respective experimental setups. CFD simulations are also a possible tool for investigating the important flow phenomena.

The physical meaning of the use of an effective viscosity in flow models must be thoroughly investigated. This is important since a proper mathematical model has not been established while the use of an effective viscosity has proven to be valuable in the investigation of the wall effects. It is also suggested that a cylindrical-packed bed with a bed-to-particle diameter ratio equal to the annular width-to-particle diameter ratio of the SAPB should be investigated to determine whether the influence of the walls for cylindrical and annular configurations are very different or not.

REFERENCES

ACHENBACH, E. 1995. Heat and flow characteristics of packed beds. *Experimental Thermal and Fluid Science,* 10:17-27.

ANON. Auslegung der Reaktorkerne von gasgekühlten Hochtemperaturieaktoren, Teil 3: Reibungsdruckverlust in Kugelhaufen. KTA 3102.3, 1981.

BARTHELS, H. 1972. Druckverlust in kugelschüttungen. *Brennstof-Wärme-Kraft*, 24:233-236.

BEDENIG, D. 1966. Experimentelle Untersuchungen zum Strömungsverhalten eines Kugelhaufens im Hinblick auf den Brennelementkreislauf im Core eines Kugelhaufenreaktors. *Dissertation Dipl. Ing, Jülich.*

BENENATI, R.F. & BROSILOW, C.B. 1962. Void fraction distribution in beds of spheres. *A.I.Ch.E. Journal*, 8:359-361.

BEY, O. & EIGENBERGER, G. 1996. Fluid flow through catalyst filled tubes. *Chemical Engineering Science*, 52(8):1365-1376.

BLAKE, F.E. 1922. Resistance of packing to fluid flow. *Transactions of American Institute of Chemical Engineers*, 14:415-421.

BRAUER, H. 1960. Eigenshaften der Zweiphasen-Strömung bei der Rektifikation in Füllkörpersäulen. In H. Bretschneider (Ed.), *Fortschritte der Destilliertechnik. Forschungsarbeiten aus dem Max-Plank-Institut für Strömungsforschung Göttingen. Dechema-Monographien.* VCH, Weinherm, 37:7-78.

CARMAN, P.C. 1937. Fluid flow through granular beds. *Transactions of the Institution of Chemical Engineers (London)*, 27:150-166.

CHENG, P. & HSU, C.T. 1986. Fully-developed, forced convective flow through an annular packed-sphere bed with wall effects. *International Journal for Heat and Mass Transfer*, 29(12):1843-1853.

DASZKOWSKI, T. & EIGENBERGER, G. 1992. A reevaluation of fluid flow, heat transfer and chemical reaction in catalyst filled tubes. *Chemical Engineering Science*. 47,9-11:2245-2250.

DU TOIT, C.G. 2006. Analysis of the radial variation in the porosity of annular packed beds. *High Temperature Reactor Conference 2006 Proceeding*.

DU TOIT, C.G., ROUSSEAU, P.G., GREYVENSTEIN, G.P. & LANDMAN, W.A. 2006. A system CFD model of a packed bed high temperature gas-cooled nuclear reactor, *International Journal of Thermal Sciences*, 45:70-85.

ERBEN, G. 1967. Messung des Wärmeübergangs und des Druckverlustes von gasdurchströmten Kugelpackungen und dessen Abhängigkeit von Packungsdichte un Temperatur. *Dissertation*, T.H. Karlsruhe, 51p.

ERGUN, S. 1952. Fluid flow through packed columns. *Chemical Engineering Progress*, 48(2):89-94.

EISFELD, B. & SCHNITZLEIN, K. 2001. The influence of confining walls on the pressure drop in packed beds. *Chemical Engineering Science*, 56:4321-4329.

ESKOM. 2006. Nuclear Programme [Web:] http://www.eskom.co.za/live/content.php?Item_ID223 [Date of access: 21 Feb. 2006].

FLOWNEX. 2006. Flownex user manual – Part 2, 424p.

GIESE, M., ROTTSCHäFER, K. & VORTMEYER, D. 1998. Measured and modeled superficial flow profiles in packed beds with liquid flow. *AIChE*, 44(2):484-490.

HOOGENBOEZEM, T.A.H. 2006a. HPTU PDTS 0.39 Test Report. *M-Tech Industrial Pty (Ltd) Report: HPTU002-PDTS039, Rev B, Potchefstroom.*

HOOGENBOEZEM, T.A.H. 2006b. HPTU PDTS SAPB pressure drop Test Report. *M-Tech Industrial Pty (Ltd) Report: HPTU002-SAPBdP, Rev B, Potchefstroom.*

HTTF001. 2006. Technical file, Calibration Secondary Standards.

HUNT, M.L. & TIEN, C.L. 1990. Non-darcian flow, heat and mass transfer in catalytic packed-bed reactors. *Chemical Engineering Science*, 45(1):55-63.

ISO 5167. 2003a. Measurement of fluid flow by means of pressure differential devices inserted in circular cross-section conduits running full – Part 1: General principles and requirements. ISO 5167-1:2003(E).

ISO 5167. 2003b. Measurement of fluid flow by means of pressure differential devices inserted in circular cross-section conduits running full – Part 2: Orifice plates. ISO 5167-2:2003(E).

JESCHAR, R. 1964. Druckverlust in Mehrkornschüttungen aus Kugeln. *Archiv für den Eisenhüttenwesen,* 35:94-108.

KOSTER, A., MATZNER, H.D.& NICHOLSI, D.R. 2003. PBMR design for the future. *Nuclear Engineering Design*, 222:231-245.

KUGELER, K., ALKAN, Z. & PöPPE, N. 2003. High Temperature Reactor Technology course
notes. Chapter 3, p10.

LABUSCHAGNE , J.T. 2005a. High Pressure Test Unit Thermal-Fluid Design Report. *M-Tech Industrial Pty (Ltd) Report: HTTF001-0009.2 Rev 3, Potchefstroom.* 101p.

LABUSCHAGNE , J.T. 2005b. High Pressure Test Unit (HPTU) Test Procedure. *M-Tech Industrial Pty (Ltd) Report: HTTF001-0004, Rev 1, Potchefstroom.* 23p.

LABUSCHAGNE , J.T. 2005c. High Pressure Test Unit (HPTU) Test Plan *M-Tech Industrial Pty (Ltd) Report: HTTF001-0003, Rev 3, Potchefstroom.* 42p.

LEROU, J.J. & FROMENT, G.F. 1976. Velocity, temperature and conversion profiles in fixed bed catalytic reactors. *Chemical Engineering Science,* 32:853-861.

LINDEBOOM, J. 2005. High pressure test unit detail design report. *M-Tech Industrial Pty (Ltd) Report: HTTF001-0027.1, Rev 1, Potchefstroom.* 53p.

MARTIN, H. 1978. Low Peclet number particle-to-fluid heat and mass transfer in packed beds. *Chemical Engineering Science,* 33:913-919.

MATZIE, R.A. 2004. Pebble Bed Modular Reactor (PBMR) Project Update.

METHA, D. & HAWLEY, M.C. 1969. Wall effects in packed columns. *I& EC Process Design and Development,* 8(2):280-282.

MORALES, M., SPINN, C.W. & SMITH, J.M. 1951. Velocities and Effective Thermal Conductivities in Packed Beds. *Engineering and Process Development,* 43(1):225 – 232.

MUELLER, G.E. 1991. Prediction of radial porosity distributions in randomly packed fixed beds of uniformly sized spheres in cylindrical containers. *Chemical Engineering Science,* 46(2):706-708.

PAPAGEORGIOU, J.N. & FROMENT, G.F. 1995. Simulation models accounting for radial voidage profiles in fixed-bed reactors. *Chemical Engineering Science,* 50(19):3043-3056.

PBMR (Pty) Ltd. 2006a. News Releases – May 2003 [Web:] http://www.pbmr.co.za/index.asp?Content=10&MState=DT&Article=46 [Date of access: 16 Feb. 2006].

PBMR (Pty) Ltd. 2006b. Why PBMR [Web:] http://www.pbmr.co.za/index.asp?Content=3& [Date of access: 16 Feb. 2006].

PBMR (Pty) Ltd. 2006c. News Releases – November 2004 [Web:] http://www.pbmr.co.za/index.asp?Content=10&MSTate=DT&Article=48 [Date of access: 16 Feb. 2006].

PRICE, J. 1968. The distribution of fluid velocities for randomly packed beds of spheres. *Mechanical & Engineering Transactions*. May:7-14.

PRINSLOO, J.H.J. 2006. HPTU Detail Control Design Report. *M-Tech Industrial Pty (Ltd) Report: HTTF001-0031 Rev 1, Potchefstroom.* 89p.

REICHELT, W. 1972. Zur Berechnung des Druckverlustes einphasig durchströmter Kugel- und Zylinderschüttungen. *Chemie Ingenieurs Technik*, 44(18):1068-1071.

ROBLEE, L.H.S., BAIRD, R.M. & TEIRNEY, J.W. 1958. Radial porosity variation in packed beds. *AIChE Journal*. 4:460-464.

ROUSSEAU, P.G. 2005a. Heat Transfer Test Facility Test Specifications. *M-Tech Industrial Pty (Ltd) Report: HTTF001-0008.1 Rev 3, Potchefstroom.* 44p.

ROUSSEAU, P.G. 2005b. Uncertainty analysis of expected results from the HTTF plant design. *M-Tech Industrial Pty (Ltd) Report: HTTF001-0031.1 Rev 2, Potchefstroom.* 43p.

SCHERTZ, W.W. & BISCHOFF, K.B. 1969. Thermal and material transport in Nonisothermal packed beds. *AIChE Journal*. 15,4:579-602.

SODRé, J.R. & PARISE, J.A.R. 1998. Fluid flow pressure drop through an annular bed of spheres with wall effects. *Experimental Thermal and Fluid Science*. 17:265-275.

SCHWARTZ, C.E. & SMITH, J.M. 1953. Flow distribution in packed beds. *Industrial Engineering and Chemistry*. 45,6:1209-1218.

SQUIRES, G.L. 1976. Practical Physics. *McGraw-Hill, Second Edition, Maiden head, Berkshire, England.* 224p.

VAN DER MERWE, J. 2006. HPTU PDTS 0.39 Test Report. *M-Tech Industrial Pty (Ltd) Report: HPTU002-PDTS039, Rev B, Potchefstroom.*

VAN DER WALT, A.J.K. & DU TOIT, C.G. 2006. Pressure drop through annular packed beds. *Proceedings of the Fifth South African Annual Conference on Computational and Applied Mechanics*, Cape Town.

VAN DER WALT, A.J.K. 2006a. Orifice flow meter installation review. *M-Tech Industrial Pty (Ltd) Report: HTTF001-0034, Rev 1, Potchefstroom.* 16p.

VAN DER WALT, A.J.K. 2006b. HPTU PDTS 0.45 Test Report. *M-Tech Industrial Pty (Ltd) Report: HPTU002-PDTS045, Rev B, Potchefstroom.*

VAN DER WALT, A.J.K. 2006c. HPTU PDTS SCPB pressure drop Test Report. *M-Tech Industrial Pty (Ltd) Report: HPTU002-SCPBdP, Rev B, Potchefstroom.*

VAN NIEKERK, W.M.K. 2006. HPTU instrument calibration plan. *M-Tech Industrial Pty (Ltd) Report: HTTF001-0027, Rev 1, Potchefstroom.* 14p.

VORTMEYER, D. & SCHUSTER, J. 1983. Evaluation of steady flow profiles in rectangular and circular packed beds by a variational method. *Chemical Engineering Science*, 38(10):1691-1699.

WENTZ, C.A. & THODOS, G. 1963. Pressure Drop in the Flow of Gases Through Packed and Distended Beds of Spherical Particles. *AIChE Journal*, 9(1):81-84.

WHITE, S.M. & TIEN, C.L. 1987. Analysis of flow channelling near the wall in packed beds. *Wärme- und Stoffübertragung*, 21:291-296.

WINTERBERG, M. & TSOTSAS, E. 2000. Impact of tube-to-particle-diameter ratio on pressure drop in packed beds. *AIChE Journal*, 46(5):1084-1088.

Appendix A: SCHEMATIC LAYOUT OF THE HPTU

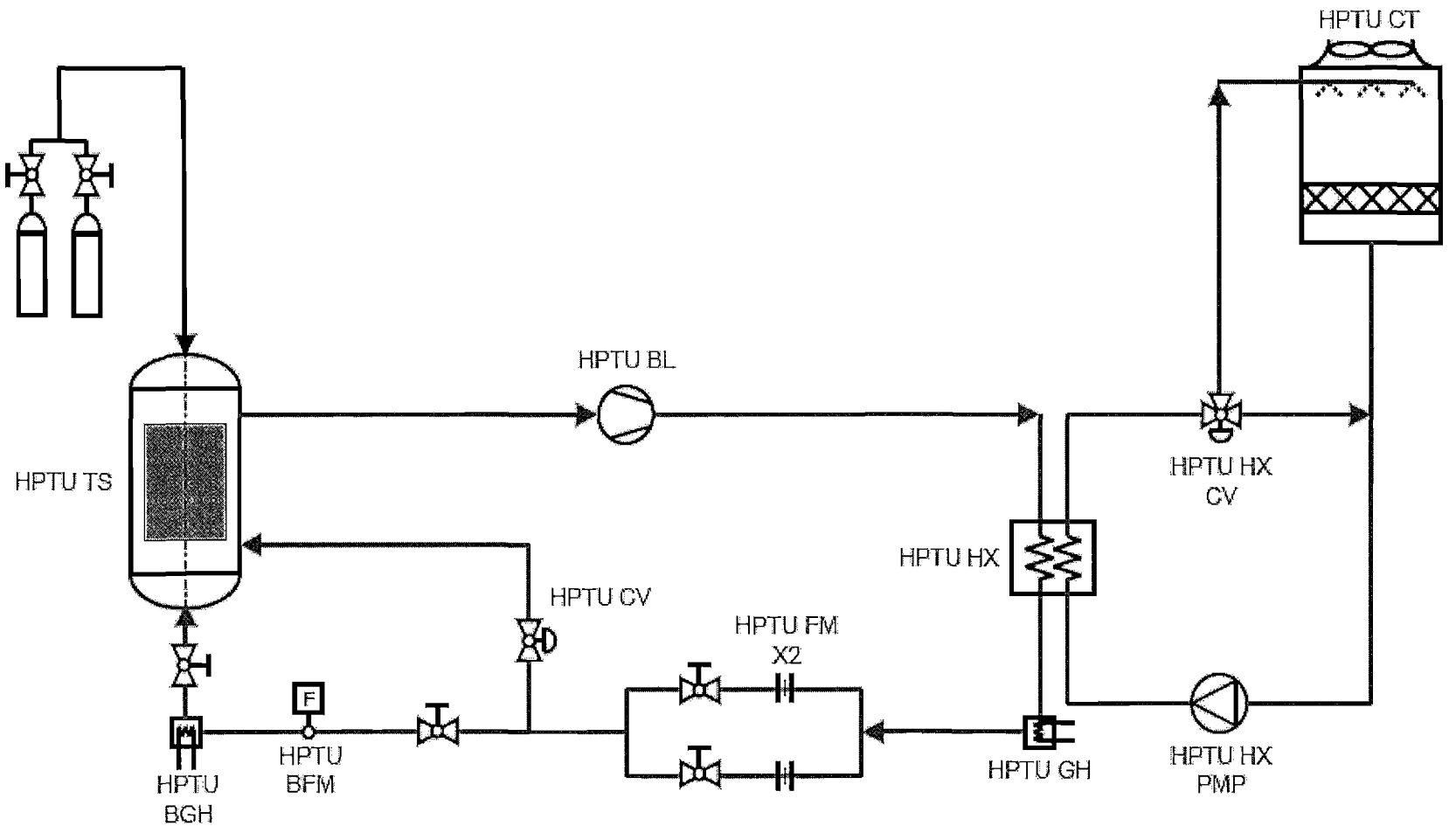

Figure A.1 *Schematic layout of the HPTU plant*

Table A.1: List of abbreviations in Figure A1

Abbreviation	Description
TS	Test Section
BGH	Braiding Gas Heater
BFM	Braiding Flow Meter
CV	Control Valve
FM	Flow Meter
GH	Gas Heater
HX	Heat Exchanger
BL	Blower
HX PMP	Heat Exchanger Pump
HX CV	Heat Exchanger Control Valve
HX CT	Heat Exchanger Cooling Tower

Appendix B: ORIFICE STATIONS DIMENSIONS AND UNCERTAINTIES

The dimensions of the orifice plates measured during the Orifice Flow Meter Installation Review (van der Walt, 2006a) are given in Table B.1. The measurements were made with a Mitutoyo vernier with a range of 150 mm and a resolution of 0.01mm. The vernier was calibrated at SANAS accredited laboratory. The uncertainty in the calibration is 0.026 mm.

Table B.1: Dimensions of the orifice measurement stations

Variable	Orifice Station OR-220		Orifice Station OR-221	
	Measured Value [m]	Standard Uncertainty [m]	Measured Value [m]	Standard Uncertainty [m]
Pipe diameter	0.097253	4.97494E-05	0.097217	2.64002E-05
Throat diameter	0.04839	[-]	0.04834	[-]
β	0.497570757 [-]	[-]	0.497239842 [-]	[-]

The discharge coefficient used in equation (24) is defined by ISO 5167 (2003a) as:

$$C = 0.5961 + 0.0261 \cdot \beta^2 - 0.216 \cdot \beta^8 + 0.000521 \cdot \left(\frac{10^6 \cdot \beta}{\mathrm{Re}_D}\right)^{0.7} + \left(0.0188 + 0.0063A'\right) \cdot \beta^{3.5} \cdot \left(\frac{10^6}{\mathrm{Re}_D}\right)^{0.3} + \left(0.043 + 0.08e^{-10L_1} - 0.123e^{-7L_1}\right).(1 - 1.011A').\left(\frac{\beta^4}{1-\beta^4}\right) - 0.031(M_2' - 0.8M_2'^{1.1})\beta^{1.3} \quad (55)$$

with

$$A' = \left(\frac{19000 \cdot \beta}{\mathrm{Re}_D}\right)^{0.8} \quad (56)$$

and Re_D the pipe Reynolds number and L_1 and M_2 constants. In the case of the orifice stations installed on the HPTU plant, pressure measurements are made from corner tappings for which $L_1 = 0$ and $M_2' = 0$. The expansion coefficient is given as:

$$\varepsilon = 1 - \left(0.351 + 0.256 \cdot \beta^4 + 0.93 \cdot \beta^8\right) \cdot \left[1 - \left(\frac{p_2}{p_1}\right)^{1/\kappa}\right] \quad (57)$$

with p_1 and p_2 the pressure before and after the orifice plate respectively. For the sake of reference in the explanation of the various uncertainties equation (25) is repeated:

$$\frac{u_s(\dot{m})}{\dot{m}}=\sqrt{\left(\frac{u_s(C)}{C}\right)^2+\left(\frac{u_s(\varepsilon)}{\varepsilon}\right)^2+\left(\frac{2\beta^4}{1-\beta^4}\right)^2\cdot\left(\frac{u_s(D)}{D}\right)^2+\left(\frac{2}{1-\beta^4}\right)^2\left(\frac{u_s(d_{or})}{d_{or}}\right)^2+\frac{1}{4}\left(\frac{u_s(\Delta p)}{\Delta p}\right)^2+\frac{1}{4}\left(\frac{u_s(\rho_1)}{\rho_1}\right)^2}$$

The minimum value for $\frac{u_s(C)}{C}$ given by ISO 5167 (2003b) is 0.5% for the specific value of β. An additional 0.5% is however added according the ISO 5167 (2003b) after the Installation Review (van der Walt, 2006a), due to the upstream pipes lengths. The value of $\frac{u_s(C)}{C}$ for all cases is therefore 1% of the calculated value. The value of $\frac{u_s(\varepsilon)}{\varepsilon}$ is given by ISO 5167 (2003b) as $3.5\frac{\Delta p}{\kappa \cdot p_1}\%$, with p_1 the upstream measured pressure.

The standard uncertainty of the pipe diameter $u_s(D)$ is shown in Table B.1 for both orifice stations. The general uncertainty in the throat diameter is assumed to be 50μ m. This is a realistic value given the standard uncertainties in the pipe diameter which is not machined. The general uncertainty of the throat diameter is without a confidence interval. The standard uncertainty is therefore calculated as $u_s(d_{or})=\frac{0.00005}{\sqrt{3}}=0.000028m$.

Appendix C: PROPERTY EQUATIONS

The equation derived for the density is given as:

$$\rho\ [\mathrm{kg/m^3}] = \left(b3_3T^3 + b3_2T^2 + b3_1T + b3_0\right)p^3 + \left(b2_3T^3 + b2_2T^2 + b2_1T + b2_0\right)p^2 + \left(b1_3T^3 + b1_2T^2 + b1_1T + b1_0\right)p + \left(b0_3T^3 + b0_2T^2 + b0_1T + b0_0\right) \quad (58)$$

Where

$b3_3 =$ 3.4e-19

$b3_2 =$ -2.32257e-16

$b3_1 =$ 4.59236e-14

$b3_0 =$ -3.73572e-12

$b2_3 =$ -7.74489e-14

$b2_2 =$ 1.67423e-11

$b2_1 =$ -1.76353e-9

$b2_0 =$ 5.78174e-8

$b1_3 =$ -4.22222e-10

$b1_2 =$ 1.58476e-7

$b1_1 =$ -4.50004e-5

$b1_0 =$ 1.23325e-2

$b0_3 =$ -1.90620e-9

$b0_2 =$ 2.79035e-7

$b0_1 =$ -1.78122e-5

$b0_0 =$ 4.19341e-4

$T[^\circ C]$ = Temperature

$p[kPa]$ = Static pressure

The maximum difference between the densities calculated using equation (58) and the original data is 0.0137%

The equation derived for the viscosity is:

$$\mu\ [\text{kg/m s}] = \left(b2_3 T^3 + b2_2 T^2 + b2_1 T + b2_0\right) p^2 + \left(b1_3 T^3 + b1_2 T^2 + b1_1 T + b1_0\right) p + \left(b0_3 T^3 + b0_2 T^2 + b0_1 T + b0_0\right) \quad (59)$$

where

$b2_3 =$ -2.31556E-21

$b2_2 =$ 5.91776E-19

$b2_1 =$ -7.83363E-17

$b2_0 =$ 6.5815E-15

$b1_3 =$ -6.22222E-18

$b1_2 =$ 1.96619E-15

$b1_1 =$ -5.86961E-13

$b1_0 =$ 1.67993E-10

$b0_3 =$ 0

$b0_2 =$ -3.25714E-11

$b0_1 =$ 4.785E-8

$b0_0 =$ 1.66207E-5

$T[^\circ C]$ = Temperature

$p[kPa]$ = Static pressure

The maximum difference between the viscosities calculated using equation (59) and the original data is 0.0025%

Appendix D: ADDITIONAL RESULTS

Some important data are included for reference. The uncertainty in the Euler number for all the pressure drop tests are firstly presented in Table D.1, showing the maximum uncertainties in each of the tests. The uncertainty in the friction factor is secondly presented in Table D.2
The repeatability results are shown in Table D.3, with the maximum deviation occurring in all the tests shown. The percentage deviation between the predicted and experimental friction factor are shown in Table D.4.
As further important results the repeatability of the PDTS 036, PDTS 039 and SCPB pressure drop tests are presented graphically in Figure D.1 to Figure D.3

Table D.1: Euler number uncertainties for all the pressure drop tests

Set point Number	PDTS036		PDTS039		PDTS045		SAPB Pressure drop		SCPB Pressure drop	
	Test run 1	Test run 2	Test run 1	Test run 2	Test run 1	Test run 2	Test run 1	Test run 2	Test run 1	Test run 2
1	4.52	4.38	4.52	4.50	4.63	4.62	4.59	4.61	4.31	4.31
2	4.14	4.14	4.18	4.16	4.24	4.23	4.57	4.56	4.33	4.31
3	4.09	4.39	4.11	4.17	4.13	4.12	4.52	4.54	4.31	4.29
4	4.07	4.12	4.14	4.13	4.11	4.16	4.52	4.52	4.29	4.29
5	4.14	4.14	4.11	4.11	4.16	4.14	4.52	4.53	3.18	3.17
6	4.09	4.09	4.10	4.10	4.10	4.11	[-]	[-]	[-]	[-]
7	4.10	4.08	4.09	4.09	4.10	4.09	[-]	[-]	[-]	[-]
8	4.08	4.09	4.09	4.09	4.10	4.10	[-]	[-]	[-]	[-]
9	4.07	4.09	4.09	4.09	4.09	4.09	[-]	[-]	[-]	[-]
10	4.11	4.06	4.10	4.10	4.12	4.10	[-]	[-]	[-]	[-]
11	4.09	4.07	4.22	4.08	4.10	4.12	[-]	[-]	[-]	[-]
12	2.89	2.87	2.93	2.92	2.97	2.98	[-]	[-]	[-]	[-]
13	2.97	2.95	4.04	4.00	3.20	3.36	[-]	[-]	[-]	[-]
14	2.88	2.91	4.04	4.28	3.33	3.30	[-]	[-]	[-]	[-]
Max	4.52	4.38	4.52	4.50	**4.63**	4.62	4.59	4.61	4.33	4.31

Table D.2: Friction factor uncertainties for all the pressure drop tests

Set point Number	PDTS036		PDTS039		PDTS045		SAPB Pressure drop		SCPB Pressure drop	
	Test run 1	Test run 2	Test run 1	Test run 2	Test run 1	Test run 2	Test run 1	Test run 2	Test run 1	Test run 2
1	5.89	5.79	5.60	5.59	5.38	5.37	17.88	17.90	16.24	16.24
2	5.61	5.62	5.33	5.32	5.05	5.04	17.86	17.85	16.25	16.24
3	5.57	5.80	5.28	5.33	4.96	4.95	17.81	17.83	16.24	16.24
4	5.56	5.59	5.30	5.30	4.94	4.99	17.81	17.81	16.24	16.24
5	5.60	5.61	5.28	5.28	4.99	4.96	17.81	17.82	15.98	15.98
6	5.57	5.57	5.27	5.27	4.94	4.94	[-]	[-]	[-]	[-]
7	5.58	5.56	5.27	5.27	4.93	4.93	[-]	[-]	[-]	[-]
8	5.56	5.57	5.26	5.26	4.93	4.93	[-]	[-]	[-]	[-]
9	5.55	5.57	5.26	5.26	4.92	4.93	[-]	[-]	[-]	[-]
10	5.59	5.55	5.27	5.27	4.95	4.93	[-]	[-]	[-]	[-]
11	5.57	5.55	5.36	5.26	4.93	4.95	[-]	[-]	[-]	[-]
12	4.76	4.75	4.42	4.41	4.05	4.05	[-]	[-]	[-]	[-]
13	4.81	4.80	5.22	5.20	4.21	4.34	[-]	[-]	[-]	[-]
14	4.75	4.77	5.23	5.41	4.31	4.29	[-]	[-]	[-]	[-]
Max	**5.89**	5.80	5.60	5.59	5.38	5.37	17.88	**17.90**	16.25	16.24

Table D.3: Summary of the percentage deviation in the Euler number for test run 1 and 2 of each test

Set point Number	PDTS036 [%]	PDTS039 [%]	PDTS045 [%]	SAPB Pressure drop [%]	SCPB Pressure drop [%]
1	0.63	0.95	0.43	0.65	0.06
2	0.22	0.77	0.71	0.54	0.19
3	1.79	0.38	0.16	0.62	0.03
4	0.01	0.31	0.63	0.26	0.08
5	0.75	0.19	0.32	0.05	0.17
6	0.07	0.06	0.49	[-]	[-]
7	0.45	0.16	0.57	[-]	[-]
8	0.47	0.09	0.48	[-]	[-]
9	0.20	0.24	0.35	[-]	[-]
10	0.11	0.33	0.21	[-]	[-]
11	0.80	0.09	0.25	[-]	[-]
12	0.18	0.15	0.16	[-]	[-]
13	0.03	0.06	0.14	[-]	[-]
14	0.01	0.05	0.15	[-]	[-]
Max	**1.79**	0.95	0.71	0.65	0.19

Table D.4: Percentage difference between predicted and experimental friction factors for the SET

Reynolds number	PDTS 036		PDTS 039		PDTS 045	
	KTA	Wentz & Thodos (1963)	KTA	Wentz & Thodos (1963)	KTA	Wentz & Thodos (1963)
1000	9.4	15.4	20.6	25.6	56.0	60.9
2000	23.8	19.3	38.0	31.7	80.7	70.9
3000	35.9	24.8	49.2	35.9	97.5	78.5
4000	44.1	28.2	59.4	40.9	110.7	84.8
5000	51.5	31.8	68.5	45.6	125.7	93.6
6000	59.5	36.3	76.9	50.2	137.4	100.3
7000	66.6	40.3	84.6	54.5	148.5	106.7
8000	72.5	43.5	91.7	58.6	158.5	112.5
9000	78.4	46.8	98.4	62.5	168.0	118.1
10000	83.5	49.7	104.9	66.3	176.9	123.5
20000	126.6	75.1	152.5	94.4	252.3	169.8
30000	139.5	80.1	173.3	104.8	291.1	191.7
40000	143.2	79.6	185.8	110.4	315.6	204.7
50000	140.7	75.5	190.1	110.9	327.7	209.7

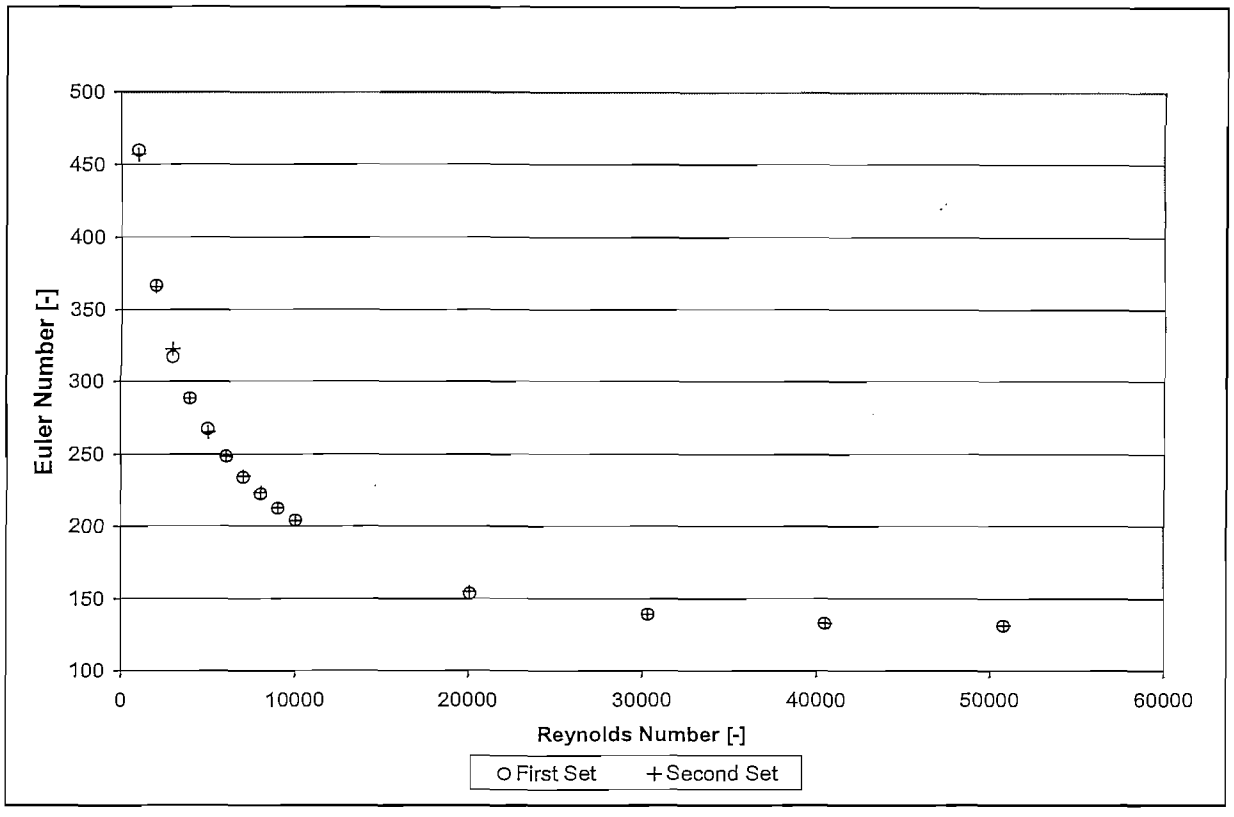

Figure D.1 *Repeatability results for the PDTS036 pressure drop test*

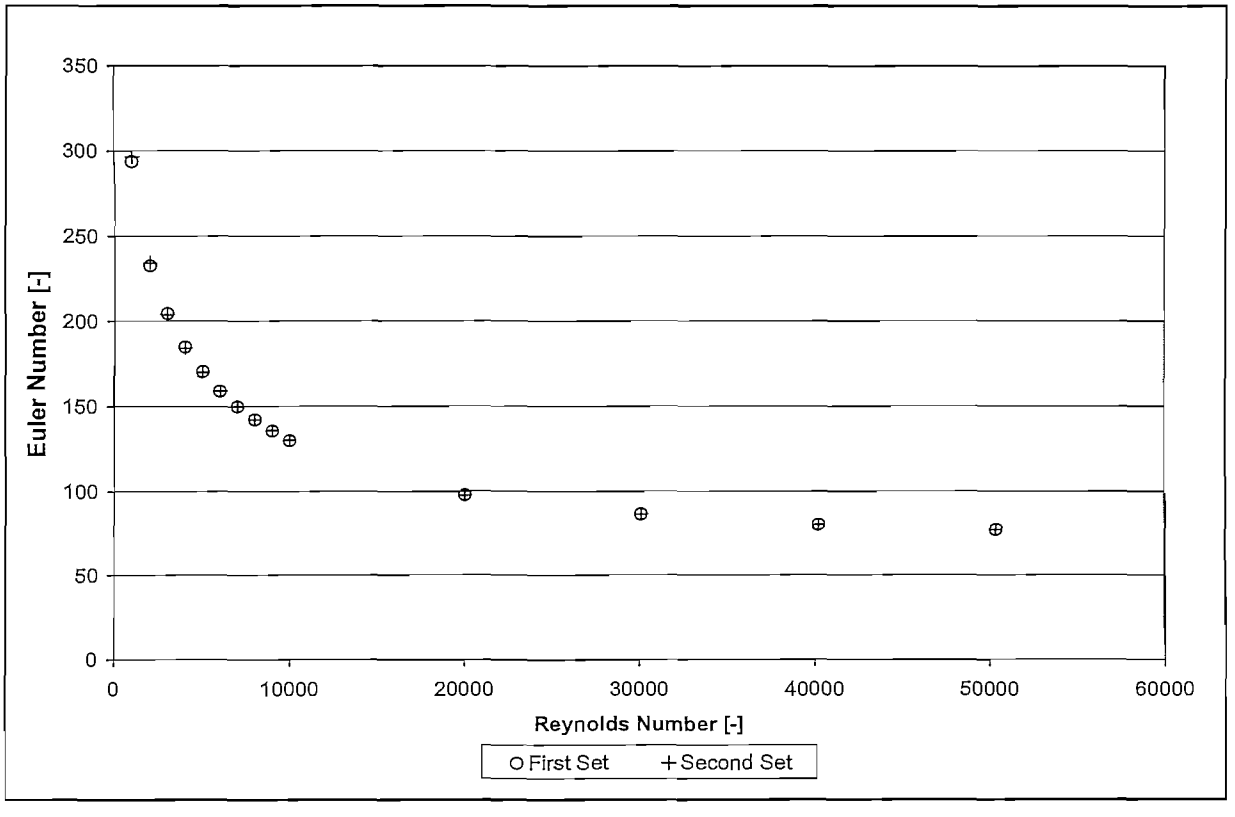

Figure D.2 *Repeatability results for the PDTS039 pressure drop test*

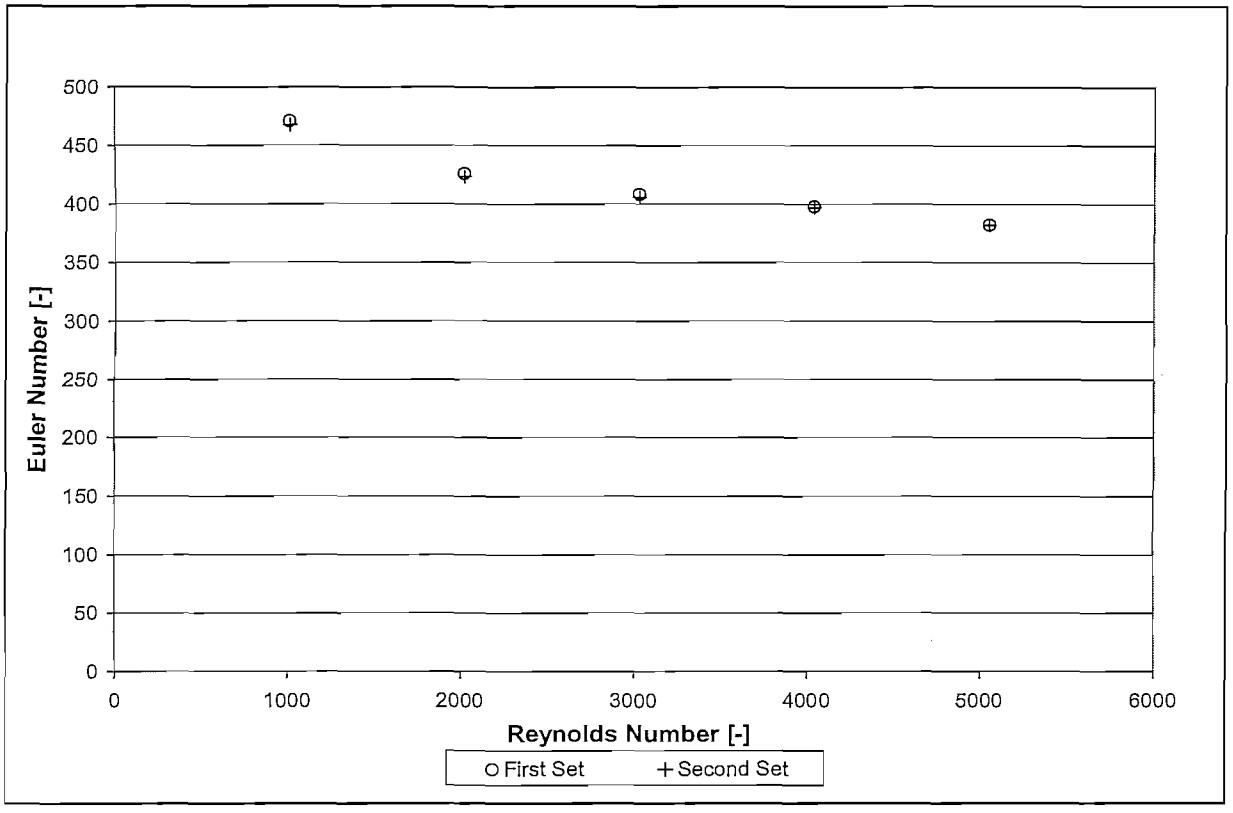

Figure D.3 *Repeatability results for the SAPB pressure drop test*